

University of Nottingham Malaysia

Department of Electrical and Electronic Engineering



**AN INTELLIGENT POWER
MANAGEMENT SYSTEM WITH ACTIVE
LEARNING PREDICTION ENGINE FOR
PV GRID-TIED SYSTEMS**

by KOW KEN WENG

Thesis submitted in candidature for the degree of Doctor of Philosophy, Sept 2019

ABSTRACT

An incremental unsupervised neural network algorithm namely time-series self-organizing incremental neural network (TS-SOINN) is developed to predict the photovoltaic output power for power fluctuation events detection in photovoltaic micro-grid system. The TS-SOINN is an unsupervised clustering algorithm that identifies the most similar patterns from a data map to predict photovoltaic output power. A novel memory layer and weighted tapped delay line is introduced to establish the time-series learning. By using real-life environment data as input data, the proposed TS-SOINN based real-time prediction engine predicts 97% of power fluctuation events with 10% false acceptance rate. These results outperform three different types of self-organizing incremental neural network, self-organizing map, and nonlinear autoregressive with exogenous input network. The proposed TS-SOINN is then integrated into an intelligent power management system (PMS) to form the novel active learning intelligent PMS. The developed system is tested in simulation and experiment environments. Results show that the developed PMS reduces 89% of power fluctuation events and battery state-of-charge maintains within 30% to 100%. It outperforms hourly rule-based controller and the ramp rate controller by 53.53% and 37.08%, respectively in terms of the number of mitigated power fluctuation events. To conclude, power fluctuation events are mitigated by a novel intelligent PMS with reduced battery energy storage system capacity.

ACKNOWLEDGEMENT

Foremost, I would like to express my sincere gratitude to my principal supervisor, Dr Wong Yee Wan for the continuous support of my PhD study and research, for her patience, motivation, enthusiasm and immense knowledge. This research work would not be possible without her guidance. Besides my principal supervisor, I would like to thank Mr Rajparthiban, and Dr Rajprasad for their encouragement, insightful comments, and the effort in proofreading my thesis. Their patience and support help me to overcome numerous obstacles I have been facing through my research. I would like to thank the Ministry of Science, Technology and Innovation (MOSTI) to offer a grant for me to carry out my research works.

I am grateful to my father, Mr. Kow Yoon Fatt, who have provided me through moral, emotional and financial support in my life. I dedicate this thesis to my late mother, Mdm. Chee Chooi Leng who supported me from another world. I would like to thank my brothers and sister for supporting me spiritually throughout writing this thesis and my life in general.

PROJECT GRANT FUNDING

This project is funded by eScience MOSTI under project reference number 03-02-12-SF0211 from the year 2013 to 2016. With the successful completion of this project, a Prototype Development Research Grant Scheme (PRGS) was then secured from the Ministry of Higher Education (MOHE) in the year 2017 (project reference code PRGS/1/2017/ICT02/UNIM/03/1).

The novel prediction algorithm (TS-SOINN) and the system developed in this project was submitted for Intellectual Property (IP) filling to fulfil one of the important requirements of the PRGS.

PUBLICATIONS

The following papers were published in international conference, book, and journals:

1. **Kow Ken Weng**, Wong Yee Wan, Rajprasad Kumar Rajkumar, and Dino Isa. "An Intelligent Real-Time Power Management System with Active Learning Prediction Engine for PV Grid-Tied Systems," *Journal of Cleaner Production*, Volume 205, PP. 252-265, 2018. 5- Year Impact Factor: 6.352
2. **Kow Ken Weng**, Wong Yee Wan, Rajphatiban Kumar Rajkumar, and Rajprasad Kumar Rajkumar, "A review on performance of artificial intelligence and conventional method in mitigating PV grid-tied related power quality events," *Renewable and Sustainable Energy Review*, Volume 56, PP. 334-346, 2016. 5-Year Impact Factor: 10.093
3. **Kow Ken Weng**, Wong Yee Wan, Rajphatiban Kumar Rajkumar, and Rajprasad Kumar Rajkumar, "*Power Quality Analysis for PV Grid Connected System Using PSCAD / EMTDC*," *International Journal of Renewable Energy Research*, Volume 5, Issue 1, PP. 121-132, 2015. Impact Factor: 1.261
4. **Kow Ken Weng**, Wong Yee Wan, Rajparthiban Kumar Rajkumar, Rajprasad Kumar Rajkumar, and Dino Isa. "*Power Fluctuation Prediction Using Unsupervised Learning Algorithms for PV Grid-Tied System*." 2016 International Conference on Engineering, Technology and Applied Science, 2016.
5. **Kow Ken Weng**, Wong Yee Wan, Rajparthiban Kumar Rajkumar, Rajprasad Kumar Rajkumar, and Dino Isa. "Incremental Unsupervised Learning Algorithm for Power Fluctuation Event Detection in PV Grid-Tied Systems." In *9th International Conference on Robotic, Vision, Signal Processing and Power Applications*, pp. 673-679. Springer Singapore, 2017.

TABLE OF CONTENTS

ABSTRACT	i
ACKNOWLEDGEMENT	ii
PROJECT GRANT FUNDING.....	iii
PUBLICATIONS	iv
TABLE OF CONTENTS	v
ABBREVIATIONS	ix
LIST OF FIGURES	xii
LIST OF TABLES.....	xvi
Chapter 1 Introduction.....	1
1.1 Overview.....	1
1.2 Problem Statement.....	4
1.3 Research Objectives.....	5

Table of Contents

1.4	Significance of Research	6
1.5	Scope of Research.....	7
1.6	Thesis Structure	7
Chapter 2	Literature Review	10
2.1	Power Quality	11
2.2	Mitigation Engine	14
2.2.1	Power Monitoring	14
2.2.2	Inverter.....	17
2.2.3	Geographical Dispersion	20
2.2.4	BESS.....	23
2.3	Prediction Engine.....	29
2.3.1	Types of Prediction Engine	30
2.4	Use of AI in Power Networks.....	37
2.4.1	Incremental Unsupervised Learning Algorithm	39
2.4.2	E-SOINN	42

Table of Contents

2.4.3	SOINN-DTW	47
2.4.4	HBSOINN	48
2.5	Summary	50
Chapter 3	Time-Series Self-Organizing Incremental Neural Network (TS-SOINN).....	52
3.1	Summary	62
Chapter 4	Intelligent Real-Time Power Management System (PMS)	63
4.1	Summary	69
Chapter 5	Real-time Implementation of Power Management System	70
5.1	PV Grid-Tied System	70
5.2	Data Acquisition System	72
5.3	Laboratory-Scale PV grid-tied system.....	76
5.4	Real-time Implementation of the PMS	78
5.5	Summary	80

Table of Contents

Chapter 6	Results and Discussions.....	81
6.1	TS-SOINN	82
6.1.1	Optimisation of Parameters	82
6.1.2	Simulation Analysis.....	88
6.1.3	Experimental Analysis.....	104
6.2	Intelligent Real-Time PMS.....	109
6.2.1	Optimisation of Parameters	109
6.2.2	Performance Evaluation.....	111
6.2.3	Performance Comparison	116
6.3	Summary.....	125
Chapter 7	Conclusions	126
7.1	Future Works	129
REFERENCES		130

ABBREVIATIONS

AARC	Average Active Reactive Control
AC	Alternating Current
AI	Artificial Intelligence
AMR	Automated Meter Reading
ANN	Artificial Neural Network
AR	Autoregressive
ARIMA	Autoregressive Moving Integrated Average
ARMA	Autoregressive Moving Average
ARMAX	Autoregressive Moving Average Exogenous
BESS	Battery Energy Storage System
BFO	Bacterial Foraging Optimisation
CB	Circuit Breaker
CHL	Competitive Hebbian Learning
DC	Direct Current
DNI	Direct Normal Irradiance
DTW	Dynamic Time Warping
E-SOINN	Enhanced Self-Organizing Incremental Neural Network
ESS	Energy Storage System
EVMS	Electric Vehicle Management System
GA	Genetic Algorithm
GHI	Global Horizontal Irradiance
GNG	Growing Neural Gas
GRC	Generation Rate Constraint
HBSOINN	Hidden Markov Model Based Self-Organizing Incremental Neural Network
HMM	Hidden Markov Model

IARC	Instantaneous Active Reactive Control
IGNG	Incremental Growing Neural Gas
IID	Independent and Identically Distributed
IPQMS	Integrated Power Quality Monitoring System
MAE	Mean Absolute Error
MLP	Multi-Layer Perceptron
MSB	Main Switchboard
NARX	Non-linear Autoregressive Exogenous
NWP	Numerical Weather Prediction
O&M	Operating and Maintenance
P.U	Per Unit
PCC	Point of Common Coupling
PI	Proportional Integral
PID	Proportional Integral Derivative
PMS	Power Management System
PQMS	Power Quality Monitoring System
PREPA	Puerto Rico Electric Power Authority
PSCAD	Power System Computer Aided Design
PSO	Particle Swarm Optimisation
PV	Photovoltaic
R^2	R-squared
RES	Renewable Energy Sources
RMS	Root Mean Square
RMSE	Root Mean Square Error
s	Forecast Skill
SCADA	Supervisory Control and Data Acquisition
SOC	State-of-Charge
SOINN	Self-Organizing Incremental Neural Network

Abbreviations

SOINN-DTW	Self-Organizing Incremental Neural Network Dynamic Time Warping
SOM	Self-Organizing Map
TSI	Total Sky Image
TS-SOINN	Time-Series Self-Organizing Incremental Neural Network
UNM	University of Nottingham Malaysia
VSC	Voltage Source Controller

LIST OF FIGURES

Figure 1: Topology of PV Grid-Tied System with BESS	23
Figure 2: Impact of Data Resolution to the Power Fluctuation Event. The System Power in Seconds to Minutes Resolution Fluctuates Largely	28
Figure 3: Illustration of Large Similarity Threshold Problem in E-SOINN.....	46
Figure 4: Associate Memory Prediction Mechanism	53
Figure 5: Learning Flowchart of the TS-SOINN.....	58
Figure 6: Prediction Mechanism of the TS-SOINN	59
Figure 7: Time-Series Self Organizing Incremental Neural Network.....	60
Figure 8: Block Diagram of the Developed Intelligent Real-Time Power Management System.....	63
Figure 9: Flowchart of the Data Acquisition System	72
Figure 10: Data Logger.....	73
Figure 11: SP Lite 2 Pyranometer	74
Figure 12: Wiring Schematic of Floating Source	74
Figure 13: WXT 520 Weather Transmitter (left) & Nokeval 7470 Analog Converter (Right).....	75

List of Figure

Figure 14: ABB 3.6 kW inverter	76
Figure 15: Simplified Electrical Schematic of the PV Grid-Tied System.....	77
Figure 16: Flowchart of Real-Time Implementation of PMS	79
Figure 17: Percentage of Predicted Power Fluctuation Events for Different Total Previous Data Point	84
Figure 18: Percentage of Predicted Power Fluctuation Events for Different Maximum Age	85
Figure 19: Percentage of Predicted Power Fluctuation Events versus Different Similarity Threshold Values	86
Figure 20: Percentage of Predicted Power Fluctuation Events for Different Periods	87
Figure 21: Graph of Actual Power versus Predicted Power (Blue) with Actual Power Fluctuation Events (Brown Dot) in Day 5.....	94
Figure 22: Graph of Actual Power versus Predicted Power (Blue) with Actual Power Fluctuation Events (Brown Dot) in Day 18.....	95
Figure 23: Graph of Actual Power versus Predicted Power (Blue) with Actual Power Fluctuation Events (Brown Dot) in Day 53.....	96
Figure 24: Methodology of Power Fluctuation Prediction where the Red Dots are the Actual Power Fluctuation Events and the Blue Line is the Predicted Range. Red Dots that Fall into the Blue Rectangle is the Early Predicted Event,	

whereas the Red Dots that Fall Outside the Blue Line is the Unpredicted Event.	99
Figure 25: Scatter of Actual Output Power versus Predicted Output Power (Experiment).....	105
Figure 26: Graph of Actual Power versus Predicted Power on 10th of January 2018	107
Figure 27: Graph of Predicted and Occurrence of Power Fluctuation Events (Experiment).....	108
Figure 28: Percentage of Mitigated Power Fluctuation Events versus Different Update Times.....	110
Figure 29: Percentage of Mitigated Power Fluctuation Events against Different Limiting Thresholds.....	110
Figure 30: Performance of the BESS Controller	112
Figure 31: PV Power (Red Dotted) versus PCC Power (Blue Line).....	113
Figure 32: Graph of PCC Power versus PV Power (Zoomed In).....	113
Figure 33: RMS Voltage (Top) and Frequency (Bottom) at the PCC.....	114
Figure 34: Simulation of PV Grid-Tied System with Developed PMS for a Complete Day. Top Plot: PCC (blue), PV (red), and Battery (brown) Active Power. Bottom plot: Battery SOC	115

List of Figure

Figure 35: SOC of BESS by the Developed PMS, Hourly Rule-Based and Ramp Rate Controller for day 3	117
Figure 36: SOC of BESS by the Developed PMS, Hourly Rule-Based and Ramp Rate Controller for day 8	118
Figure 37: SOC of BESS by the Developed PMS, Hourly Rule-Based and Ramp Rate Controller for day 15	119
Figure 38: Cumulative Distribution Function Analysis of Ramp Rate at PCC of Original Data (blue), Developed PMS (Red), Ramp Rate Method (Orange), and Hourly Control (Purple).....	120
Figure 39: PI Error for Developed System and Ramp Rate Controller	122

LIST OF TABLES

Table 1: Summary of Prediction Engine	37
Table 2: Advantages and Disadvantages of Existing Clustering Techniques ..	41
Table 3: Summary of Tested Algorithms Performances in Predicting Output Power	92
Table 4: Summary of Performances Metrics during Power Fluctuation Events' Instance	98
Table 5: Prediction Rate of Power Fluctuation Events for Tested Algorithms	101
Table 6: False Acceptance Rate for Tested Algorithms	102
Table 7: Summary of Prediction Performances for Tested Algorithms	103
Table 8: Performance Metrics of TS-SOINN in Simulation and Experiment	105
Table 9: Performances in Predicting Power Fluctuation Events	108
Table 10: Number of Mitigated and Unmitigated Event	114
Table 11: Summary of PMS Performances	124

Chapter 1 Introduction

1.1 Overview

In power networks, poor power quality could cause damage to electrical appliances and cause power distribution component to operate in undesired regions. In Malaysia, photovoltaic (PV) system has become popular and it is being integrated to the grid. The downside of PV grid-tied system is that PV output highly relies on the solar irradiance and ambient temperature which are stochastic and intermittent. Hence, power fluctuation events could happen and cause an imbalance between power generation and load.

Power fluctuation event prediction and mitigation is the aim of this research work. To identify the most effective method to mitigate the power fluctuation events, a thorough review is conducted [1]. Most of the existing works in power fluctuation mitigation set the desired output power by assuming a prediction engine is available [2]–[5]. In addition, ancillary power from batteries usually dispatch constantly for an hour or power fluctuation level is calculated at an hourly basis [2]–[4]. It is not applicable to solar PV as cloud moves rapidly. Furthermore, the existing mitigation engines [6] are passive as they are only able to solve power quality problems after the occurrence. According to Rodway et al. [7], the current power network's protection system is insufficient to ensure the reliability of the power distribution system in terms

of response time due to the integration of renewable energy sources (RES). In addition, they showed that there is no research work done on predicting power quality events from environmental variables. They also suggested that prediction of power quality events could enhance the reliability of micro-grid by varying power contribution of RES.

Therefore, to actively predict and mitigate power fluctuation events in a PV grid-tied system, an active learning power fluctuation events prediction and mitigation engine based on a novel incremental unsupervised neural network is presented. The Time-Series Self-Organizing Incremental Neural Network (TS-SOINN) is the first time-series unsupervised incremental neural network algorithm. It actively learns new data and predicts occurrence of power fluctuation events. The TS-SOINN uses a clustering technique to form a data map, identifies the most similar pattern for the solar power prediction and then predicts power fluctuation events. A novel weighted tapped delay line is incorporated to establish time-series learning. It predicts the output power of the PV system in 30 seconds resolution. The developed algorithm outperforms the conventional Enhanced Self-Organizing Incremental Neural Network (E-SOINN) [8] in three aspects: 1) It is applicable in time-series learning, 2) It reduces the number of unknown parameters from five (as in the E-SOINN with associate memory) to three, and 3) It improves the prediction accuracy by solving the data overlapping issues caused by the adaptive similarity threshold in the E-SOINN.

The TS-SOINN based prediction algorithm is then implemented in a power management system (PMS). The developed PMS uses a novel control strategy to control the battery energy storage system (BESS) to mitigate power fluctuation events. When the difference of the predicted output power within a minute exceeds 10% of the rated PV system, the prediction engine maintains call of power fluctuation events for a short period (T_{active}). When there is a call of power fluctuation event, the mitigation engine switches on to alleviate the power fluctuation events and then it will be switched off when there is no event predicted. By doing so, the power fluctuation events can be mitigated prior to its occurrence. It subsequently updates the required ancillary power to the grid by every 2.5 minutes to reduce the difference between actual output power and ancillary power. The mitigation engine maintains the state of charge (SOC) of the BESS within 30% to 100% to prolong the battery lifespan [9]. The TS-SOINN based mitigation engine is novel as it is the first incremental unsupervised learning used in real-time PV output fluctuation prediction [10], [11].

The performance of the developed system is tested in both simulation and experimental environments. Real-life irradiance and temperature data are fed into the modelled 270 kWp PV grid-tied system to simulate power fluctuation events due to a real-life scenario. Next, a 1.2 kWp laboratory scale PV grid-tied system is designed and constructed in the solar cabin of the University of Nottingham Malaysia (UNM). Irradiance, ambient temperature,

and output power of the PV system are collected in real-time to predict power fluctuation events.

1.2 Problem Statement

Some of the research issues which may be regarded as problem statements are as follows:

- The highly fluctuating and random behaviour of the PV output in Malaysia imposes a great challenge in accurately predicting the occurrence of the power fluctuation events. Most of the existing works [2]–[5] in power fluctuation mitigation is passive and to have an active mitigation engine, the power fluctuation events need to be accurately predicted.
- Difficulty in time-series incremental unsupervised learning. Conventional prediction algorithm [12] requires collectively exhaustive set of data to achieve high prediction rate. Incremental learning helps to increase the prediction accuracy of the highly fluctuating PV output power by learning new weather data in real-time. Other than being incremental, the algorithm should also be an unsupervised learning algorithm as it is impractical to label real-time data manually. There is no such prediction algorithm done in the field.

- Reduced capacity of the BESS. Most of the existing power fluctuation mitigation engines [2]–[5] require the BESS to operate all the time including during non-power fluctuation period. In consequence, it reduces the effective capacity of the BESS to mitigate power fluctuation events.

1.3 Research Objectives

The aim of this research is to develop an active learning prediction and mitigation engine to accurately predict power fluctuation events and then mitigate them prior to its occurrence.

To accomplish the above-stated aim, the following are the research objectives:

1. To develop an active learning neural network to accurately predict the power output of the solar PV system based on external weather conditions and generated power from the PV system. The predicted output power will be subsequently used in power fluctuation events detection.
2. To develop a power fluctuation mitigation system which will be able to determine the best control strategies to mitigate power fluctuation events.
3. To test the developed prediction and mitigation system on a PV grid-tied system in a real-time manner

1.4 Significance of Research

Three significant contributions have been made:

- 1) A thorough review is done to investigate the negative impacts of PV grid-tied system to the power networks, and to study on the performance of artificial intelligence (AI) and conventional methods in mitigating power quality event. From the review, AI methods are found to usually outperform conventional methods in terms of response time and controllability. The review shows that the incremental unsupervised learning AI is the future trend in the PV grid-tied systems as it can adapt to the environment without the need for collecting a large amount of data before the AI is implemented.
- 2) An incremental unsupervised neural network algorithm namely TS-SOINN is developed to predict the occurrence of power fluctuation events in a PV grid-tied system. The TS-SOINN is the first time-series unsupervised incremental neural network algorithm. It outperforms the E-SOINN [8], Hidden Markov Based Self-Organizing Incremental Neural Network (HBSOINN) [13], Self-Organizing Incremental Neural Network Dynamic Time Warping (SOINN-DTW) [13], Non-linear Autoregressive Exogenous (NARX) [14] and Self-Organizing Map (SOM) [15] algorithms in predicting output power of the PV system and power fluctuation events.

- 3) The TS-SOINN and a mitigation engine are integrated to form an intelligent PMS to smooth power fluctuation events. It is the first incremental unsupervised learning used in real-time PV output fluctuation prediction [10], [11]. This system outperforms two state-of-the-art system [2], [16] in terms of the number of mitigated power fluctuation events.

1.5 Scope of Research

This research covers and focuses on predicting output power and power fluctuation of a PV system using a neural network, and mitigating power fluctuation events. Other power quality events that may happen in a PV grid-tied system are not within the scope of this research work.

1.6 Thesis Structure

In *Chapter 2*, the background on the PV grid-tied system, and adverse impacts to local distribution system is presented. A comprehensive literature review on performances of AI and conventional methods in mitigating power fluctuation events due to PV grid-tied system is presented. It then describes different types of prediction engine in predicting the output power of the PV system. Use of AI

in the power networks and unsupervised active learning AI are discussed. This chapter justifies the developed system.

Chapter 3 discusses the proposed TS-SOINN algorithm. The method for unsupervised learning AI to conduct prediction is shown. Next, it describes the associate memory and weighted tapped delay line function to the TS-SOINN. Then, the TS-SOINN algorithm is shown in detail.

In *Chapter 4*, the developed intelligent real-time PMS is presented in detail.

Chapter 5 shows the real-time implementation of the proposed algorithm. Firstly, it describes the modelled PV grid-tied system used in this research together with the data acquisition system. Then, it presents the constructed laboratory-scale PV grid-tied system. Lastly, it presents the real-time implementation of the PMS.

Chapter 6 presents the results and discussions. It is separated into two main sections. The first section discusses results obtained in the TS-SOINN evaluation. Optimal values for unknown parameters used in the proposed TS-SOINN and its prediction performance are presented. In the second section, the performance of the developed PMS is shown. Optimal parameter values for the developed PMS is shown. Then, the performance in mitigating power fluctuation events is presented.

Chapter 1 - Introduction

Lastly, *Chapter 7* concludes the research work. Possible future works are also presented.

Chapter 2 Literature Review

This chapter begins by providing a background review on the negative impacts of power fluctuation event and their causes and effects to the PV grid-tied system. The power fluctuation event is found to be able to cause different power quality events such as voltage flicker, frequency fluctuation and voltage sag.

It proceeds to describe the current state-of-the-art mitigation methods on alleviating the power fluctuation event that is caused by the PV grid-tied system. Mitigation methods range from power monitoring, use of an inverter, geographical dispersion and BESS. Advantages and disadvantages of each method are described. It justifies the mitigation method used in this work.

Next, a thorough literature review is presented on methods to predict the intermittent power output of the PV system. Different types of prediction engines are reviewed.

Lastly, a review on the use of AI in the power networks is presented. This includes a thorough review on the E-SOINN, HBSOINN, and SOINN-DTW.

2.1 Power Quality

Generation, transmission, distribution and protection have been integrated into power networks for a safe and reliable system. By integrating renewable energy resources into power networks, it is believed to be able to meet the energy challenges that are unable to be solved by traditional centralised power plants. These resources increase the variety of energy supply market, decrease global emissions and increase long-term sustainable energy supply. However, the integration of renewable energy resources into the power networks has changed the flow of power from unidirectional to bidirectional. Since the power system is not designed to handle bidirectional power flow, false tripping and non-operations of protective devices may occur [17], [18]. This behaviour affects current power networks adversely.

Among the renewable energy resources available today, solar PV is the one in favour by most utility companies. Its inherent characteristics encourage the development of micro-grid PV system. Despite the benefits of PV system, the downside of the PV system is that the output power highly relies on the intermittent solar irradiance and ambient temperature that may cause PV power to fluctuate. Power fluctuation is a phenomenon where the generated power is unstable. It is one of the main issues in a PV system. The effect of power fluctuation becomes more serious when the penetration of the PV system is high

Chapter 2 – Literature Review

(up to gigawatt). It is because the output power of PV farm for example could have a power drop of 63% during a power fluctuation event [19].

Simulations and experiments are carried out to validate the occurrence of power fluctuation event in [20], [21]. From experiments, these events are triggered during noon time (from 1000 to 1300) because of fast-moving cloud in Malaysia [21]. Since the cloud behaves as an obstacle to block the irradiance from the sun, active power generated from the PV system is reduced greatly. Sizing and topology of the PV system are other culprits to power fluctuation event [21]. A low power rating PV system has a relatively smaller area. In consequence, the PV system has a higher chance of being shaded by the cloud. From research finding [22], power fluctuation of a PV system's standard is only available in the technical requirement of Puerto Rico Electric Power Authority (PREPA) for interconnecting wind and solar generation. From PREPA, it only allows 10% fluctuation rate of rated capacity within a minute. This rate is chosen because higher fluctuation rate breaks the supply and demand of electrical power and creates more power quality events such as voltage flicker, frequency fluctuation, and voltage sag.

Voltage flicker is one of the adverse impacts caused by power fluctuation event in a PV grid-tied system. Variation in output power is the cause of the voltage fluctuation. Research papers [23], [24] show that PV systems are mostly invulnerable to voltage flicker events. However, this is not applicable to

Chapter 2 – Literature Review

countries that have high frequency and intensity of moving cloud [25]. In addition to voltage flicker, frequency fluctuation causes by power fluctuation event of the PV system. Funabashi et al. report that the intermittent output power worsens the frequency deviation scenario [26].

Voltage sag is another consequence of the power fluctuation. Voltage sag is a well-known power quality issue among consumers. From research findings [27], [28], voltage sag contributes 80% and 72% of the reported complaints in Malaysia and China, respectively. A PV grid-tied system is believed to be able to improve the voltage profile of distribution systems. However, it is applicable to low penetration of PV system only as observed from [29]. Yamashita et al. [30] show that by increasing penetration of PV system in a high voltage network, PV system exacerbates the voltage sag issue and post-disturbance steady state voltage. It is because a utility operator expects a higher volume of electrical power from the PV system, but the PV system generates a lower volume of electrical power due to power fluctuation event. This shows that the power fluctuation event could cause voltage sag to electrical distribution system.

2.2 Mitigation Engine

This section describes the current state-of-the-art mitigation methods such as power monitoring, inverter, geographical dispersion and BESS to deal with power fluctuation event in the PV grid-tied system.

2.2.1 Power Monitoring

Power monitoring mitigates power fluctuation by identifying the source of power fluctuation events and supply ancillary power to it. Thus, it mainly focuses on data classification. In general, utility companies monitor high voltage distribution network to identify a fault in a short time [31]. An example is a Malaysia energy utility company installs a power quality monitor system in five regions [31]. They are used to detect and record power quality events in order to take corrective action in the shortest possible time. Kilter et al. [32] initiate a guideline for power quality monitoring. However, extensive works are required to complete it. Music et al. [33] integrate Supervisory Control and Data Acquisition (SCADA), Automated Meter Reading (AMR), Power Quality Monitoring System (PQMS), and Electric Vehicle Management System (EVMS) as the Integrated Power Quality Monitoring System (IPQMS) to monitor a smart distribution system. They show that power networks are easier to be controlled and monitored through IPQMS.

Chapter 2 – Literature Review

AI techniques have also been implemented in power system monitoring. Zang and Zhao [34] develop an algorithm to identify types of power quality disturbance by using a support vector machine. This algorithm is developed from wavelet transform and multi-layer support vector machines. Results show that the algorithm locates six types of disturbances [34]. Power quality classification has been carried out by Ding et al. [35] as well. They utilise the least square support vector machine theory to classify power quality events [35]. In addition, Chan et al. [36] prove the validity of AI in micro-grid fault detection classification. Radial basis function, decision tree, K-nearest neighbour, and Naïve Bayes are used to classify seven groups of power quality events. Results show that the Naïve Bayes has the best performance in terms of average classification error, which has an average of 20% of error [36]. Next, Bentley et al. show the validity of an unsupervised neural network, SOM to identify power quality disturbance source in an IEEE 6-bus system [37].

Mallesham et al. [38] introduce an automatic generation control of micro-grid, which is equipped with a diesel generator, fuel cell generator, aqua electrolyser, battery, wind and solar energy. The gains of each source which are confined by Generation Rate Constraint (GRC), are calculated by AI techniques. The GRC is a ramp rate limit of increasing or decreasing a power source to ensure power balance between load and sources. From the results, they show that the frequency of micro-grid without GRC fluctuates within 2 Hz, whereas micro-grid with GRC maintains the frequency. In addition, they show that

Chapter 2 – Literature Review

conventional proportional integral derivative (PID) controller, Genetic Algorithm (GA), Bacterial Foraging Optimisation (BFO), and Particle Swarm Optimisation (PSO) are capable of maintaining frequency due to an increase in wind power generated, increasing and decreasing of the load. Among the methods, BFO has the lowest integral time squared error overall [38]. Llanos et al. [39] implement an online neural network for load prediction in an off-grid system. From the results, the load prediction from the SOM network can track the actual trend. This shows that AI can be used for load prediction. Other than Llanos et al., Loewenstern et al. [40] compare five methods for very short-term load forecasting (five minutes in advanced). The very short-term forecast horizon (five minutes) is used for balancing the supply and demand of electrical power in the grid. From the results, difference averaging with moving average method achieves the lowest mean absolute percentage error in overall [40].

Research findings [31]–[40] show that AI techniques outperform conventional methods in classification of power quality event and identification of the source of the disturbance. However, only one research work [38] shows the use of power monitoring in power fluctuation mitigation.

2.2.2 Inverter

Next, power curtailment wastes excess energy which causes it to be an inefficient mitigation method. It can be seen from the inverter. Since the inverter has no energy storage system (ESS) to store and dispatch the power deficit, it converts the active power of a PV system into other types of power to prevent power fluctuation events. Power system configuration and additional compensator equipment are methods to mitigate power quality events in the power networks [41]. In a PV grid-tied system, the inverter is the core component to vary the output of a PV system. Therefore, the configuration of the inverter is used to mitigate major power quality issues.

Huang et al. [42] find that an inverter which is controlled by Instantaneous Active Reactive Control (IARC) and average active reactive control (AARC) has issues as it is unable to output sinusoidal current and the output power consists 120-Hz ripples, respectively. Therefore, they propose a flexible active and reactive power control to command operation of the inverter [42]. The new algorithm verifies the validity in reducing power fluctuation and current harmonics. However, it is found that the algorithm is unable to be implemented in the PV system. It is because it can only reduce the power fluctuation or current harmonic at a time. Another control scheme based on instantaneous power theory and hysteresis current is found in [43]. Results show that it is effective in regulating the voltage at the point of common coupling

(PCC). Moreover, it can recover the voltage profile due to a fault with a shorter time. Hao and Xu [44] propose a new control algorithm based on the current reference for a PV system to work under unbalanced voltage condition. Outputs of simulation prove that the validity in eliminating power fluctuation with increasing control parameter, k . However, it must sacrifice the balance of the current waveform. Shou et al. [45] suggest current adjustment coefficients control strategy to alleviate output power fluctuation and total harmonic distortion of current under unbalanced voltage environment. Results show that power fluctuation and harmonic distortion can be alleviated by regulating current adjustment coefficient with second control mode.

AI also shows its good performance in commanding equipment like the inverter. Dasgupta et al. [46] apply spatial iterative learning in an inverter controller. They find that conventional methods such as the resonant controller, repetitive controller and proportional controller are ineffective in maintaining the voltage waveform. Experiments and simulations have been conducted to compare spatial iterative learning method with the conventional methods. Results show that the controller can converge load voltage error to zero within 0.65 seconds, perform auto synchronisation while maintaining voltage profile automatically when frequency varies, and generate harmonic to inverter's voltage to counter grid harmonic voltage to ensure unity of load voltage waveform. Al-Saedi et al. propose a PSO algorithm to control the inverter of a distributed generator for switching distributed generator from grid-connected to

Chapter 2 – Literature Review

islanding mode. Simulation results show that the control algorithm enables a micro-grid system to switch from grid-connected mode to islanding mode autonomously [47]. Next, it can maintain its voltage profile within 10% of fluctuation, maintain the supply of active power and frequency profile within 1.2% of fluctuation during the switching stage.

From research findings [41]–[47], advanced conventional methods are built on complex algorithms. For AI controlled based inverter, its structure enables it to be used in different fields which diversify its usage and it could achieve similar performance as in advanced conventional methods. Therefore, the AI techniques outperform advanced conventional methods in terms of controllability and response time [46] [47]. Due to lack of ESS from the inverter, the inverter usually mitigates the power fluctuation events by power curtailment method. In another word, it converts the excess electrical energy into another form of energy such as reactive power. Thus, it is an inefficient method to mitigate the power fluctuation events as it mitigates the event by reducing the output power.

2.2.3 Geographical Dispersion

Smoothing output power can be done by either geographical dispersion or ESS. Geographical dispersion is usually used for a large-scale PV system that installed in a wide area. It smooths the output power of a PV system in a passive method and requires several large areas to disperse a PV system. It separates a large PV farm into several PV farms to reduce the adverse impact of the fast-moving cloud. This is because the chances of having a big cloud to cover up 10 KM² is rare. Thus, this method reduces the chances of a whole PV farm is shaded by the cloud.

Jewell et al. observe that a PV system with a penetration level of 15% can cause a significant effect on the electric utility system [48]. This increases the operating cost of utility companies as it causes different protection problems in the transmission line such as power swing, transmission line overload and reverses power flow. Therefore, Jewell et al. suggest to disperse a large scale PV system over 100,000 KM² to reduce the adverse impact of the transmission line [48]. Marcos et al. agree with geographical dispersion of large PV plant can reduce short-term power fluctuation events [49]. However, it is unable to deal with large amplitude of output power fluctuation. From the results, the combined output power of six PV plants maintains in between 0.5 to 0.7 per unit (P.U). In contrast, the output power of a single PV system ranges from 0.15 to 0.95 P.U within 30 minutes.

Chapter 2 – Literature Review

Other than U.S.A [48] and Spain [49], similar research has been carried out in Japan as well. Murata and Otani [50] find that the unstable output power can be reduced by integrating the output of PV systems that installed over a wide area. In addition, they find that the capacity of conductor cable in between PV systems and grid affects the smoothing capability. In [51], Lave et al. show that power fluctuation can be reduced by separating a PV system into six different locations. From [52], Hoff and Perez develop a model to calculate the output variability of PV systems. They find that the frequency and amplitude of short-term power fluctuation for a single PV site are larger than the 16 PV sites. Although integrating a group of PV systems reduces the power fluctuation level, this method fails during fast-moving cloud scenario as shown in [52].

In [53], Hoff and Perez show that geographical dispersion reduces the power fluctuation events and the adverse impacts of geographical dispersion method are voltage issues, and tripping of power distribution line. Rowlands et al. [54] investigate 16 PV systems in Ontario, Canada for 3 years on an hourly basis. From their finding, geographical dispersion leads to lower power variability and higher energy production. In [55], Junior et al. propose to combine regional forecast technique and principal component analysis to forecast and smooth output power of the PV system. However, this method is unable to forecast production of individual PV system.

Chapter 2 – Literature Review

Although smoothing output power of the PV system is achievable by geographical dispersion method, Wiemken et al. find that this method has weaknesses [56]. They analyse 100 distributed PV systems in Germany and find that the power fluctuation events of the combined PV systems are suppressed significantly. However, the maximum power production of the 100 PV systems is unable to reach the rated power of the PV systems. In addition, they find geographical dispersion is unable to smooth short-term power fluctuation effectively. Moreover, power fluctuation events increase with decreasing number of PV system in the local distribution system [56].

From the above findings [48]–[56], it can be concluded that smoothing of PV system is achievable by dispersing a large scale PV system into several small PV farms with sufficient distance and capacity of cables in between them. However, it is found that this method has its weaknesses. Firstly, it requires several vast areas to divide a large-scale PV system into several smaller-scale PV systems. Secondly, it is unable to smooth power fluctuation events due to the fast-moving cloud which is the principal cause of power fluctuation in the PV grid-tied system. Thirdly, the smoothing effect reduces with decreasing number of integrated PV systems. In addition, the maximum power generation from the PV systems is less than the rated power of the total PV systems.

2.2.4 BESS

Inherent characteristics of BESS as a medium to store and release electrical power provide an opportunity for micro-grid PV system to compensate intermittent behaviour due to environmental factors. Among the ESS, battery is cost-effective in storing large amount of energy. Since production of renewable energy resources is well-known for intermittency problem, these inherent characteristics of battery enable an active method to smooth output power of the renewable energy resources as it is able to dispatch energy while there is a short of production from renewable energy resources and vice versa. For PV systems, generation could drop up to 63% within a minute. This creates significant adverse impacts on the grid, and this scenario can be mitigated by the BESS.

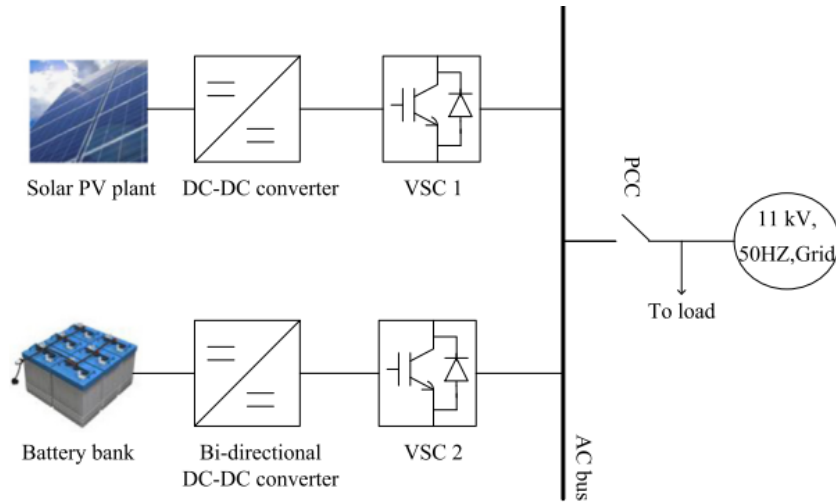


Figure 1: Topology of PV Grid-Tied System with BESS [1]

Chapter 2 – Literature Review

Figure 1 shows a BESS is integrated into a PV grid-tied system at the PCC which can mitigate the power fluctuation events due to intermittent weather condition. According to Shivashankar et al. [1], smoothing output power of solar PV by ESS is the most efficient method. Although it increases the overall operating and maintenance (O&M) cost, it is applicable to all types of output power range. In [57], it shows that the length of an operational period has a strong relationship with BESS, which shorter time-window requires lower rated BESS. However, a longer operational period has a better performance in smoothing output power [51]. In addition to that, frequency of power fluctuation events decreases with increasing step size of the moving average method. However, the drawback of the moving average method is that it requires a large battery capacity to reserve vast amount of electrical energy in order to supply the power deficit to the grid.

Abdelkarim et al. [58] find that reactive power can enhance voltage profile with BESS. However, it fails in fast cloud transient phenomenon. They suggest the use of plug-in hybrid electric vehicles as a solution for power fluctuation events. Results indicate that this method increases the reliability of the voltage profile [58]. Noro et al. [20] find that the BESS can reduce fluctuation and maintain high efficiency of the PV system. Hossain and Ali [59] discover spatially diverge PV plant equipped with small energy storage is able to have the same performance as in a centralised PV plant. Besides, it is more cost efficient. To further enhance the reliability of BESS to micro-grid, control

Chapter 2 – Literature Review

theory has been implemented to configure BESS. Liu et al. [60] introduce a coordinated control to mitigate voltage swell event due to the high penetration of PV system. Both experimental and simulation results show that it can increase the life cycle of the BESS, and decrease switching operation times, stress and losses to the BESS. Most importantly, peak load shaving function is achievable through this technique [60]. Parra et al. [16] implement a BESS with ramp rate limiter to mitigate the power fluctuation event. This approach requires the BESS to standby all the time for any power fluctuation event.

AI is also found to be able to generate power reference for the BESS as well. From research findings [2]–[5] smoothing output power by ESS is usually done by a prediction engine to predict solar irradiance or output power of the PV system. ESS such as the battery is used to supply or absorb power deficit (which is the difference of predicted output power and desired output power) to smooth the power fluctuation.

Teleke et al. [2] introduce a rule-based controller for smoothing power fluctuations. It is a PMS where they assume a prediction engine is available to predict output power hourly and set desired output power to smooth power fluctuation. They develop rules to constraint state-of-charge (SOC) and output power deviation. The battery is dispatched hourly to smooth output power and the results are verified in a one bus PV system. Similar to the research finding in [2], Daud, Mohamed, and Hannan [3] assume a prediction engine is available

Chapter 2 – Literature Review

to forecast the output power of the PV system. It is found that, when the prediction engine has a higher mean absolute error (MAE), this methodology suffers from higher frequency of power fluctuation events and decreases in battery lifespan as the SOC of the battery varies within 19.8% to 100% [3].

Other than hourly dispatched PMS, Li et al. use a day ahead dispatching smooth model to maximise the profit and smooth power fluctuation for a PV, wind, and battery connected grid system [4]. Instead of supplying 100% of generated power to the local distribution system, Li et al. [4] store part of the energy in the BESS to produce for smoothing purpose. Although this approach has a smooth power generation graph, the renewable energy experiences power curtailment while the BESS is fully charged to smooth power fluctuation event. It also requires a larger size of BESS which is 35.71% of the total rated of wind and solar PV generation as compared with the research finding in [2] and [3], which are 25% and 24.5%, respectively. Moreover, this research paper [4] assumes an accurate and reliable prediction engine available to predict a day ahead output power of renewable energy. Instead of solely relying on the predicted output power, Sam, Rahim and Mokhlis [5] apply the moving average method to the predicted output power. The processed output power is used as the desired output power for the PMS. Although this approach smooths power fluctuation events, the capability of this method to deal with real-life data is not shown as the prediction engine is assumed to be available.

Chapter 2 – Literature Review

From research findings [2]–[5], [20], [58]–[60], AI outperforms conventional method in terms of predicting upcoming usage pattern. It is found that a control system that is equipped with a prediction engine can increase the financial benefit of the system. Despite the popularity of AI method in BESS control, the performance of this kind of control system highly relies on the accuracy of the AI prediction engine. Most of the recent research works [2]–[5] assume the availability of an accurate and reliable power output prediction engine and this assumption is not practical for the actual implementation of the system. In [3], Daud, Mohammed and Hannan show that the unmitigated power fluctuation events are increased by 4.7% with an increment of 10% in MAE. This shows the existing methods [2]–[5] are unreliable as their systems do not have a prediction engine.

Figure 2 shows the impact of data resolution to the power fluctuation events. From the figure, it shows high-resolution data reveals the actual performance of the output power and low-resolution data smoothens the output power. As a result, power fluctuation events could be hidden within low-resolution data. This is proved in Figure 2 where resolution tens of minutes to hours and day have a relatively smooth graph, whereas resolution in seconds to minutes fluctuates largely. This explains the reason for high reduction rate of the power fluctuation events in [2]–[5]. This scenario is not realistic as real-life environmental variables are changing from time to time. To achieve a PMS that is able to deal with this real-life problem, the PMS is required to operate at a

very high resolution such as a minute to deal with the unpredicted changes to the environment.

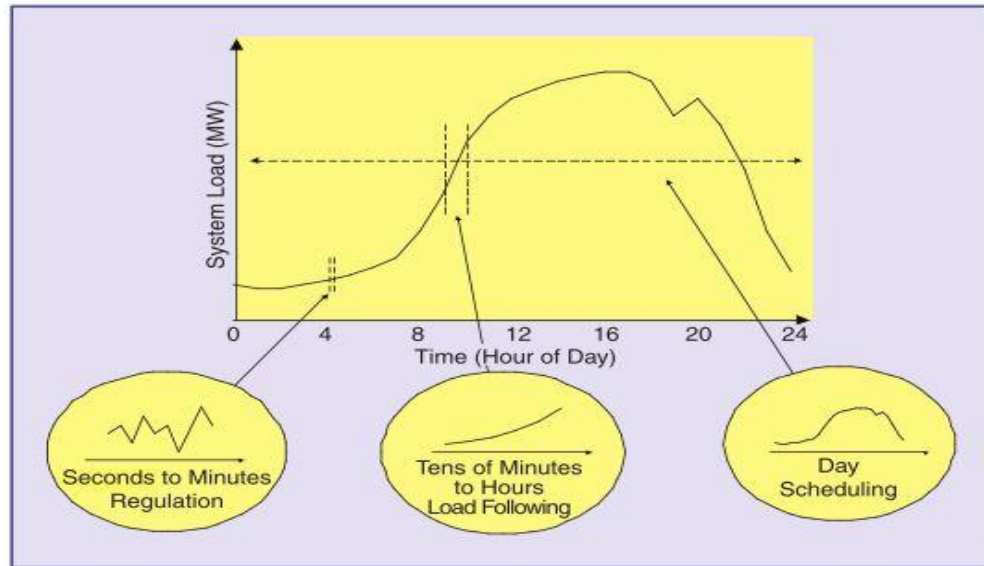


Figure 2: Impact of Data Resolution to the Power Fluctuation Event. The System Power in Seconds to Minutes Resolution Fluctuates Largely [61]

Other than the absence of a prediction engine and low-resolution in identifying power fluctuation events, batteries are usually dispatched every hour or power fluctuation level is scheduled at an hourly basis. This might be sufficient for wind energy however, it is not practical for solar PV where clouds move rapidly. This is supported by Mills et al. [61], where their research shows that a moving cloud takes several minutes to shade a 100 MW PV system. To respond to these downfalls, a real-time prediction engine capable in high-frequency prediction (within a minute) has to be integrated into the mitigation engine to deal with the highly intermittent behaviour of weather condition that causes power fluctuation events.

2.3 Prediction Engine

This section first explains the needs of the prediction engine in a PV grid-tied system. It then describes the suitable temporal aspect for the prediction engine. Lastly, the current state-of-the-art of PV system's prediction engine is reviewed.

According to Shivashankar et al. [1], coupling an ESS into the micro-grid PV system is the most optimum method to mitigate power fluctuation events. However, the period and amount of energy to be dispatched into the micro-grid is unknown to the BESS. Inadequate or excessive power supply could further deteriorate the power system. Besides, inappropriate PMS shortens the battery lifespan which increases the implementation cost of the PV grid-tied system. These issues can be solved by integrating a prediction engine to an ESS. The prediction engine predicts the abnormal condition of the PV system, and switches on the ESS when there is an abnormal condition. However, Barbieri et al. [62] claim that there is only a few literature [63]–[65] on very short-term (within 30 minutes) output power prediction.

It is important to determine the temporal aspect of a prediction engine as this aspect introduces a vital parameter which is the forecast horizon. It defines a time range of prediction. Each forecast horizon has its own function. Firstly, the very short-term horizon or nowcasting ranges from several seconds to 30 minutes. It is used for immediate action or real-time control of PV system [66]–

[68]. In the research findings [66], [67], they find that research in this time frame is rare. Secondly, the short-term horizon which is from 30 minutes to 6 hours ahead is used for economic dispatch. Most of the research works are done in this forecast horizon [66]–[68]. The medium-term horizon which is ranged from 6 hours to 1 day is for the operational security purpose, and the long-term horizon which is more than a day is used for maintenance scheduling to optimise the operating cost.

Since power fluctuation events could occur within a minute due to the fast-moving cloud, the sampling time for the prediction engine should be within a minute. This is because sampling time that is greater than a minute could miss some power fluctuation events. From [66]–[69], they show that the shortest time horizon is important for automatic real-time control to protect power grids as the prediction in this horizon allows immediate action to be carried out. It is also important for the prediction engine to detect power fluctuation events under all types of different environmental scenarios. To achieve this, a very short-term (30 seconds) active learning prediction engine is developed in this research work to learn the most updated data and give accurate prediction within a second.

2.3.1 Types of Prediction Engine

The main cause of power fluctuation in the very short-term horizon is the presence of clouds [10], [62]. Therefore, prediction engine mainly focuses on forecasting of cloud movement using Global Horizontal Irradiance (GHI),

Chapter 2 – Literature Review

Direct Normal Irradiance (DNI), weather condition, and output power of the PV system. From the research findings [76-102], output power of a PV system or solar irradiance prediction engine can be done by satellite imaging, Numerical Weather Prediction (NWP), Total Sky Image (TSI) and AI methods.

Meteorological satellite is a type of national scale weather monitoring satellite. It offers a wide spatial range which can go up to several thousands of kilometres. From Dambreville et al. [70], this approach is accurate to forecast the GHI for the horizons shorter than 6 hours. In particular, Dambreville et al. find satellite imaging outperforms the NWP method to forecast GHI in the horizon of 5 hours ahead [70].

Although the satellite images method has a good performance in the horizon of 30 minutes to 6 hours, Lonij et al. [63] find that it is not suitable to observe in high frequency or fast cloud motion. In consequence, it is unable to determine the velocity of clouds. In addition, cloud-radiation studies are not allowed from the satellites images because the images are in low-resolution [62]. Moreover, since the spatial resolution is high, persistence models usually outperform the satellite-based forecast in short forecast horizon [71].

NWP is another type of global scale ground weather monitoring network. NWP was found by Vilhelm Bjerknes in 1904 [72]. It discretises a domain into small resolution and applies physical laws of motion and thermodynamics law

Chapter 2 – Literature Review

on the discrete spatial grid. An analysis of different spatial and horizons is done by Lorenz et al. [73]. The NWP model is found to perform well in forecasting weather condition with a large spatial and temporal resolution [73]. These results are agreed by Bacher et al. [74] where the NWP performs better in longer forecast horizon and larger spatial area.

From the research findings, [75]–[78] use NWP to predict for 1-36 hours forecast horizon. These characteristics enable the NWP to predict well in the day-ahead horizon, which makes it suitable for determining energy pricing purposes. However, this method is found to be accurate to the scenario with large-scale cirrus clouds and fail in scenario with small clouds in a cloudy day [62]. Thus, this drawback causes it unsuitable to forecast for low forecast horizon. In addition, substantial computation power is required by the NWP method. The NWP method requires two hours of computation time to forecast for two minutes in [63].

TSI is an alternative to provide higher frequency prediction compared to the NWP and satellite imaging technique. From research findings [79]–[82], TSI forecasts for time horizon from 5 minutes to 30 minutes. The TSI works by mounting a fisheye lens on a whole sky camera to observe the entire sky cloud condition. The types of cloud and movement of clouds data are collected to make the prediction of GHI or output power accordingly. Chow et al. use TSI technique to predict the GHI for intra-hour forecast [83]. Ferreira et al. [84]

Chapter 2 – Literature Review

make use of TSI data as input to the Artificial Neural Network (ANN) model to forecast cloudiness, GHI, and temperature for forecast horizon ranges from 5 minutes to 4 hours. Coimbra and Marquez use TSI data for intra-hour DNI forecast [85]. It is found that TSI images achieve the highest forecast accuracies on time horizons of 5 minutes.

Compared to the NWP and satellite imaging technique, the TSI uses the local meteorological information to forecast for intra-hour irradiance. The local meteorological information restricts the TSI image to have the maximum time horizon of 30 minutes [86]. It is because the fisheye lens has a limited field of view. Other than this, this technique has a lower boundary of time horizon. A complex mask is required to remove shadow bands that are caused by the circumsolar glare. This difficulty causes the TSI to be unable to forecast for the time horizon shorter than 3 minutes [83], [85]. Therefore, the TSI technique only has an effective forecast horizon from 3 minutes to 30 minutes.

AI is another alternative that can forecast in the short time horizon. Input data to the AI can be images, temperature, irradiance, and output power of a PV system. There are various types of AI model for prediction engine. AI technique also has the flexibility in forecast horizon.

In [87], Azedah et al. use supervised learning AI which is Multi-Layer Perceptron (MLP) to predict solar radiation with no solar measurement devices

Chapter 2 – Literature Review

for the time horizon of a month. MLP model is also used by Mellit and Pavin in [88] to predict irradiance for the time horizon of 24 hours. It uses daily mean irradiance and temperature to predict the next 24 hours irradiance. Previous output power, humidity and temperature are used by Chen et al. to forecast the next 24 hours GHI in [89] for the purpose of operational planning in power networks. Lonij et al. use data from sensor networks in [64], [65] to forecast the time horizon of 30 seconds to 6 hours. The most optimum results are obtained from the forecast horizon of 15 minutes. Compared to sky image, NWP and satellite imaging, Lonij et al. find that this method directly measures the irradiance and it does not need to convert irradiance level from optical properties of clouds or used of radiative models [63]. In [90], Chow et al. use the MLP model to forecast output power of the PV system with irradiance, temperature, solar elevation and solar azimuth angles. However, performance metrics show in the paper is limited.

Apart from supervised feedforward network, the autoregressive (AR) network model is used in forecasting the irradiance and output power of the PV system. The NARX, Autoregressive Moving Average (ARMA), Autoregressive Moving Integrated Average (ARIMA), and Autoregressive Moving Average Exogenous (ARMAX) are examples of AR networks. In [91], the ARIMA model is used by Craggs et al. to forecast irradiance in time horizons of 10 minutes to 1 hour. In [92], Combra and Kleissl show that the NARX model outperforms the persistence model for time horizons of 10 hours to 200 hours.

Chapter 2 – Literature Review

It is proven that the AR model that takes in exogenous data can improve prediction accuracy [10].

Other than the supervised ANN and AR network, unsupervised learning ANN is another type of ANN. Unsupervised learning ANN is a type of ANN which learns without target data. It is shown in [86] that the unsupervised learning ANN is accurate in pattern classification. However, there is no research paper done on using it to predict the irradiance or output power of the PV system.

From the above findings [76-102], it is found that the performance of existing prediction engines can be maintained if the environmental conditions remain which is not realistic in real-life. These exiting prediction engines are confined by their limited training data and unable to update themselves accordingly. In addition, these types of learning methods are sensitive to the training data. When the input in an unseen data type, these prediction engines are unable to predict accurately.

Among the four techniques discussed (satellite imaging, NWP, TSI, and AI), each of them has its unique advantages and disadvantages. Satellite imaging has a national scale (1km – 10km) distribution of cloud image. This enables it to forecast effectively for the horizon up to 6 hours. NWP discretise a large domain into small resolution and the physical laws of motion and thermodynamics law on the discrete spatial grid to model the local weather

Chapter 2 – Literature Review

scenario. This allows the NWP to forecast for a wider region (5km – 20km) and longer time horizon (4 hours – 36 hours) as it models a larger map. However, this is not suitable for short time horizon as the instantaneous cloud movement is unable to be predicted by it. Compared to the previous two techniques, TSI has a smaller scale (1m – 2km) image. In consequence, it is able to predict for short time horizon (3 minutes – 30 minutes). The AI equipped with sensor network is found to be the most flexible method where it predicts from the very short-time horizon (real-time) to very long-time horizon (a month). Coverage of sensor network is the limitation of the AI technique. Although it can be solved by installing a sensor network to a wider area, the cost of a sensor and the installation cost are high. Table 1 shows the summary of the prediction engine. From Table 1, AI technique is the only method that is able to forecast within a minute. Therefore, AI method is chosen as the prediction engine in this project.

Table 1: Summary of Prediction Engine

Techniques	Forecast Horizon	Spatial Resolution
Satellite Image	30 minutes – 6 hours	1 KM – 10 KM
NWP	4 hours – 36 hours	5 KM – 20 KM
TSI	3 minutes – 30 minutes	1 m – 2 KM
AI	1 second – 1 month	1 m – 2 KM

2.4 Use of AI in Power Networks

AI algorithms are used in prediction and mitigation of power quality events in Xu et al. [6], and Kanirajan and Kumar [93]. Xu et al. [6] use a supervised neural network to predict short-term voltage stability and achieve high prediction rate. Kanirajan and Kumar [93] use AI to conduct classification of power quality events. Their proposed supervised AI method achieves high accuracy in the classification of power quality events. However, these methods [6], [93] are passive. It can only solve the power quality problems after the occurrence. This type of passive method could still cause damage to the power networks.

Quan et al. [94] use PSO to optimise supervised neural network's parameters to predict short-term load and wind power. Bai et al. [95] use supervised AI to predict next-day power quality events for a wind farm. It uses trend analysis approach and decision support method to perform power quality prediction. Although supervised learning usually achieves high performance in short-term or application with stationary data, its data labelling cost is expensive and time-consuming [96]. Furthermore, the accuracy of supervised AI in a non-stationary data application could drop drastically due to the incomplete dataset used during the training stage. This weakness can be solved by providing complete data to train the AI. Nevertheless, labelled data are usually inadequate [96].

Unsupervised learning AI is introduced to solve data labelling issue where it is able to cluster data without prior knowledge [97]. It is trained by observing the input data [98]. Due to the absence of the desired output, the weight of the nodes is altered according to the cluster of the node. Despite the advantages of unsupervised learning, Tscherepanow et al. [99] find that off-line learning approach is insufficient to achieve high performance because the behaviour of non-stationary data such as the weather data in PV system is inconsistent and they are not collectively exhaustive [99]. To overcome these issues, incremental online learning or active learning is used. Active learning is a type of learning method where it learns in a real-time manner. Although the active learning method seems to be a perfect learning methodology, it could

neglect to learn useful data [100]. This is due to the stability-plasticity dilemma where AI is unable to differentiate which type of data should be learned or forgotten [101].

2.4.1 Incremental Unsupervised Learning Algorithm

In machine learning, data clustering is usually used for unsupervised learning. Kohonen [15] develop the SOM, which maps input data into a topological structure. It is also well-known for decreasing high dimensional data to low dimensional data. From several findings [97], [102], constraints of the SOM are its predefined structure and size. These limitations yield a poor result for the SOM in the incremental learning task. To overcome the constraints, Growing Neural Gas (GNG) [103] which is based on Competitive Hebbian Learning (CHL) [104] and neural gas [105], is proposed by Fritzke. However, this algorithm suffers from noise and stability-plasticity dilemma. Incremental Growing Neural Gas (IGNG) was introduced by Prudent and Ennaji [102] to solve the stability-plasticity dilemma. It is a situation to learn significant data and yet remain stable to previously learnt input. From the results, IGNG outperforms GNG in terms of the number of iteration cycle and accuracy. However, Hebboul, Hacini, and Hachouf [97] claim that IGNG is unsuitable to be applied in a noisy environment as IGNG is unable to separate small overlapped clusters and perform noise elimination.

Shen and Hasegawa [106] introduce the Self-Organizing Incremental Neural Network (SOINN) to solve the noise issue. It adopts GNG to build the network. In addition, SOINN is a two-layered structure which makes it different to other clustering networks. The neuron's learning rate decays as the number of neuron activation increases. As a result, a stable network is achieved. The weaknesses of the SOINN are the algorithm requires eight parameters to be determined *a priori* and its two-layer structure is unable to perform online learning efficiently [8],[97]. In addition, Hebboul, Hacini, and Hachouf [97] claim that the SOINN has a tendency to delete useful information. Shen and Hasegawa [8] improve SOINN to the E-SOINN. Unlike SOINN, the E-SOINN has a one-layer structure only which smoothens the online learning task. In addition, it reduces *a priori* parameters from eight to four and a denoising function is added to the E-SOINN. Table 2 summarises the advantages and disadvantages of existing clustering techniques. From the table, it is found that the E-SOINN is the most outstanding algorithm among the listed unsupervised learning algorithms because it can carry out incremental learning with the least parameters that are required to be determined *a priori*.

Table 2: Advantages and Disadvantages of Existing Clustering Techniques

Ref.	Algorithm	Advantage	Disadvantage
[15]	Self-Organizing Map	1. Decreasing multidimensional into two dimensional 2. Map input data into topological structure	1. Pre-defined structure and size
[103]	Growing Neural Gas	1. It does not require a pre-defined structure and size	1. Suffer from noise 2. Permanently increasing from number of node
[102]	Incremental Growing Neural Gas	1. It is able to perform incremental task	1. Adaptive threshold 2. Unable to separate cluster in low density overlapping 3. Suffer from noise
[106]	Self-Organizing Incremental Neural Network	1. It is able to perform incremental task 2. Noise elimination is included	1. Eight parameters have to be determined <i>a priori</i> 2. Unable to perform online learning efficiently 3. Have the tendency to delete useful information
[8]	Enhanced Self-Organizing Incremental Neural Network	1. Smoothen online learning task	1. Five parameters (as in the E-SOINN with associate memory function) are required to be determined <i>a priori</i> 2. Sequence of data affects the results 3. Not usable for time-series data

2.4.2 E-SOINN

The E-SOINN is found to be useful in processing online non-stationary task while clustering sufficient number of classes. Similar to the SOM, it preserves the topological structure of input data. One of the major differences between the SOM and the E-SOINN is the E-SOINN is introduced for online/active learning.

The E-SOINN technique is built on GNG and CHL method. It initialises node set A to contain two nodes with weight vectors as the first two input. It then initialises connection set C to establish linkage edge for the first two input. The new input data \mathcal{E} is inputted to the E-SOINN, where the input data \mathcal{E} is a subset of real coordinate space of n dimensions R^n .

It searches for the nearest node a_1 and the second nearest node a_2 by Equation (1) and Equation (2), respectively, where W_A is the weight vectors of node set A . If the Euclidean distance between new input data \mathcal{E} and the nearest node a_1 or second nearest node a_2 is greater than similarity threshold T_{a1} (when the winner node has neighbour node) or T_{a2} (when the winner node has no neighbour node), a new node is created for the input signal. This new node is added to the node set A and a new input is fed into the E-SOINN. Threshold T is calculated by using Equation (3) when the node has neighbour node or Equation (4) when the node has no neighbour node.

$$a_1 = \arg \min_{a \in A} \|\mathcal{E} - W_A\| \quad (1)$$

$$a_2 = \arg \min_{a \in A \setminus \{a_1\}} \|\mathcal{E} - W_A\| \quad (2)$$

$$T_{a1} = \max_{j \in A} \|W_i - W_j\| \quad (3)$$

$$T_{a2} = \min_{j \in A} \|W_i - W_j\| \quad (4)$$

If the minimum Euclidean distance between input data \mathcal{E} and the nearest node a_1 or second nearest node a_2 is smaller than any similarity threshold, the new input data merges into the winner node and age of edges that linked with the winner node increments by 1. Next, it uses three rules to determine the connection between nodes which are as follow: 1) connect the two nodes with an edge if the winner or second winner is a new node. 2) Connect the two nodes with an edge if the winner and second winner belong to the same subclass. 3) If the winner and second winner belong to difference subclass and Equation (5) or Equation (6) is satisfied, connect the two nodes, and combine subclasses Z and Y , where h is density of node, α is a parameter that belongs to $[0,1]$ which can be calculated by using the threshold function as in Equation (9) and Z_{max} and Y_{max} are the nodes that have a local maximum density within subclass Z and subclass Y , respectively. Otherwise, do not connect the two nodes, and remove the connection if a connection exists. If there is an edge between nearest node a_1 and second nearest node a_2 , refreshes the age of edge to 0. The density of the

Chapter 2 – Literature Review

node h is updated by Equation (7), where N is total number of input signal, λ is number of input signal during one learning period and \bar{d}_i is mean distance of node i from its neighbour nodes j which can be obtained by Equation (8). The activation number of winner node M_{a1} is incremented by 1 as in Equation (10). The weight vectors of the winner node W_{a1} and its direct topological neighbours W_i are updated according to Equation (11) and Equation (12), respectively. For the edges with age which is greater than age_{\max} , that particular edge is removed.

$$\min(h_{\text{winner}}, h_{\text{second winner}}) > \alpha_z Z_{\max} \quad (5)$$

$$\min(h_{\text{winner}}, h_{\text{second winner}}) > \alpha_z Z_{\max} \quad (6)$$

$$h_i = \frac{1}{N} \sum_{j=1}^N \left(\sum_{k=1}^{\lambda} \frac{1}{(1+\bar{d}_i)^2} \right), \quad (7)$$

$$\bar{d}_i = \frac{1}{m} \sum_{j=1}^m \|W_i - W_j\| \quad (8)$$

$$\alpha_z \begin{cases} 0.0 & \text{if } 2.0 \text{ mean}_z \geq Z_{\max} \\ 0.5 & \text{if } 3.0 \text{ mean}_z \geq Z_{\max} > 2.0 \text{ mean}_z \\ 1.0 & \text{if } Z_{\max} > 3.0 \text{ mean}_z \end{cases} \quad (9)$$

$$M_{a1}(t+1) = M_{a1}(t) + 1 \quad (10)$$

$$W_{a1} = \frac{1}{t} (M_{a1})(\mathcal{E} - W_{a1}) \quad (11)$$

$$W_i = \frac{1}{100t} (M_i)(\mathcal{E} - W_i) \quad (12)$$

Chapter 2 – Literature Review

When the number of input data is an integer multiple of parameter calls lamda, the E-SOINN begins to denoise. It updates the subclass label of every node. Next, it deletes nodes resulting from noise as follows: 1) For all nodes in node set A , if node a has two neighbours and Equation (13) is met, where c_1 is the first denoising factor and N_A is the total number of nodes in the node set A , then remove the node a . 2) For all nodes in node set A , if node a has a neighbour and Equation (14) is met, where c_2 is the second denoising factor, then remove node a . 3) For all nodes in node set A , if node a has no neighbour, then remove node a . New input data is inputted to the E-SOINN after the denoising step.

$$h_a < c_1 \sum_{j=1}^{N_A} \frac{h_j}{N_A} \quad (13)$$

$$h_a < c_2 \sum_{j=1}^{N_A} \frac{h_j}{N_A} \quad (14)$$

Although the E-SOINN has denoising factor, it is found that the E-SOINN has data overlapping issue which is caused by the adaptive similarity threshold. Data overlapping issue is a scenario where different characteristics data fall into the same node. The similarity threshold is a parameter to decide the insertion of a new node. If the first two nodes to the E-SOINN have a large difference with each other, the adaptive similarity threshold assigns a large similarity threshold value to both nodes. Thus, upcoming nodes that have different characteristic might be categorised wrongly as they fall into a large radius of the first and second node. This can be visualised as in Figure 3.

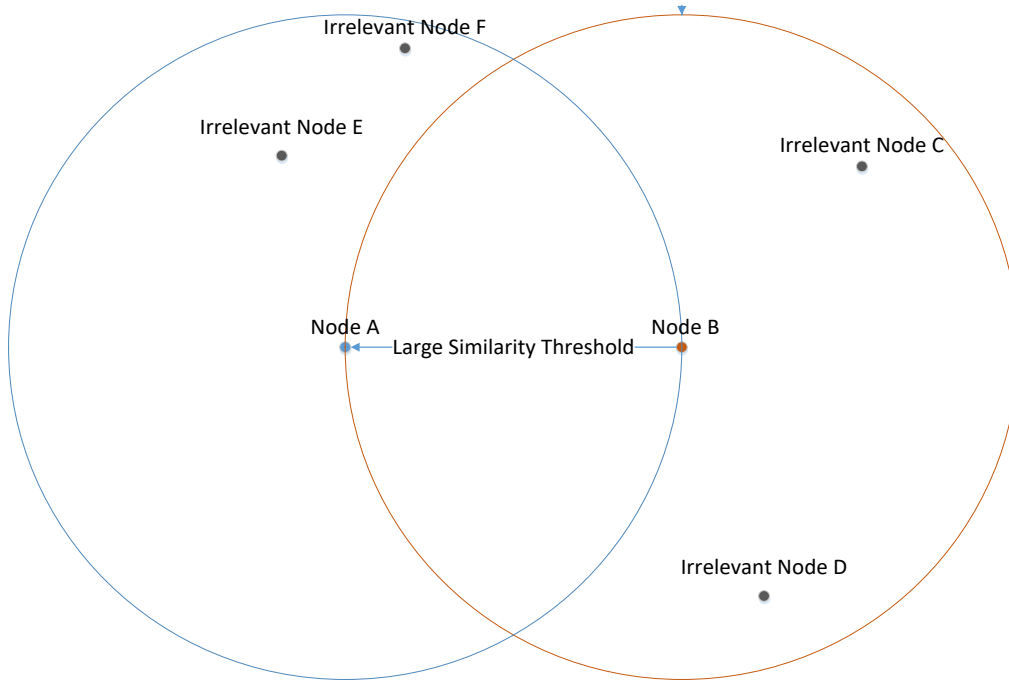


Figure 3: Illustration of Large Similarity Threshold Problem in E-SOINN

Node A and Node B are the first two nodes in the E-SOINN network. Even though the upcoming nodes C, D, E and F have different characteristics with node A and node B (because they are far away from node A and B), these nodes are unable to form their own clusters as they have smaller similarity threshold values compared with node A and node B. Although the E-SOINN is able to reform a new node due to this type of error, it takes time for this type of error to be identified which is unsuitable to be used in an online time-series prediction engine. Moreover, the adaptive similarity threshold is found to be unsuitable to be used as an online time-series prediction engine due to data overlapping. In addition, this algorithm is capable to deal with independent and identically distributed (IID) data only. Therefore, it is not suitable for the field

Chapter 2 – Literature Review

of application in this research work because the prediction engine has to deal with time-series data. In consequence, a novel unsupervised time-series active learning AI prediction engine is developed in this research work.

2.4.3 SOINN-DTW

Since the SOINN and E-SOINN are unable to perform time-series task, Okada, Hasegawa and Nishida [13] propose two time-series SOINN which are Self Organising Incremental Neural Network Dynamic Time Warping (SOINN-DTW) and Hidden Markov Based Self Organising Incremental Neural Network (HBSOINN) to achieve time-series learning. In [13], SOINN-DTW is used for phoneme classification and HBSOINN is used for gestures classification.

In SOINN-DTW, number of classes in the training data needs to be determined and data needs to be labelled prior to the training. A standard data P^* of the template model is selected among training data that belong to each class. The P^* is calculated by Equation (15).

$$P^* = \arg \min_{P_m} \{ \sum_{n=1}^N D(P_m, P_n) \} \{ (P_n, P_m) \in C \} \quad (15)$$

where P_m, P_n denote training data that belong to class C , $D(P_m, P_n)$ is the global distance that is calculated by DTW. Data that has the shortest distance with other training data from the same class is selected as P^* . Then, each P^* and respective training data undergo DTW to determine the optimal warping path. The training

Chapter 2 – Literature Review

data that have the optimal warping path with the P^* is input into the SOINN. The topological structure of the training data is then learned by the SOINN. SOINN-DTW performs time-series learning by pre-processing the training data prior to SOINN. The drawback of this algorithm is that DTW requires data to be labelled and hence SOINN-DTW is not a fully unsupervised incremental learning algorithm.

2.4.4 HBSOINN

In HBSOINN, Hidden Markov Model (HMM) is used to reduce the number of dimensions of the time-series data to map the variable length sequences to vectors of a fixed dimension [13]. The HBSOINN uses the output probability element B within the HMM to feed into the SOINN algorithm to achieve dimension reduction. Firstly, the training data is labelled. Then, each class of training data is trained by the HMM to obtain the HMM parameters which consist of initial probability π , transition probability A , and the Gaussian component B . The B has a mean μ and a covariance σ^2 . To prevent the curse of dimensionality, only the mean vector μ is used as input to the SOINN.

Other than dimension reduction, HBSOINN includes a random sampling function to the SOINN. When the Euclidean distance between input data and winner node is greater than the similarity threshold, a random sample is generated from the HMM. This is because existing nodes are different from

Chapter 2 – Literature Review

input data. Input data has a high possibility to be an unknown pattern. Thus, HMM generates a vector that is similar to the input data for learning purpose.

Similar to SOINN-DTW, HBSOINN achieves time-series learning with SOINN by pre-processing training data using HMM algorithm. HBSOINN also requires data labelling prior to the learning stage and this makes it not a fully unsupervised incremental learning algorithm.

2.5 Summary

To conclude, the highly intermittent output power of PV system creates power fluctuation events. This event could introduce several types of power quality events to the power networks such as voltage flicker, frequency fluctuation, and voltage sag. This phenomenon limits the penetration of the PV system to the power networks as the reliability of the PV system is low.

Next, this chapter reviews the current state-of-the-art mitigation methods on alleviating the power fluctuation event that is caused by PV grid-tied system. The BESS is found to be the most appropriate method to mitigate power fluctuation event as it can mitigate power fluctuation event actively. However, existing mitigation methods [2]–[5] assume the availability of an accurate and reliable prediction engine is coupled with the BESS, which is unrealistic.

Thirdly, the current state-of-the-art of PV system prediction engine is reviewed. Among the four different types of prediction engine, AI technology is the most suitable technique to be used in this research work due to its ultra-short forecast horizon, as power fluctuation event is calculated in one-minute basis.

Lastly, this chapter discusses on the use of AI in power networks. Since weather data is inconsistent and not collectively exhaustive, active unsupervised learning AI is selected for this research work. This is because active unsupervised learning AI learns without target data and in a real-time manner.

Chapter 2 – Literature Review

Among the unsupervised learning AI, the E-SOINN can smoothen online learning task. In addition, DTW and HMM techniques are integrated into the E-SOINN to enable the E-SOINN to achieve time-series learning. However, both DTW and HMM techniques are supervised learning AI algorithms.

Chapter 3 Time-Series Self-Organizing Incremental Neural Network (TS-SOINN)

This chapter describes in detail about the developed TS-SOINN algorithm. This algorithm is the first time-series fully unsupervised SOINN algorithm. This is achieved by modifying the conventional E-SOINN algorithm with a novel memory layer and a weighted tapped delay line. It does not need any supervised pre-processing prior to the incremental learning as in SOINN-DTW [13] and HBSOINN [13]. The TS-SOINN is also designed to solve the adaptive threshold problem in the conventional E-SOINN by using a fixed threshold. Unlike other incremental SOM models such as E-SOINN [8], IGNG [102], GNG [103], and SOINN [106], the TS-SOINN algorithm uses competitive learning as in the SOM network to identify the best matching unite to update the network in a continuous manner. Therefore, it omits the step of creating an edge in between nodes.

An associate memory function is developed in the TS-SOINN to enable time-series prediction. It is done by combining multiple dimensions data a_t and previous data points, n into an input array X_i as in Equation (16).

$$X_i = [a_t | a_{t-1} | \dots | a_{t-n}], \text{ for } i = 1, 2, \dots \quad (16)$$

Since the input array contains current and previous values, it creates a memory layer to the unsupervised TS-SOINN. This allows the TS-SOINN to establish the relationship of current value to previous values.

Figure 4 and Equation (17) show the mechanism of associate memory to perform prediction without a target data. In this example, $n = 4$. The recent observation $X_{current}$ is compared with the neuron X_i in the TS-SOINN network. Note that, the recent 4 observations from $X_{current}$ are compared with the 4 previous points in neuron X_i . The neuron X_i which has the shortest Euclidean distance with $X_{current}$ is the winner node and the data point $a(t)$ (as highlighted in

Figure 4) from the winner node is the predicted output.

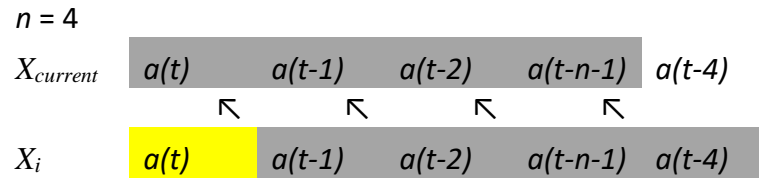


Figure 4: Associate Memory Prediction Mechanism

$$\begin{aligned}
 X_{current} &= [a_t | a_{t-1} | \dots | a_{t-n-1}] \\
 X_i &= [a_{t-1} | a_{t-2} | \dots | a_{t-n}], \text{ for } i = 1, 2, \dots \\
 s &= \arg \min \|X_i - X_{current}\|, \text{ for } i = 1, 2, \dots
 \end{aligned} \tag{17}$$

where s is the index of the winner node.

Although the associate memory function creates a memory layer for the TS-SOINN, it is found that the associate memory function is insufficient to

predict time-series data accurately. It is because the difference of current values, $X_{current}$ and output nodes in each data point carry the same weightage. According to Bishop [107], past observation has a relatively smaller impact to the next state prediction compared to the recent observation. A novel weighted tapped delay line is proposed to address this problem. It is a function to assign different weightage to input data in each data point. Since recent observation has a bigger impact on the predicted value, a higher weightage is assigned to the recent observation and vice versa. The weighted tapped delay line function is as shown in Equation (18).

$$X_i = [a_t \times (n + 1) | a_{t-1} \times (n) | a_{t-2} \times (n - 1) | \dots | a_{t-n} \times 1] \quad (18)$$

For example, if ten previous data points are included in the input array, the current input data, a_t is multiplied with 11.

For the TS-SOINN algorithm, every node contains four variables which are similarity threshold value th , age, number of activation M , and weight vector W . Age of each node is incremented by 1 during merging of a node and the node that exceeds maximum age is removed to reduce the burden of the network. Three-dimensional data which include irradiance, temperature and output power are the input to the network. These data are selected because variances in irradiance and temperature cause an impact on the output power. They are collected and cascaded with other data point to form an input delay array X and

together with the weighted tapped delay line function, the input array X_i is shown in Equation (18).

After the first input data is formed, the node set A is initialised where the first node's weight vector W_{A1} is generated from the first input data X_1 . New input data X_i is fed into the network for learning in a real-time manner. The network searches node set A to determine the index of winner node S_i which is obtained from the minimum Euclidean distance of the input data with the node in set A as shown in Equation (19). Equation (20) shows the minimum Euclidean distance of the winner node to the testing data. The minimum Euclidean distance D_j is used as a criterion whether a new insertion is required to the network. If D_j is greater than the similarity threshold th as in Equation (21), a new node is formed. Otherwise, the input data is merged into the winner node. The age, weight vector and number of activation are updated according to Equation (22).

$$S_1 = \arg \min \|X_i - W_j\|, (\forall j) \quad (19)$$

$$D_j = \min \|X_i - W_j\|, (\forall j) \quad (20)$$

$$D_j > th \rightarrow A = A \cup X_i, age_{x_i} = 1, M_{x_i} = 1, \quad (21)$$

$$W_{x_i} = X_i, \text{ for } i = 1, 2, \dots$$

$$D_j < th \rightarrow age_{s_1} = 1, M_{s_1} = M_{s_1} + 1, \quad (22)$$

$$age_j = age_j + 1 \quad (A \setminus \{S_1\}, j \in A),$$

$$W_{S_1} = W_{S_1} + [\frac{1}{M_{S_1}} \times (X_i - W_{S_1})]$$

Next, the network removes nodes with an age greater than the predefined maximum age as in Equation (23). It is used to remove nodes that are idle for a long period as these nodes burden the network. The network is repeated from Equation (19) to Equation (23) for the next epoch.

$$age_j > age_{dead} \rightarrow A = A/j \quad (j \in A) \quad (23)$$

After two learning epochs, the initial network is formed, and the prediction of output power begins. In this research work, it predicts output power and subsequently the power fluctuation events. To predict the output power, Equation (17) is used. The winner node which has the highest similarity with the recent observation, $X_{current}$ contains the predicted output information (predicted irradiance, predicted ambient temperature and predicted PV output power), only the predicted PV output power will be used for power fluctuation events prediction.

Since the weighted tapped delay line is implemented into the TS-SOINN, the predicted data, a_t need to be divided by $n+1$ as in Equation (24) because it is multiplied by $n+1$ as in Equation (18). TS-SOINN updates the network when

there is a new input and predicts the next state value subsequently. The learning flowchart, prediction mechanism and diagram of TS-SOINN are show in Figure 5, Figure 6 and Figure 7, respectively.

$$\text{Predicted Data, } a_t = \frac{w_{S1}^{(t=1)}}{n+1} \quad (24)$$

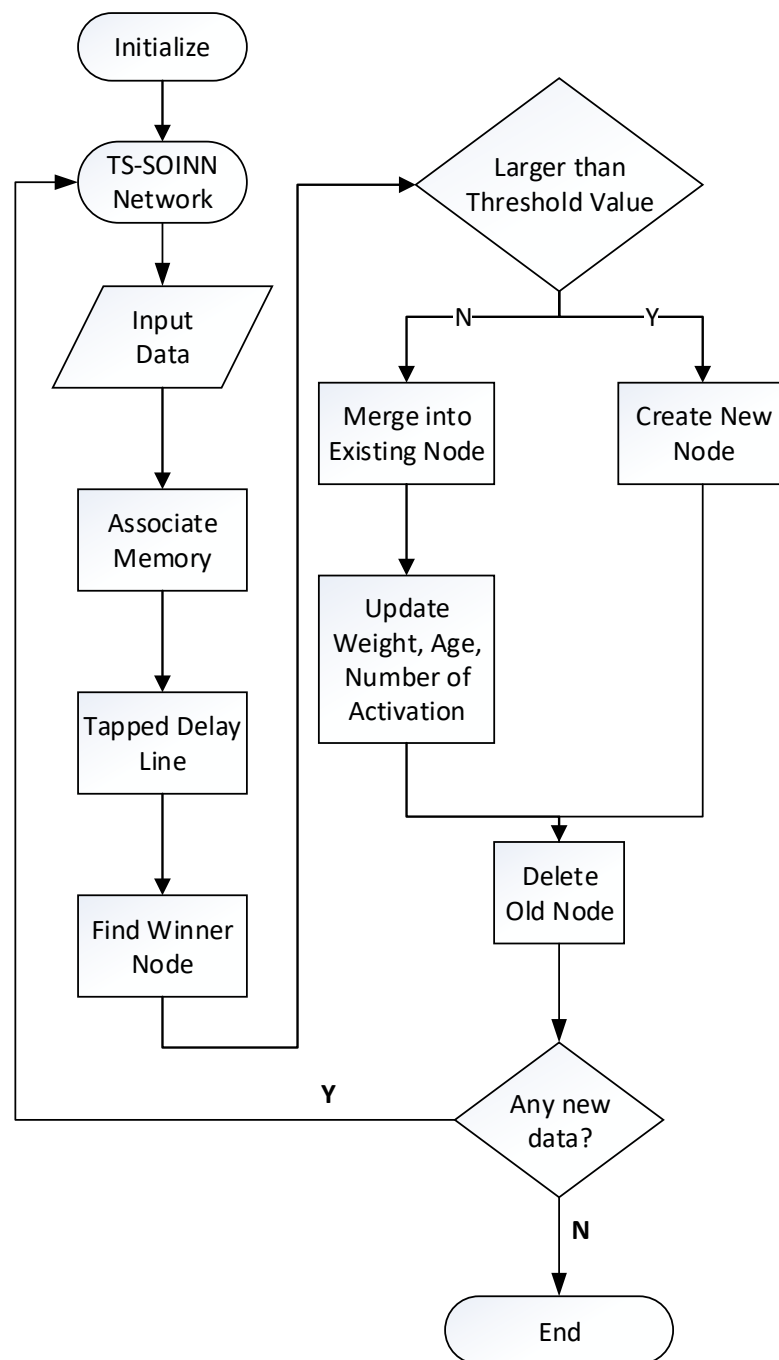


Figure 5: Learning Flowchart of the TS-SOINN

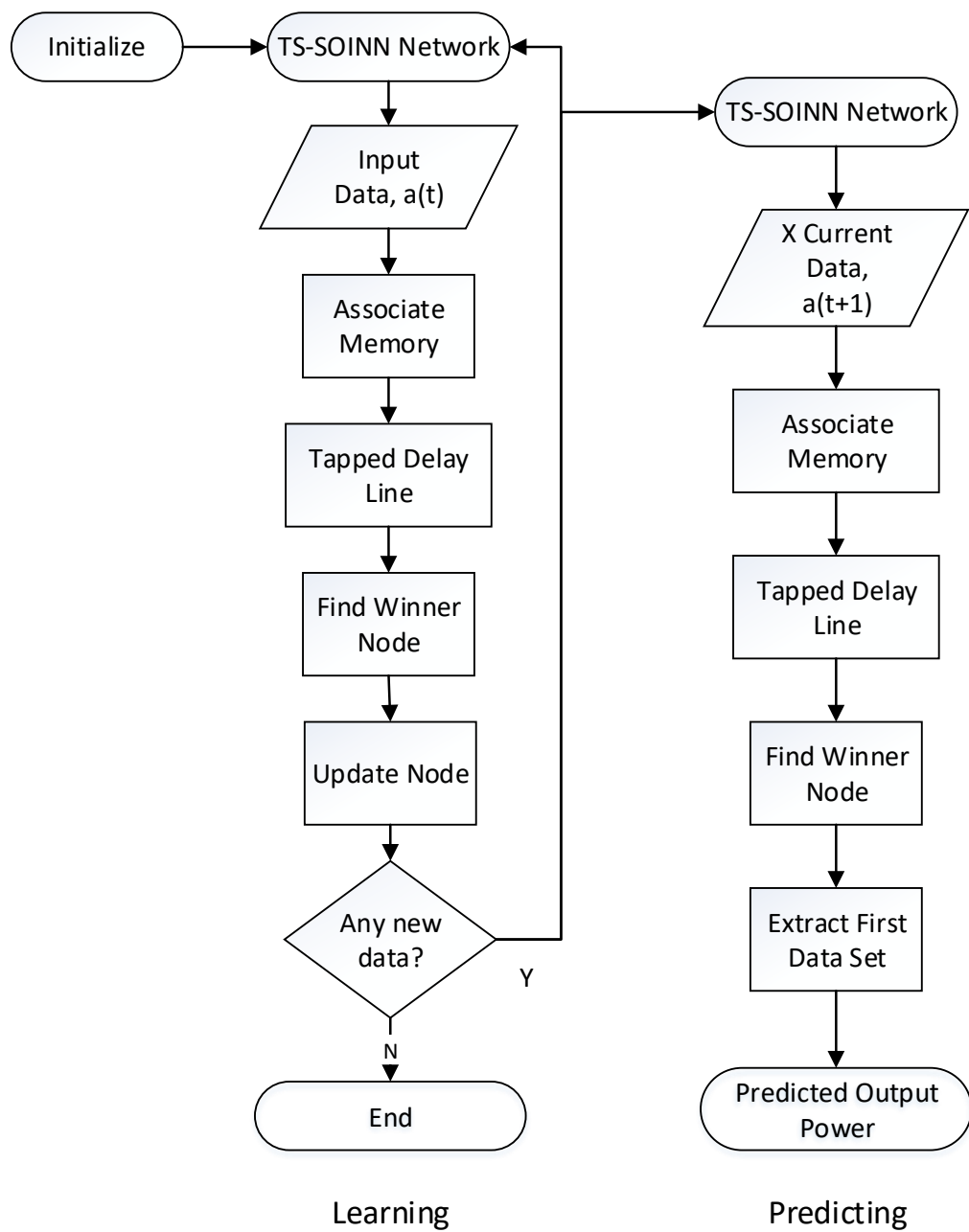


Figure 6: Prediction Mechanism of the TS-SOINN

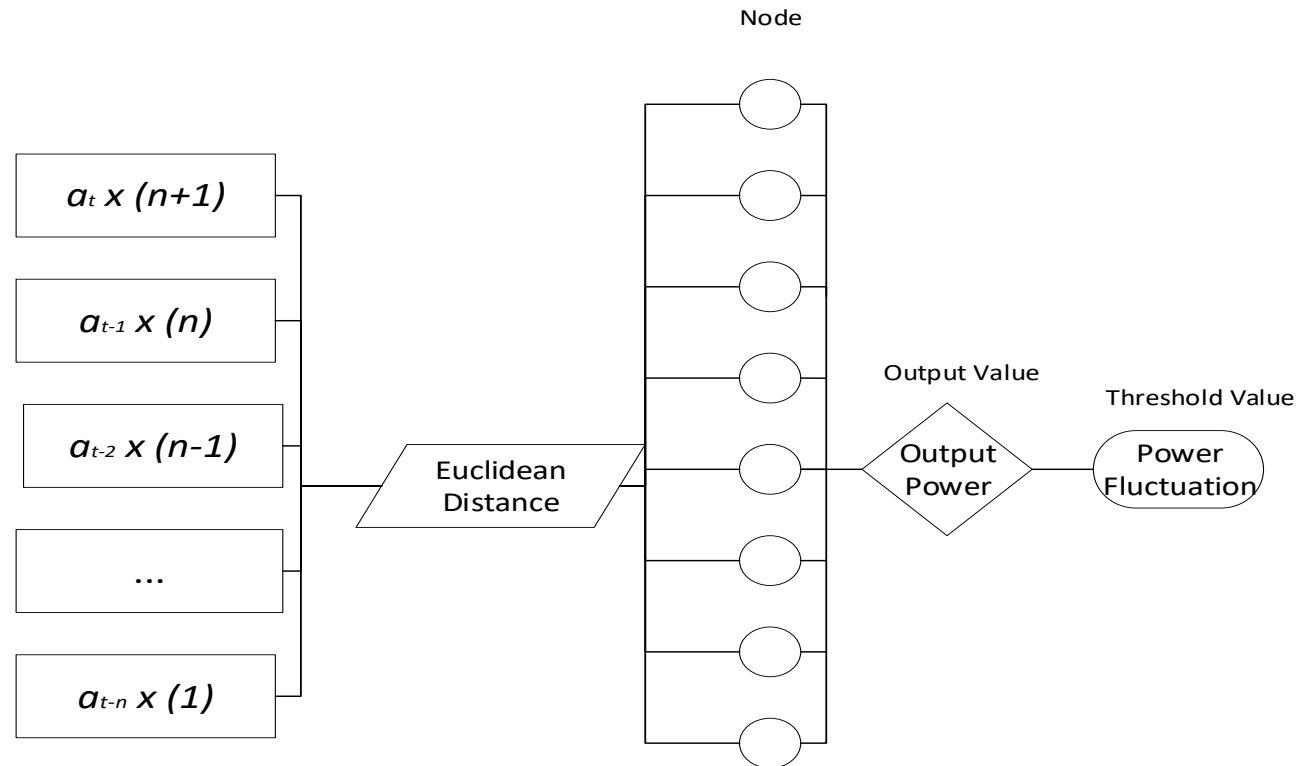


Figure 7: Time-Series Self Organizing Incremental Neural Network

If the difference of the predicted output power within a minute is more than 10% of the rated PV system, the TS-SOINN algorithm predicts a power fluctuation event. The mitigation engine is then switched on for a short period of time (T_{active}) to alleviate the power fluctuation events. It will be switched off when there is no event predicted. By doing so, the usage time of the BESS is reduced as compared to [2]–[4], [16] which switch on for an hour. The impact and selection of T_{active} to the prediction performance are further discussed in Chapter 6.1.1.

Lastly, the unknown parameters are discussed. There are three unknown parameters in the TS-SOINN to be determined which are the similarity threshold th , the maximum age age_{dead} , and total previous data points n . These parameters are determined through experiment to obtain the optimum values. Selection of these parameters will be discussed in detail in Chapter 6.1.1.

3.1 Summary

To conclude, an associate memory function is introduced to the TS-SOINN to enable active unsupervised learning algorithm for time-series prediction. A novel weighted tapped delay line is then proposed to assign higher weightage to the recent observation and vice versa. This could help the learning by emphasizing on the recent observation. Then, the detail mathematic model of TS-SOINN in learning and predicting is elaborated. Lastly, T_{active} concept is introduced to reduce switch on time of BESS.

Chapter 4 Intelligent Real-Time Power Management System (PMS)

This section describes an intelligent real-time PMS that focuses on smoothing intermittent behaviour of the PV grid-tied system. With the aid of the intelligent real-time PMS, the PV system supplies its maximum available power to the grid and the BESS behaves as an ancillary device to dispatch the power deficit in order to smooth power fluctuation events. The intelligent real-time PMS is made up of two engines, which are a prediction engine using the developed TS-SOINN algorithm and a mitigation engine which made up of a rule-based controller and a BESS. The schematic diagram of the developed system is shown in Figure 8.

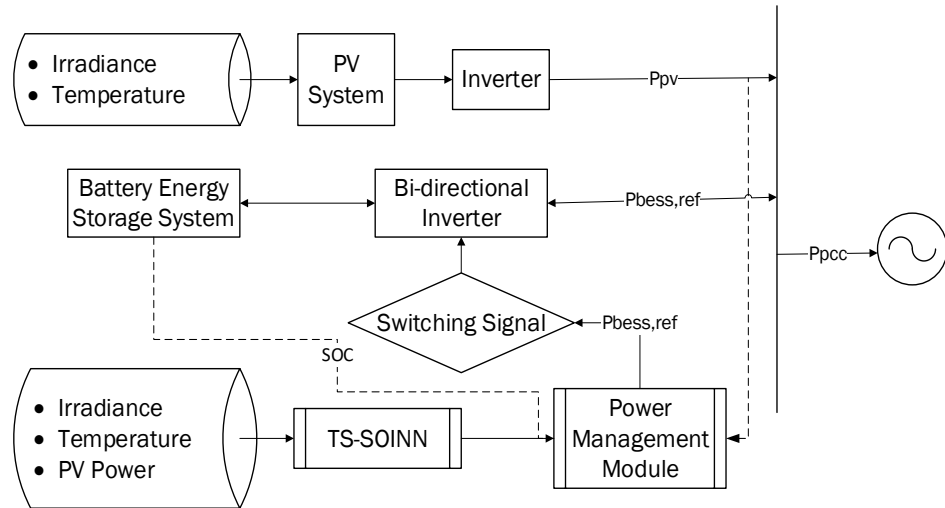


Figure 8: Block Diagram of the Developed Intelligent Real-Time Power Management System

When a power fluctuation event is predicted by the TS-SOINN algorithm, the mitigation engine is activated. The amount of energy to be dispatched by the BESS $P_{BESS,ref}$ is then determined. Insufficient or excessive electrical energy dispatched to the grid system could worsen the power fluctuation scenario. Therefore, a reliable controller that is used to assign charge and discharge rate of the BESS and to maintain SOC, is needed to smooth the power fluctuation events. The power management module in this research work uses a rule-based controller and it is to satisfy two objectives which are to smooth output power and maintain SOC of the BESS in between 30% and 100%. Here, the desired power to the PCC $P_{PCC,ref}$ is used as an ancillary power reference. $P_{PCC,ref}$ is used instead of $P_{BESS,ref}$ because it is easier to explain in terms of smoothing intermittent power as power fluctuation events occur at the PCC. $P_{BESS,ref}$ can be obtained from Equation (25).

$$P_{BESS,ref}(t) = P_{PCC,ref}(t) - P_{PV}(t) \quad (25)$$

where P_{PV} is actual PV output power

Smoothing of power fluctuation is achieved by regulating the current state of power at the PCC to be equivalent to the previous state of PV power. This can be found in Equation (26).

$$P_{PCC,ref}(t) = P_{PV}(t - 1) \quad (26)$$

Equation (26) is used as the primary equation to smooth the power fluctuation. This equation ensures that $P_{PCC,ref}(t)$ closely behaves as $P_{PV}(t)$ to reduce stress on the BESS. In addition, a short update time T_{update} is required to ensure the $P_{PCC,ref}(t)$ closely behaves as the $P_{PV}(t)$. Next, the power deficit of $P_{PCC,ref}(t)$ and $P_{PV}(t)$ will be supplied or absorbed by the BESS to smooth the output power. The following conditions are used to form the first rule in the developed controller:

While Mitigation Engine is ON:

$$P_{PCC,ref}(t) - P_{PV}(t) > Th_m \rightarrow P_{PCC,ref}(t + 1) \quad (27)$$

$$= P_{PCC,ref}(t) - Th_m$$

$$P_{PCC,ref}(t) - P_{PV}(t) < Th_m \rightarrow P_{PCC,ref}(t + 1) \quad (28)$$

$$= P_{PCC,ref}(t) + Th_m$$

$$-Th_m < P_{PCC,ref}(t) - P_{PV}(t) < Th_m \quad (29)$$

$$\rightarrow P_{PCC,ref}(t + 1) = P_{PCC,ref}(t)$$

While Mitigation Engine is OFF:

$$P_{PCC,ref}(t) = P_{PV}(t) \quad (30)$$

where Th_m is a limiting threshold. The limiting threshold can be in a range from 1% to 10% of the rated capacity of the PV system. This is to ensure output power at the PCC fluctuates within 10% of rated capacity per minute. From Equation (27) and Equation (28), while $P_{PCC,ref}(t)$ is greater than $P_{PV}(t)$ by the limiting threshold, it reduces the next state level, $P_{PCC,ref}(t + 1)$ by the limiting threshold and vice versa. Next, the $P_{PCC,ref}$ remains same if the predicted power difference is within the limiting threshold as in Equation (29). When the mitigation engine is not turned on, the P_{PCC} varies according to P_{PV} as in Equation (30).

In general, battery does not tolerate deep discharge and full discharge as these operations cause permanent damage to the battery [9]. Hence, battery is recommended to operate within a healthy SOC of 30% to 100%. The second rule of the proposed controller is to maintain the SOC within this range and it is achieved following the rules below:

$$30\% \leq SOC \leq 100\% \rightarrow P_{PCC,ref}(t) = P_{PCC,ref}(t) \quad (31)$$

$$\begin{aligned} SOC < 30\% \cap P_{PCC,ref}(t) > P_{PV}(t) &\rightarrow P_{PCC,ref}(t) \\ &= P_{PCC,ref}(t) \end{aligned} \quad (32)$$

$$\begin{aligned} SOC > 100\% \cap P_{PCC,ref}(t) > P_{PV}(t) &\rightarrow P_{PCC,ref}(t) \\ &= P_{PCC,ref}(t) \end{aligned} \quad (33)$$

$$\begin{aligned} SOC < 30\% \cap P_{PCC,ref}(t) > P_{PV}(t) &\rightarrow P_{PCC,ref}(t) \\ &= P_{PV}(t) \end{aligned} \quad (34)$$

$$\begin{aligned} SOC > 100\% \cap P_{PCC,ref}(t) < P_{PV}(t) &\rightarrow P_{PCC,ref}(t) \\ &= P_{PV}(t) \end{aligned} \quad (35)$$

From Equation (31), the BESS operates as usual under the control of the first rule while the SOC of the battery is within the healthy range. When the SOC falls below 30% and the $P_{PCC,ref}$ is less than the P_{PV} as in Equation (32), this scenario indicates the BESS operates as a charging system. Hence, the BESS operates according to the $P_{PCC,ref}$. When the SOC is more than 100% and the $P_{PCC,ref}$ is more than the P_{PV} as in Equation (33), the PMS allows the operation as the BESS discharges power to the grid. However, when the SOC is less than 30% and the $P_{PCC,ref}$ is more than the P_{PV} as in Equation (34), or when the SOC is more than 100% and the $P_{PCC,ref}$ is less than the P_{PV} as in Equation (35), the $P_{PCC,ref}$ is set to be the same as the P_{PV} . In consequence, the BESS does not discharge or charge when the SOC is less than 30% and more than 100%, respectively.

From Equation (27) to Equation (35), it concludes that while the BESS does not reach the SOC limitation, $P_{PCC,ref}$ is able to smooth the intermittent behaviour of the PV system. Since the BESS system does not need to operate for 24 hours, it can be recharged to 65% to 70% of SOC at night to prepare for

next day operation. These range of SOC are chosen as it is the mean value of the healthy SOC range (30% and 100%).

Lastly, the two unknown parameters of the PMS are discussed which are the update time T_{update} and the limiting threshold Th_m . These two parameters are determined experimentally to find out the optimised values. Seven days of irradiance and temperature data are used to generate actual power fluctuation events due to the PV grid-tied system. To identify the optimum update time T_{update} for the rule-based controller, it is tested from 1 minute to 10 minutes with increment steps of 30 seconds. The update time that is longer than 10 minutes is not shown in the research work because they are tested and found to have a lower performance than 10 minutes. Next, the optimal value for the limiting threshold, Th_m is discussed. It has to be set within 1% to 10% of the rated capacity of the PV system. A large limiting threshold increases the stress in the BESS and fluctuation rate of the PV system. In contrast, a small limiting threshold increases the stress in the controller. The results of the optimum update time T_{update} and the optimum limiting threshold Th_m are shown in Chapter 6.2.1.

4.1 Summary

To conclude, with the aid of the intelligent real-time PMS, the PV system can supply maximum available power to the power networks, and the BESS behaves as an ancillary device to dispatch the power deficit to the power distribution system to smooth power fluctuation events. The intelligent real-time PMS is composed of a prediction engine (TS-SOINN) and a mitigation engine which made up of a rule-based controller and a BESS. The mitigation engine will be switched on for T_{active} when the prediction engine predicts a power fluctuation event. The detailed mathematical equations of the intelligent real-time PMS are shown in this chapter.

Chapter 5 Real-time Implementation of Power

Management System

This section describes the methodology to connect the developed intelligent prediction and mitigation system to real-life data. Firstly, a PV grid-tied system is modelled in the PSCAD environment. Secondly, a data acquisition system is built to collect irradiance and temperature data as input data to the modelled PV system. Thirdly, a laboratory scale PV grid-tied system in the UNM solar cabin is constructed. It is used to validate the proposed TS-SOINN's simulation result. Lastly, real-time implementation of the intelligent real-time PMS is presented.

5.1 PV Grid-Tied System

The modelled PV grid-tied system consists of a PV source, a maximum power point tracker, an inverter, a high pass filter, transformer and a grid. A 270 kWp PV system is modelled in the PSCAD environment.

To demonstrate that the PMS with the aid of the TS-SOINN can compensate the most critical environmental factors, a 54 kWh BESS is modelled [108] in Power System Computer Aided Design (PSCAD). The BESS model [108] is composed of a controlled voltage source in series with a resistance, a capacitor and a bidirectional inverter. A bidirectional inverter is chosen for the BESS to carry out charge and discharge operations.

Chapter 5 – Real-Time Implementation of PMS

The basic power flow equation as shown in Equation (36) is used to control the inverter's output power, where V_1 is the voltage from the BESS's inverter, V_2 is the voltage from the grid, X_{12} is the impedance between two ports and δ is the power angle between two ports. To obtain adequate power deficit to prevent power fluctuation events, the desired PCC power $P_{PCC,ref}$ is compared with the actual PCC output power P_{PCC} to yield an error. The error is passed to a proportional integral (PI) controller to generate a power angle for the inverter to supply sufficient power deficit to the grid.

$$P_{12} = \frac{V_1 V_2}{X_{12}} \sin \delta \quad (36)$$

Chapter 5 – Real-Time Implementation of PMS

5.2 Data Acquisition System

Irradiance and temperature are collected and fed into the modelled PV system to simulate the real-life event. Three devices are required to construct this data acquisition system which are SP Lite 2 pyranometer, a WXT520 weather station, and a data logger. The data logger transmits and saves the data to a computer via LabVIEW. Figure 9 shows the flowchart of the data acquisition system.

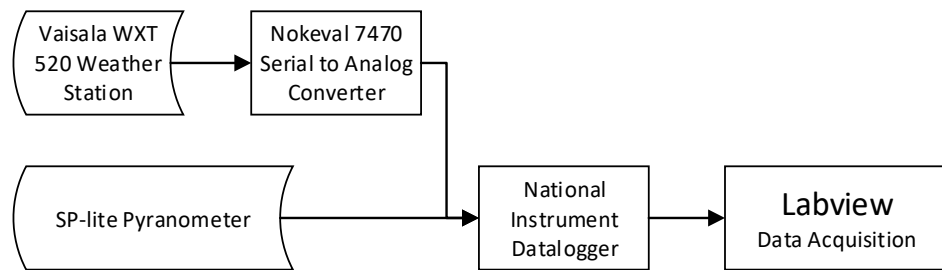


Figure 9: Flowchart of the Data Acquisition System

The features of the data acquisition system include:

- **CompactDAQ 9178:** Compact DAQ 9178 is a rugged DAQ platform that integrates connectivity and signal conditioning into modular I/O for direct interaction with any sensor or signal [109]. It allows eight modules to be installed into the chassis. The NI 9209 which is a 16 channels voltage module and the NI 9203 which is an 8 channels current module are integrated into the CompactDAQ 9178 data logger [110], [111]. Therefore, this CompactDAQ is able to collect data in

Chapter 5 – Real-Time Implementation of PMS

terms of voltage and current as well. Figure 10 shows the National Instruments CompactDAQ 9178 data logger system.

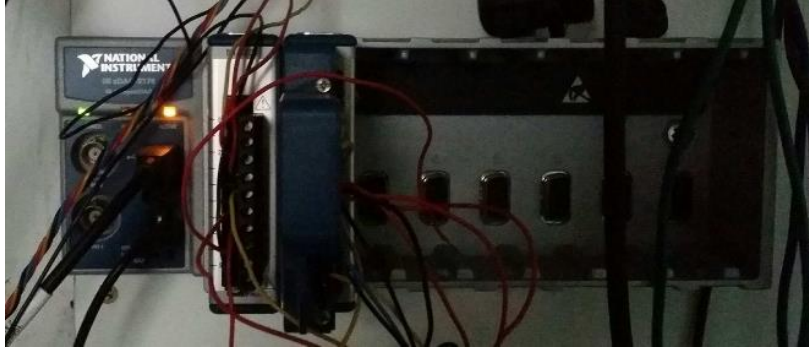


Figure 10: Data Logger

- SP Lite2 Pyranometer: Figure 11 shows the SP Lite 2 Pyranometer. SP Lite2 pyranometer is designed for PV module monitoring [112]. It can be used in all weather conditions and measures irradiance received from the entire hemisphere. It uses a photodiode detector to create an output voltage that is proportional to the incoming radiance. Its sensitivity is up to $60 \mu\text{V}/\text{W}/\text{m}^2$. However, a special wiring is required due to its floating voltage source. Two bias resistors, R which are within range of $10\text{k}\Omega$ to $100\text{k}\Omega$ are used to provide a direct current (DC) path from the instrumentation amplifier inputs to the instrumentation amplifier ground. These ranges are selected because it allows the source to float with respect to the measurement reference (data logger's ground) and not load the signal source. The

Chapter 5 – Real-Time Implementation of PMS

bias resistor is connected between each input and the data logger's ground as in Figure 12.



Figure 11: SP Lite 2 Pyranometer

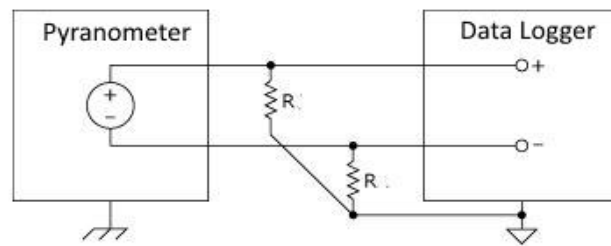


Figure 12: Wiring Schematic of Floating Source

- Vaisala WXT 520 & Nokeval 7470: WXT 520 weather transmitter is a flexible, integrated building block for weather applications. It senses the weather parameters and returns in a serial form. Thus, a serial to analogue converter is required to convert the collected data into the analogue format and send to the data logger. A Nokeval 7470 is able to convert four parameters from serial format to analogue format. The output of the Nokeval 7470 is determined through Mekuwin software. Figure 13 shows the WXT 520 weather

Chapter 5 – Real-Time Implementation of PMS

transmitter and Nokeval 7470 analog converter at the left and right, respectively.



Figure 13: WXT 520 Weather Transmitter (left) & Nokeval 7470 Analog Converter (Right)

After the data logger acquires the weather data, it transmits and saves the data to a computer via LABVIEW. The collected data is used to simulate real-life events for a PV grid-tied system in PSCAD to verify the reliability and accuracy of the TS-SOINN in prediction.

5.3 Laboratory-Scale PV grid-tied system

A laboratory-scale PV grid-tied system is constructed in this research to validate the reliability and accuracy of the TS-SOINN experimentally. The PV grid-tied system is installed in the solar cabin of the UNM. It is constructed with a 1.2 kWp PV panel, 3.6 kW ABB single-phase inverter as in Figure 14 and main switchboard (MSB) of the solar cabin. The output power of the PV system is collected by using a voltage and current transducers. These transducers collect the current and voltage data and send to the data acquisition system.



Figure 14: ABB 3.6 kW inverter

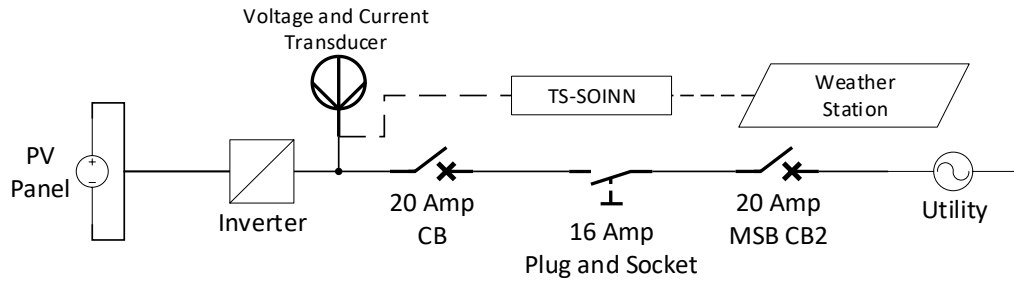


Figure 15: Simplified Electrical Schematic of the PV Grid-Tied System

Figure 15 shows the simplified electrical schematic of the PV grid-tied system. Two 20 A circuit breaker (CB) are used between the inverter and the MSB. These two circuit breakers are used to prevent large current flow into the circuit and destroy other electrical appliances. High current rating circuit breakers are used because the maximum output power of the inverter is 3.6 kW, which is equivalent to 16 A. Thus, 20 A circuit breaker is used in this project. Since the inverter outputs high current to the circuit, an industry level 16 A plug and socket are used to connect the inverter to the grid.

The voltage and current transducers are installed at the PCC. The voltage and current data are multiplied to obtain the output power of the 1.2 kWp PV system. Next, the output power is grouped with the instantaneous irradiance and temperature data to form input data to MATLAB. It is because these input data are used to validate the accuracy of the TS-SOINN experimentally, where the TS-SOINN is modelled in MATLAB environment.

5.4 Real-time Implementation of the PMS

A real-time data acquisition system is constructed to achieve real-time implementation. The MATLAB is used as an agent to command the data logger, the TS-SOINN, and the mitigation engine. A custom block is designed for the purpose of communication between MATLAB and PSCAD. It is written in FORTRAN environment. After retrieval of real-time environmental data, these data are fed into the modelled PV micro-grid system to generate real-time outputs. Next, these outputs are returned to MATLAB for training and prediction of the TS-SOINN. If a power fluctuation event is predicted, the MATLAB switches on the mitigation engine and returns the power reference to the BESS's inverter. Otherwise, the BESS is not turned on. Therefore, an intelligent real-time PMS is constructed to mitigate power fluctuation events. Figure 16 shows the flowchart of the real-time implementation.

Chapter 5 – Real-Time Implementation of PMS

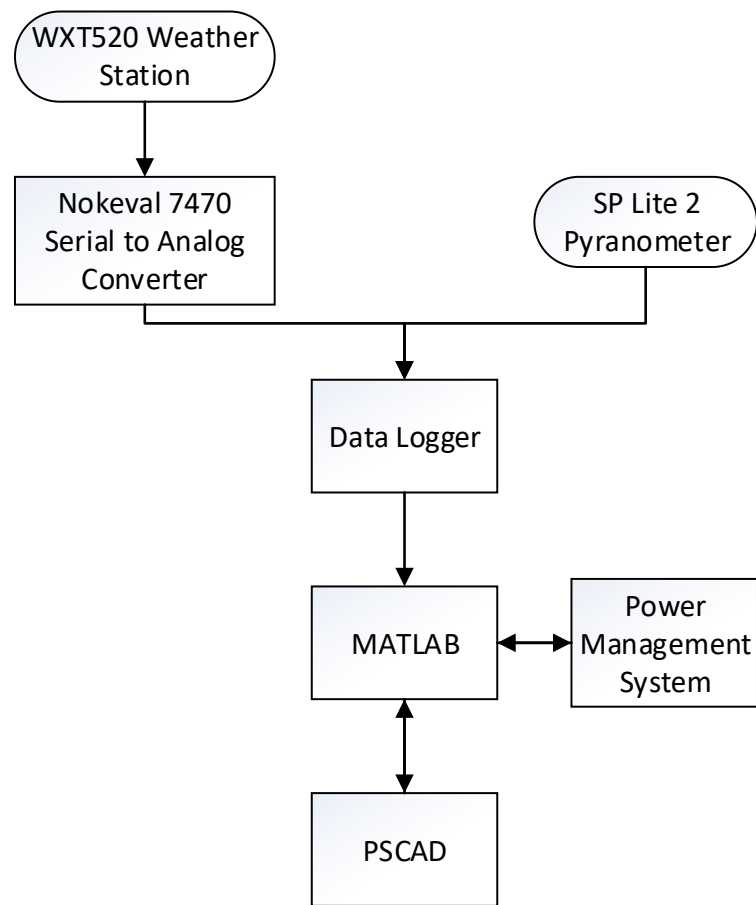


Figure 16: Flowchart of Real-Time Implementation of PMS

Chapter 5 – Real-Time Implementation of PMS

5.5 Summary

To conclude, this chapter presents the methodology to connect the developed intelligent real-time PMS to real-life data. A PV grid-tied system with BESS is modelled in the PSCAD environment to demonstrate the developed PMS is capable to mitigate power fluctuation events effectively. Next, it shows the data acquisition system that is used in this research work. The data acquisition system collects real-life environmental data and these data are used as input to the modelled PV grid-tied system in PSCAD. Therefore, the developed system can be tested with actual real-life data. A laboratory-scale PV grid-tied system is then shown in this chapter. It is used to test the performance of TS-SOINN experimentally. Lastly, this chapter describes the real-time implementation of the developed PMS. The data acquisition system sends collected data into MATLAB, and the MATLAB serves as an agent to communicate with PSCAD to train the TS-SOINN and sends a signal to the BESS to mitigate power fluctuation events.

Chapter 6 Results and Discussions

The first section of this chapter presents the performance of the proposed TS-SOINN. It discusses the optimal parameter values, for the total previous data points, maximum age, and similarity threshold for the TS-SOINN and value for T_{active} for all tested AI algorithms. It then shows the performance of the TS-SOINN in predicting power fluctuation events in real-time simulation. The performance of the TS-SOINN is compared with E-SOINN [8], HBSOINN [13], SOINN-DTW [13], NARX [14], and SOM [15]. The simulation results of the TS-SOINN are then validated experimentally.

The second section discusses the performance of the developed intelligent real-time PMS. Performance of the PMS is measured by reduction of power fluctuation events and variation in output energy to the grid. The performance of the developed PMS is then compared with the hourly rule-based controller [2], and the dynamic ramp rate controller [16].

6.1 TS-SOINN

This section evaluates the prediction accuracy of the TS-SOINN. Firstly, the optimal parameter values for the TS-SOINN are obtained. Then its accuracy in predicting the output power and power fluctuation events are evaluated. Its performance is compared with E-SOINN [8], HBSOINN [13], SOINN-DTW [13], NARX [14], and SOM [15].

Power fluctuation occurs when the output power fluctuates more than 10% of the rated capacity of the PV system within a minute. Thus, the power fluctuation threshold value is 27 kW. In other words, when the difference in output power within a minute is more than 27 kW, a power fluctuation event occurs.

6.1.1 Optimisation of Parameters

The weighted tapped delay line (the total previous data points in the memory layer n), maximum age age_{dead} , similarity threshold th , and the value for T_{active} are the parameters to be determined. Seven days of irradiance and temperature data are used as input to the modelled PV grid-tied system to obtain the output power. To identify the most optimum total previous data points n , values from 2 to 20 are tested against the prediction. Values that are greater than 20 are not discussed in this research work because they are tested and found to have similar or lower performance than 20. Prediction rate refers to the total percentage of

Chapter 6 – Results & Discussions

power fluctuation events correctly predicted by the TS-SOINN as in Equation (37).

$$\text{Prediction Rate} = \frac{\text{Correctly predicted Events}}{\text{Total Events}} \times 100\% \quad (37)$$

Figure 17 shows the prediction rate against n of value 2, 3, 5, 8, 10 and 11. These data points are shown because they have significant differences in the results. It can be seen that, total previous data point of 2 and 3 show a relatively lower prediction rate compared to others. Although total previous data point of 5 achieves the highest prediction rate in the first three days, it drops to less than 95% in the later days. The total previous data point of 8 achieves 98% prediction rate on the first day and it maintains above 96% of prediction rate for the next 6 days. Total previous data point of 8 is selected as it achieves a relatively higher and more stable prediction rate as compared to the other values in the 7 days.

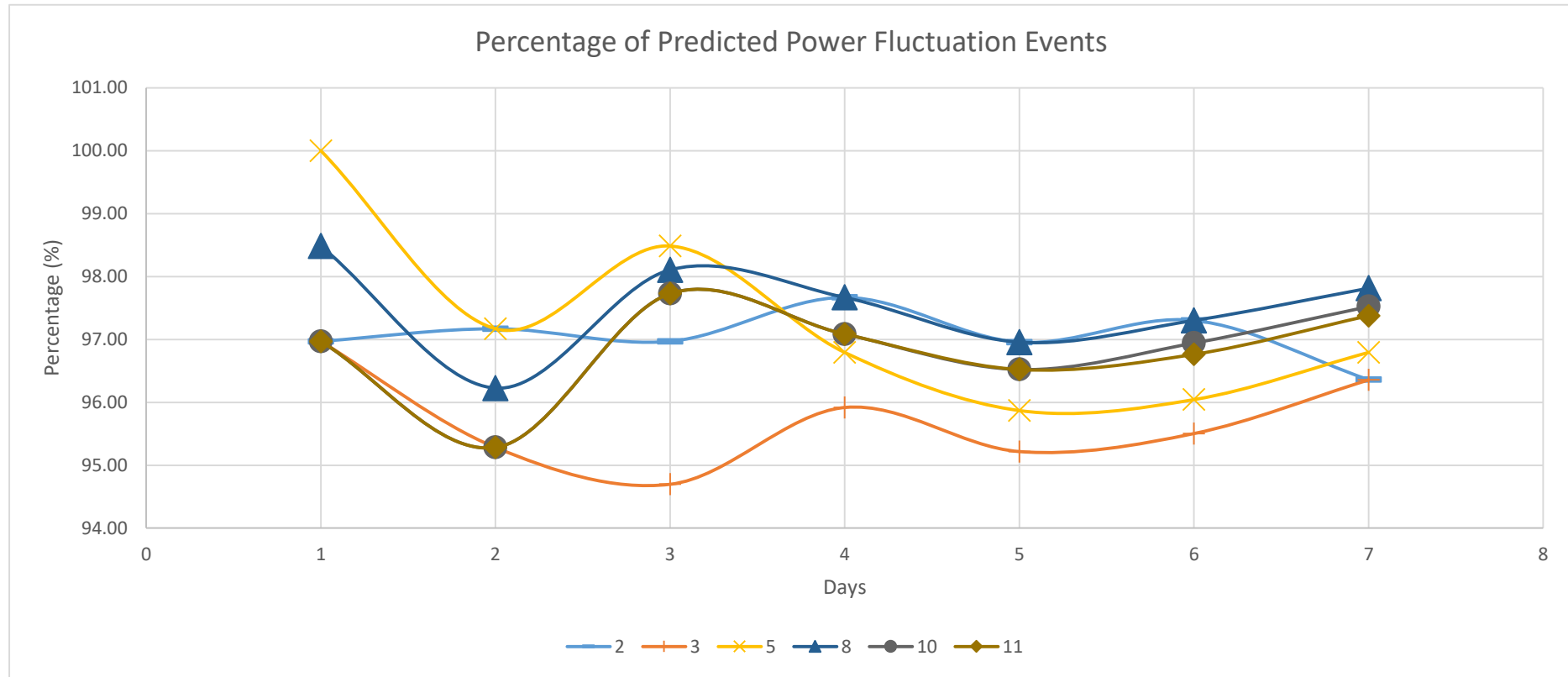


Figure 17: Percentage of Predicted Power Fluctuation Events for Different Total Previous Data Point

Chapter 6 – Results & Discussions

Next, the optimal parameter value for the maximum age age_{dead} , is evaluated. A high maximum age increases the network's size and carries a higher volume of data. This will increase the computational complexity of the network. Thus, the maximum age, is tested on a log scale of 5, 50, 500, 5000, and 50000. Figure 18 shows the prediction accuracy against different maximum ages. It is found that, maximum age, of 50 achieves the highest prediction rate. Also, when the maximum age increases to more than 500, the prediction rate decreases. Thus, the optimal maximum age should be chosen within the range of 50 to 500. From this range, 50 is chosen because it achieves the same prediction rate with other higher maximum ages.

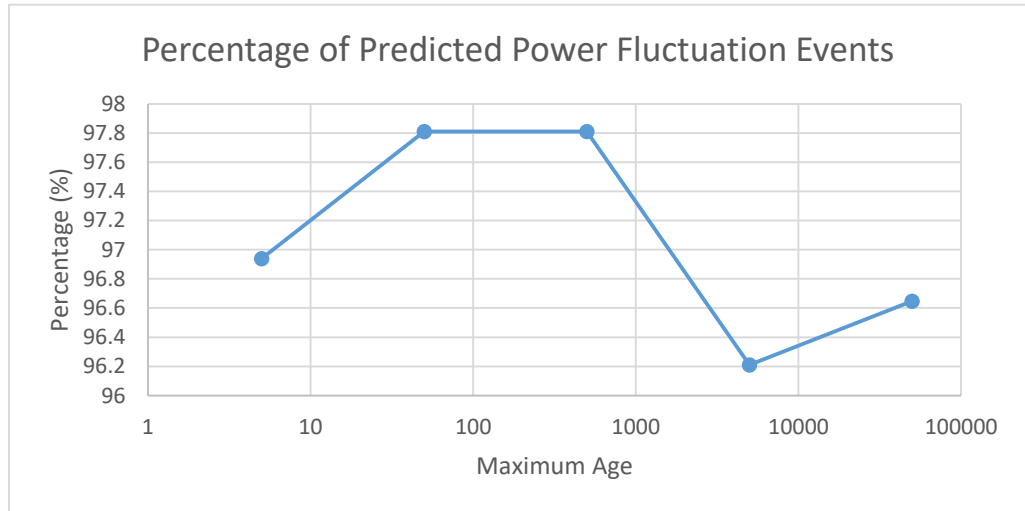


Figure 18: Percentage of Predicted Power Fluctuation Events for Different Maximum Age

The similarity threshold th determines the insertion of a new class to the network. A large value of similarity threshold causes the TS-SOINN to be

Chapter 6 – Results & Discussions

unable to create sufficient node to represent different output power patterns. In contrast, a small value of similarity threshold causes TS-SOINN to generate many nodes which could burden the network. The smallest similarity threshold of the E-SOINN [8] is used as a reference value. Then, variation is made on the reference value to obtain the most optimum similarity threshold value for the TS-SOINN. For the E-SOINN, the smallest similarity threshold is 27. To identify the most optimum similarity threshold, values from 22 to 33 are tested. Other values are not shown because they have lower performance than the tested values. Figure 19 shows the percentage of predicted power fluctuation events using different similarity threshold values. It shows that the similar threshold value of 25 achieves the highest prediction rate. It is found that when the similarity threshold further increases, the prediction accuracy decreases.

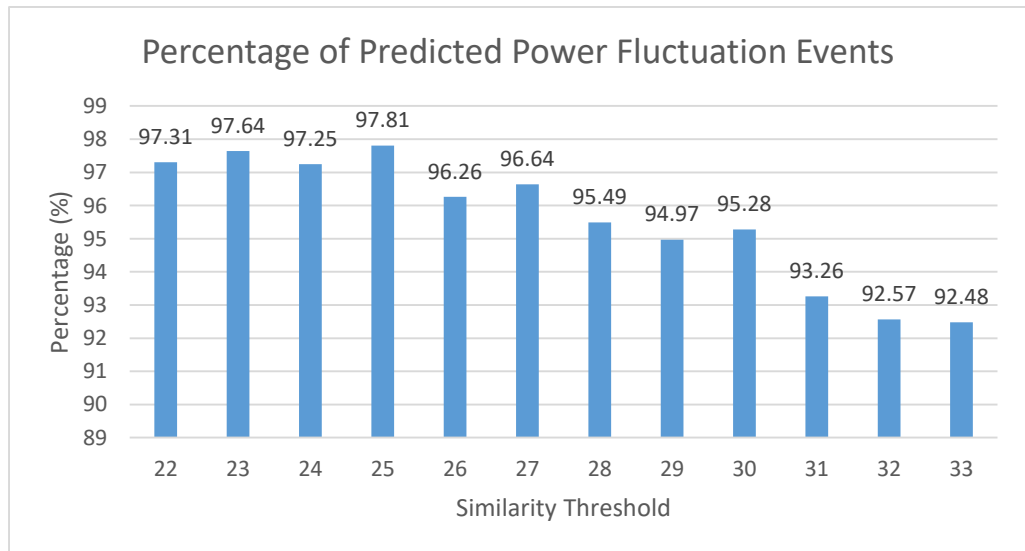


Figure 19: Percentage of Predicted Power Fluctuation Events versus Different Similarity Threshold Values

Chapter 6 – Results & Discussions

Lastly, the value for T_{active} is discussed. Figure 20 shows the impact of implementing the T_{active} into the TS-SOINN for seven days. It can be observed that, when the T_{active} is not implemented into the TS-SOINN (0 mins), the TS-SOINN predicts 55.10% of power fluctuation events. The predicted power fluctuation events increase to 91.69% while the T_{active} is 5 minutes. The predicted power fluctuation events reach its peak at 65 minutes, which predicts 97.96% of power fluctuation events. Although this period predicts the most power fluctuation events, it has to maintain the switched-on time for the longest which increases the usage of the BESS. T_{active} of 30 minutes switched on period is selected for this research work.

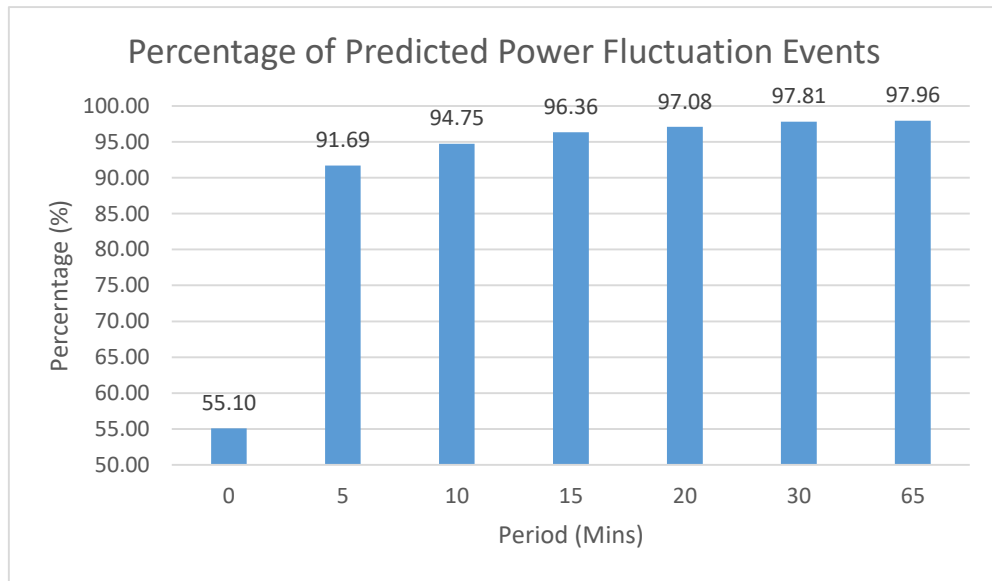


Figure 20: Percentage of Predicted Power Fluctuation Events for Different Periods

6.1.2 Simulation Analysis

The prediction performances of the TS-SOINN is thoroughly evaluated in this section. The prediction performance of the TS-SOINN is compared with five algorithms which are E-SOINN [8], HBSOINN [13], SOINN-DTW [13], NARX [14], and SOM [15]. A 20 by 20 network size are assigned to the SOM. For the NARX, it has 30 hidden neurons, 8 input delays and 8 feedback delays. For the E-SOINN, it has a maximum age of 50, lamda value of 50, c_1 and c_2 denoising factor values of 10 and 100, respectively. For the SOINN-DTW and HBSOINN, they have 40 initial classes. All the parameter values discussed above for SOM, NARX, SOINN-DTW, and HBSOINN networks are optimal values as they achieve the highest performance in terms of MAE and root mean square error (RMSE). 1-week data is used for training and a different 1-week data is used for testing in this process. To enable time-series prediction in E-SOINN and SOM, the associate memory layer is implemented into them. Total of 11 previous data points ($n = 11$) are assigned to both networks. In addition, all tested algorithms have the same value of T_{active} .

Similar to the TS-SOINN, irradiance, ambient temperature, and the output power are used as the input to the E-SOINN, SOINN-DTW, HBSOINN, SOM and NARX networks. Since the SOM and NARX networks learn in a non-incremental manner, both networks are trained with one month (16.7%), two months (33.3%), three months (50%) and four months (66.7%) data and tested

Chapter 6 – Results & Discussions

separately with five months, four months, three months and two months data, respectively. This analyses the impacts of training data on the prediction accuracy of SOM and NARX. Since the SOINN-DTW and HBSOINN are semi-supervised algorithms, they are trained with a month data. Then, they are tested with five months data. Compared to the non-incremental learning algorithms, the TS-SOINN and E-SOINN are tested with half a year data because these algorithms can learn and predict in real-time.

Firstly, the prediction accuracy is evaluated in terms of MAE, RMSE, R-square (R^2) and forecast skill (s). These four performance metrics are used commonly in assessing the performance of PV power forecasting techniques [11]. The MAE measures the difference between the forecast and actual value whereas the RMSE finds the standard deviation of the prediction error. Compared to the MAE, it amplifies large errors. The R^2 measures how well the data fits on to the regression line. The formulae for the MAE, RMSE and R^2 are listed in Equation (38), Equation (39), and Equation (40), respectively. Other than these three conventional performance metrics, s which is introduced by Coimbra and Kleissl [92] is used. It is a method to normalise forecast accuracy. It is done by comparing RMSE of different algorithms to the RMSE of the persistence model as in Equation (41). Persistence model is the simplest prediction engine and used as a benchmark for output power prediction. The s favours large positive value as it indicates the performance of the selected methodology achieves better performance than the persistence model.

$$MAE = \frac{1}{n} \sum_{i=1}^n |y_i - x_i| \times 100\% \quad (38)$$

$$RMSE = \sqrt{\frac{1}{n} \sum_{i=1}^n (y_i - x_i)^2} \times 100\% \quad (39)$$

$$R^2 = 1 - \frac{\sum_{i=1}^n (y_i - x_i)^2}{\sum_{i=1}^n (y_i - \bar{y})^2} \quad (40)$$

$$s = 1 - \frac{RMSE_{method\ X}}{RMSE_{Persistence\ model}} \quad (41)$$

where y_i is the actual output power, x_i is the predicted output power and n is the total number of predicted output power. Other than evaluating the prediction accuracy, the prediction rate and false acceptance rate for power fluctuation events prediction are tested. False acceptance rate is the total percentage of wrongly predicted events as shown in Equation (42).

$$\begin{aligned} & \text{False Acceptance Rate} \\ &= \frac{\text{False Predicted Events}}{\text{Total Predicted Events}} \times 100\% \end{aligned} \quad (42)$$

Table 3 summarises the performance of six algorithms in predicting output power of the PV system. From MAE column, both non-incremental learning algorithms, NARX and SOM show decreasing trends in MAE with increasing size of training data, which decreases from 3.08% to 2.89% for the NARX, and from 3.92% to 3.58% for the SOM. The MAE of HBSOINN and SOINN-DTW are 2.97% and 3.48%, respectively. These values are slightly

Chapter 6 – Results & Discussions

lower than the best NARX performance. Although both NARX and SOM networks mark their lowest MAE with 4 months of training data, the active learning algorithms, TS-SOINN and E-SOINN perform better than the best performance from SOM and NARX, which are 1.56% and 1.70%, respectively. Among the tested algorithms, the TS-SOINN has the lowest MAE value.

Similar results are shown in terms of RMSE. Both NARX and SOM show a decreasing trend in RMSE with increasing size of training data, which decreases from 5.83% to 5.59% for the NARX, and from 8.12% to 7.84% for the SOM. The RMSE of HB-SOINN and SOINN-DTW are 5.75% and 6.42%, respectively. These results are slightly higher than the best NARX network. The RMSE of TS-SOINN and E-SOINN are 3.75% and 4.23%, respectively. The TS-SOINN outperforms E-SOINN, HBSOINN, SOINN-DTW, NARX, and SOM by 0.48%, 2.00%, 2.67%, 1.84% and 4.09%, respectively.

For the R^2 , it improves with increasing training data's size for the NARX and SOM, which increases from 0.85 to 0.90 for the NARX, and from 0.70 to 0.78 for the SOM. The TS-SOINN achieves the highest R^2 value which is 0.95 follows by the E-SOINN, HBSOINN, and SOINN-DTW which are 0.93, 0.87, and 0.82, respectively. The TS-SOINN outperforms E-SOINN, HBSOINN, SOINN-DTW, NARX and SOM by 0.02, 0.08, 0.13, 0.05 and 0.17, respectively. The RMSE of the persistence model is 5.80% and it is used to determine the s . Among the tested algorithms, the TS-SOINN has the best forecast skill, which

Chapter 6 – Results & Discussions

is 0.35, followed by the E-SOINN, the NARX, the HBSOINN, the SOINN-DTW, and the SOM which are 0.27, 0.04, 0.01, -0.11, and -0.35, respectively. The negative value of the SOM shows that its performance worse than the persistence model.

Table 3: Summary of Tested Algorithms Performances in Predicting Output Power

Algorithm	Training Data	MAE (%)	RMSE (%)	R ²	<i>s</i>
TS-SOINN	Active Learning	1.56	3.75	0.95	0.35
E-SOINN	Active Learning	1.70	4.23	0.93	0.27
HBSOINN	Semi-Supervised	2.97	5.75	0.87	0.01
SOINN-DTW	Semi-Supervised	3.48	6.42	0.82	-0.11
NARX	4 Months	2.89	5.59	0.90	0.04
SOM		3.58	7.84	0.78	-0.35
NARX	3 Months	2.94	5.72	0.88	0.01
SOM		3.84	7.96	0.76	-0.37
NARX	2 Months	3.02	5.78	0.87	0.00
SOM		3.89	8.05	0.73	-0.39
NARX	1 Month	3.08	5.83	0.85	-0.01
SOM		3.92	8.12	0.70	-0.40

Chapter 6 – Results & Discussions

Figure 21, Figure 22 and Figure 23 show the graphs of actual output power versus forecast power and actual occurrence of power fluctuation events for three different days. The data is plotted in 30 seconds resolution and power fluctuation events are assigned to 0.5 value of the right axis. From the graphs, the output power of the PV system fluctuates largely from 0900 (as in Figure 21) to 1700 (as in Figure 22), instead of increasing steadily in the afternoon and reducing slowly in the evening. This phenomenon occurs due to the rapid moving speed of cloud in Malaysia. In addition, the graphs show that the actual power fluctuation events could occur anytime between 0900 and 1700. This indicates that the occurrence of power fluctuation events are highly random and occurrence of the next events could be 2 hours later. This phenomenon shows that switching on the BESS for daytime is a waste of energy as there might be a long period without power fluctuation events. Besides, the maximum error between the actual and predicted PV power is 0.07MW which is about 30% of rated capacity. Although the maximum prediction error is large, it does not affect the PMS performance as the predicted values are not being used as a power reference to the PMS. The predicted value is used to determine whether a power fluctuation event would occur for the T_{update} period and then the BESS controller would instructs the PMS to switch on if there is a predicted power fluctuation event.

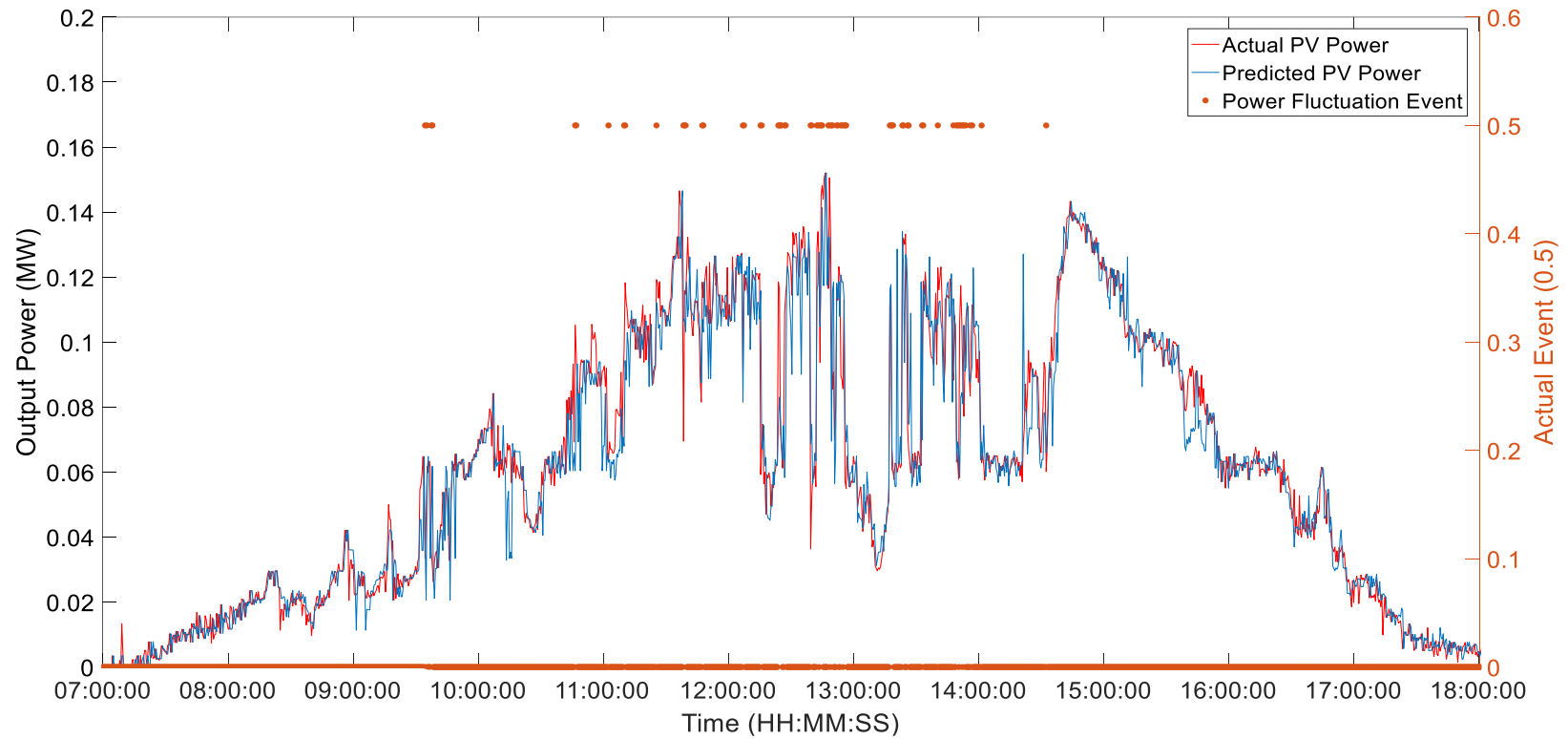


Figure 21: Graph of Actual Power versus Predicted Power (Blue) with Actual Power Fluctuation Events (Brown Dot) in Day 5

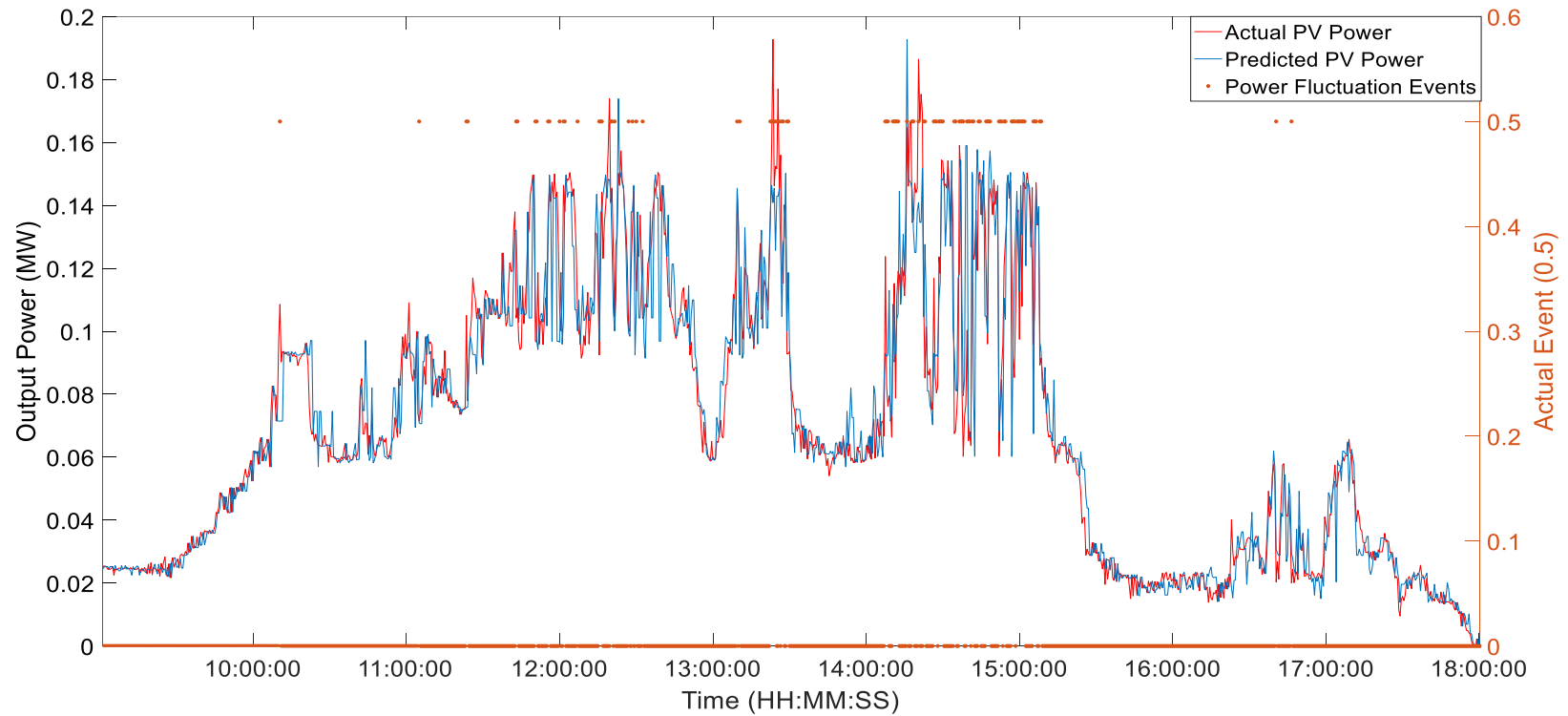


Figure 22: Graph of Actual Power versus Predicted Power (Blue) with Actual Power Fluctuation Events (Brown Dot) in Day 18

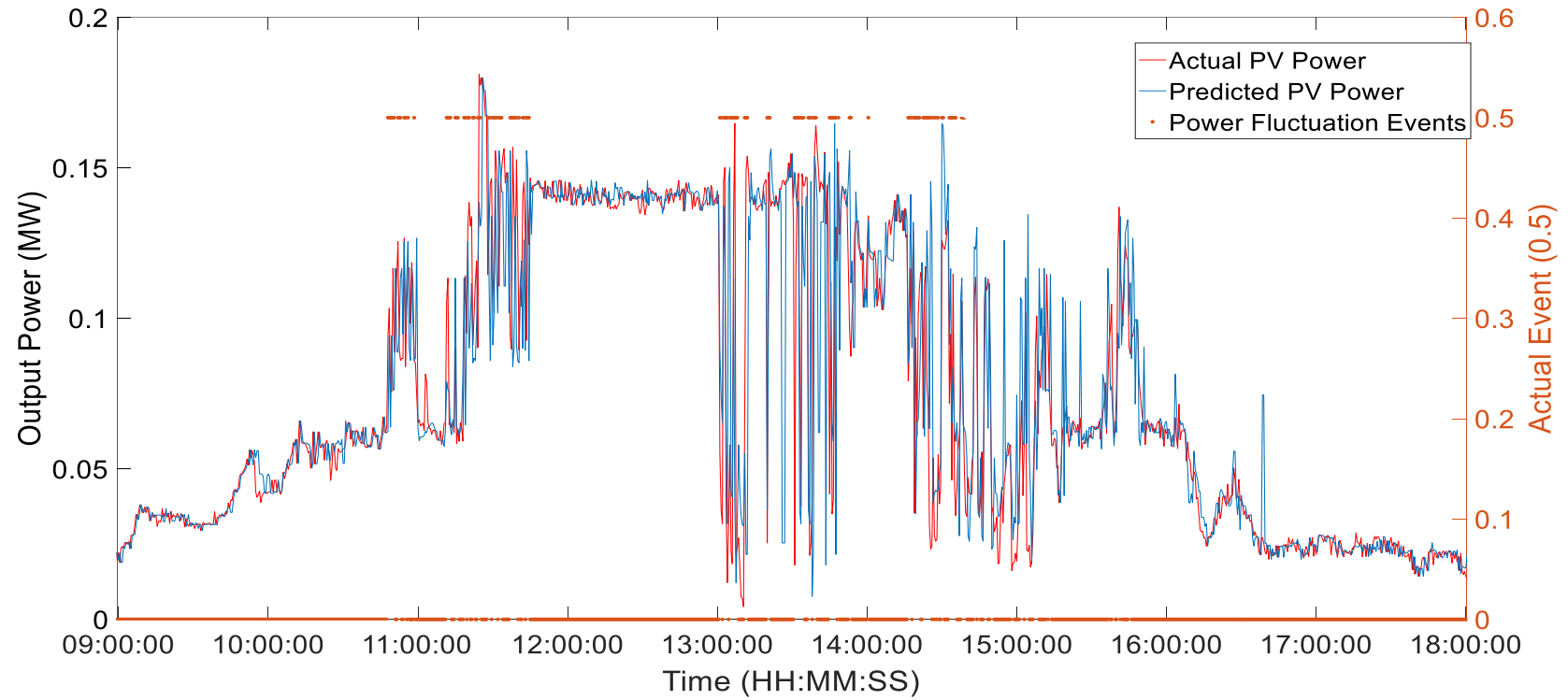


Figure 23: Graph of Actual Power versus Predicted Power (Blue) with Actual Power Fluctuation Events (Brown Dot) in Day 53

Table 4 shows the performance metrics of all tested algorithms in predicting output power of the PV system during the power fluctuation events' instance. From the table, the predicted power fluctuation events (next instance) for the TS-SOINN, E-SOINN, HBSOINN, SOINN-DTW, NARX and SOM are 55.10%, 39.07%, 34.28%, 30.61%, 28.65% and 6.71%, respectively. The low prediction rate does not reflect the high prediction accuracy as per achieved in Table 3. This is because the prediction algorithms can predict accurately most of the time of the day when the irradiance is relatively constant. This can be seen from Figure 21, Figure 22, and Figure 23 where the predicted output power follows the trend of the actual output power. However, it is not exactly the same with the actual output power especially when it is highly fluctuating. This is one of the most challenging tasks when the forecast horizon is in very short-term. This is further illustrated in Table 4 where the performance metrics during power fluctuation events' instances have relatively higher MAE, RMSE, and lower R^2 values than the ones obtained in half a year data. To solve this problem, the BESS is switched on for T_{active} when an event is predicted by the prediction engine. Its prediction rate with respect to T_{active} with 7 days of data is presented in Figure 18. The prediction rate of the developed TS-SOINN is improved to 91.69% when T_{active} is 5 minutes and 97.81% when T_{active} is 30 minutes.

Chapter 6 – Results & Discussions

Table 4: Summary of Performances Metrics during Power Fluctuation Events' Instance

	MAE (%)	RMSE (%)	R ²	Predicted Power Fluctuation Events (%)
TS-SOINN	5.82	9.42	0.90	55.10
E-SOINN	7.74	12.12	0.85	39.07
HBSOINN	8.76	13.57	0.80	34.28
SOINN-DTW	10.31	14.18	0.73	30.61
NARX	11.08	15.51	0.69	28.65
SOM	12.79	17.87	0.62	6.71

Next, the prediction rate of power fluctuation events is discussed. Figure 24 shows the methodology of power fluctuation prediction with 30 minutes of T_{active} . In the figure, the actual events are assigned to level 0.5 with red dots and prediction range are assigned to level 1 with blue line. The number within the blue rectangle are numbers of predicted power fluctuation events, whereas numbers above the blue rectangle are numbers of unpredicted power fluctuation events. There are 157 predicted power fluctuation events predicted and 1 unpredicted power fluctuation events as shown in Figure 24. This shows that the developed TS-SOINN can predict 99.4% of power fluctuation events in a day.

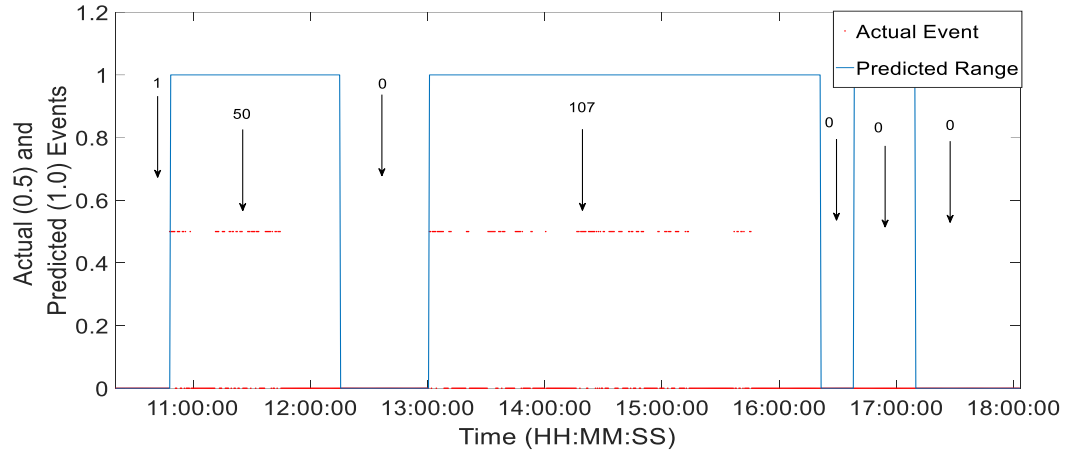


Figure 24: Methodology of Power Fluctuation Prediction where the Red Dots are the Actual Power Fluctuation Events and the Blue Line is the Predicted Range. Red Dots that Fall into the Blue Rectangle is the Early Predicted Event, whereas the Red Dots that Fall Outside the Blue Line is the Unpredicted Event.

Table 5 shows the prediction rate of power fluctuation events for all tested algorithms. From the table, the prediction rate of the developed TS-SOINN and E-SOINN range from 96.23% to 98.48% and 91.25% to 93.75%, respectively throughout the six months duration. The TS-SOINN and E-SOINN have a mean value of 97.46% and 92.69%, respectively. The HBSOINN and SOINN-DTW predict 81.66% and 74.72% of power fluctuation events, respectively. The NARX and SOM networks which are trained with 4 months data predict 84.25% and 68.00% power fluctuation events, respectively. Both NARX and SOM predict 79.87% and 62.71% of power fluctuation events with a month of training data. These scenarios show that increasing sizes of training data increases the performance of the non-incremental algorithms in predicting power fluctuation events. From the table, the developed TS-SOINN outperforms

Chapter 6 – Results & Discussions

other tested algorithms, E-SOINN, HBSOINN, SOINN-DTW, NARX and SOM by 4.77%, 15.80%, 22.74% 13.21% and 29.46%, respectively in terms of predicted power fluctuation events.

Table 6 shows the false acceptance rate of the power fluctuation events for all tested algorithms. The developed TS-SOINN and E-SOINN performance range from 9.58% to 12.23%, and from 11.9% to 12.8%, respectively. The TS-SOINN and E-SOINN have a mean value of 10.51% and 12.39%, respectively. The HBSOINN and SOINN-DTW have a mean false acceptance rate of 13.52% and 11.35%, respectively. For the best NARX and SOM networks have a mean false acceptance rate of 13.16% and 12.44%, respectively. The TS-SOINN outperforms the E-SOINN, HBSOINN, SOINN-DTW, NARX, and SOM by 1.88%, 3.01%, 0.84%, 2.65%, and 1.93%, respectively. The results in these two tables show that the developed TS-SOINN has the highest prediction rate of power fluctuation events, and lower false acceptance rate than the E-SOINN, HBSOINN, SOINN-DTW, NARX and SOM networks.

Table 7 shows the summary of prediction performances from all tested algorithms. Performance metrics such as MAE, RMSE, R^2 and s are collected from the best performing network. The prediction rate and false acceptance rate are collected from the mean value. From the results, the TS-SOINN outperforms E-SOINN, HBSOINN, SOINN-DTW, NARX, and SOM in terms of MAE, RMSE, R^2 , s , predicted power fluctuation events and false acceptance rate.

Table 5: Prediction Rate of Power Fluctuation Events for Tested Algorithms

	Training Data	Jul	Aug	Sept	Oct	Nov	Dec	Mean
TS-SOINN	Active Learning	96.23%	96.96%	98.11%	97.67%	98.48%	97.30%	97.46%
E-SOINN	Active Learning	91.25%	92.67%	91.56%	93.23%	93.68%	93.75%	92.69%
HBSOINN	Semi-Supervised	-	81.27%	81.33%	81.62%	82.59%	81.47%	81.66%
SOINN-DTW	Semi-Supervised	-	74.58%	75.21%	74.64%	74.39%	74.76%	74.72%
NARX	4 Months	-	-	-	-	85.30%	83.20%	84.25%
SOM		-	-	-	-	67.35%	68.65%	68.00%
NARX	3 Months	-	-	-	84.26%	82.35%	81.25%	82.62%
SOM		-	-	-	65.82%	65.81%	66.69%	66.11%
NARX	2 Months	-	-	80.19%	81.68%	80.57%	80.96%	80.85%
SOM		-	-	63.89%	62.34%	63.12%	64.25%	63.40%
NARX	1 Month	-	79.52%	79.85%	79.82%	80.02%	80.16%	79.87%
SOM		-	62.30%	61.65%	63.25%	62.78%	63.59%	62.71%

Table 6: False Acceptance Rate for Tested Algorithms

	Training Data	Jul	Aug	Sept	Oct	Nov	Dec	Mean
TS-SOINN	Active Learning	12.23%	11.87%	10.19%	9.60%	9.59%	9.58%	10.51%
E-SOINN	Active Learning	12.46%	12.84%	12.65%	12.40%	11.90%	12.10%	12.39%
HBSOINN	Semi-Supervised	-	13.27%	13.52%	13.89%	13.43%	13.48%	13.52%
SOINN-DTW	Semi-Supervised	-	11.43%	11.27%	11.52%	11.17%	11.38%	11.35%
NARX	4 Months	-	-	-	-	13.46%	12.85%	13.16%
SOM		-	-	-	-	12.20%	12.68%	12.44%
NARX	3 Months	-	-	-	13.39%	13.54%	13.28%	13.40%
SOM		-	-	-	10.87%	12.25%	11.98%	11.70%
NARX	2 Months	-	-	13.28%	13.69%	14.02%	13.69%	13.67%
SOM		-	-	10.36%	11.85%	12.04%	11.46%	11.43%
NARX	1 Month	-	13.38%	13.57%	14.38%	14.82%	14.38%	14.11%
SOM		-	10.85%	11.57%	11.38%	10.93%	10.82%	11.11%

Table 7: Summary of Prediction Performances for Tested Algorithms

Algorithm	TS-SOINN	E-SOINN	HBSOINN	SOINN-DTW	SOM	NARX
MAE (%)	1.56	1.70	2.97	3.48	3.58	2.89
RMSE (%)	3.75	4.23	5.75	6.42	7.84	5.59
R ²	0.95	0.93	0.87	0.82	0.78	0.90
s	0.35	0.27	0.01	-0.11	-0.35	0.04
Prediction Rate of Power Fluctuation Events (%)	97.46	92.69	81.66	74.72	68.00	84.25
False Acceptance Rate (%)	10.51	12.39	13.52	11.35	12.44	13.16

6.1.3 Experimental Analysis

This section shows the experimental analysis of the proposed TS-SOINN. The setup of this experiment is described and shown as in Figure 16. This experiment ran on 7th of January 2018 (5.00 P.M) to 7th of February 2018.

Compared to the simulation results, the MAE of the experimental result is higher by 0.17%. The experimental result of RMSE is higher than the simulation result by 0.20%. Figure 25 shows the scatter plot of actual versus predicted output power in the experiment. The experimental R^2 value is close to the simulation result which is 0.92. The s of the experimental result is 0.32 which is 0.03 lower than the simulation result. Slight reductions in measurements are due to factors that are unable to be considered during simulation such as shading from the environment obstacles (building and tree). Thus, these results validate the proposed TS-SOINN is applicable in real life.

Chapter 6 – Results & Discussions

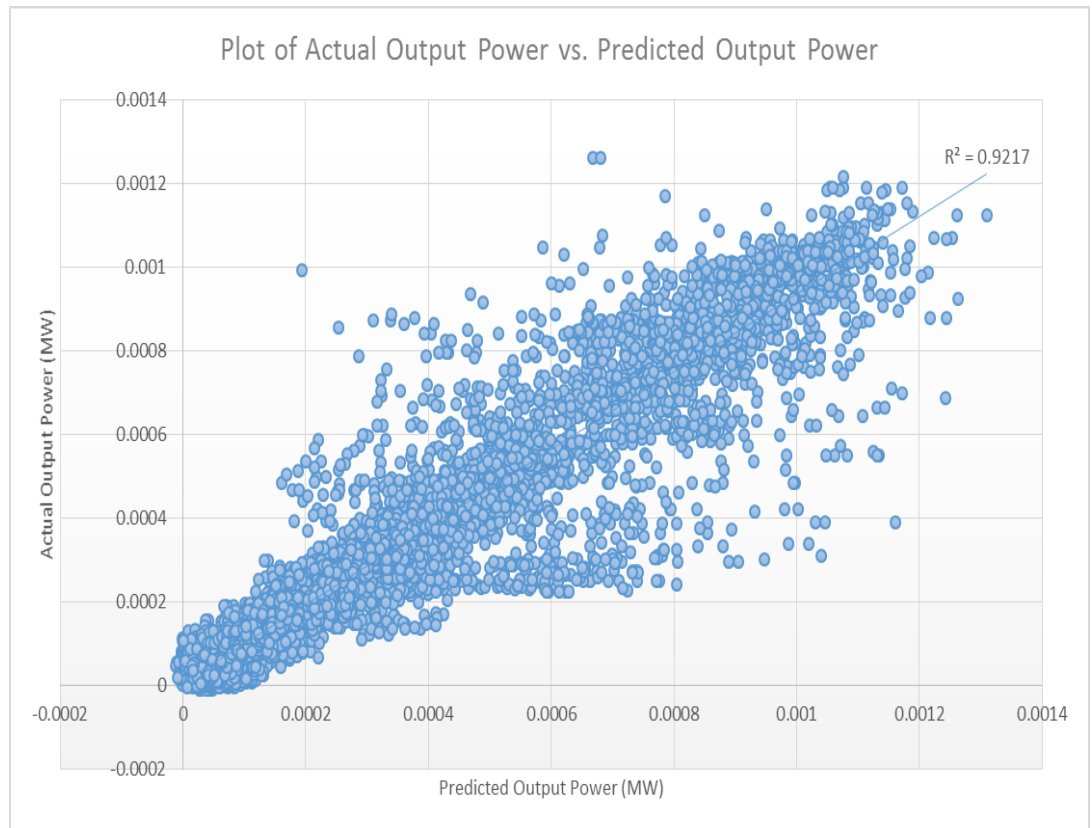


Figure 25: Scatter of Actual Output Power versus Predicted Output Power (Experiment)

Table 8: Performance Metrics of TS-SOINN in Simulation and Experiment

Measurement	Simulation	Experiment
MAE (%)	1.56	1.73
RMSE (%)	3.75	3.95
R^2	0.95	0.92
s	0.35	0.32

Chapter 6 – Results & Discussions

The predicted and actual output power of the PV system are shown in Figure 26. From the graph, the output power of the PV system fluctuates largely from 1030 to 1500 on the 10th of January 2018. Although the actual output power fluctuates largely, the predicted output power follows the actual output power's trend closely. This plot shows that the proposed TS-SOINN predicts the output power in real-life accurately.

Figure 27 shows the plot of predicted and occurrence of power fluctuation events on the 10th of January 2018. From the plot, the TS-SOINN predicted the events before its occurrence and all 108 power fluctuation events happened on 10th of January 2018 are predicted. Figure 27 also shows a scenario where the TS-SOINN predicted a non-existence event. This can be seen in the smaller blue rectangle in Figure 27, as there is no event in the second rectangle. This type of early warning is switched off in short time as the TS-SOINN does not identify any possible power fluctuation events later. Since the TS-SOINN is able to predict and give early prediction warning before the power fluctuation events happen, it is able to prevent the power fluctuation events while the ESS is available.

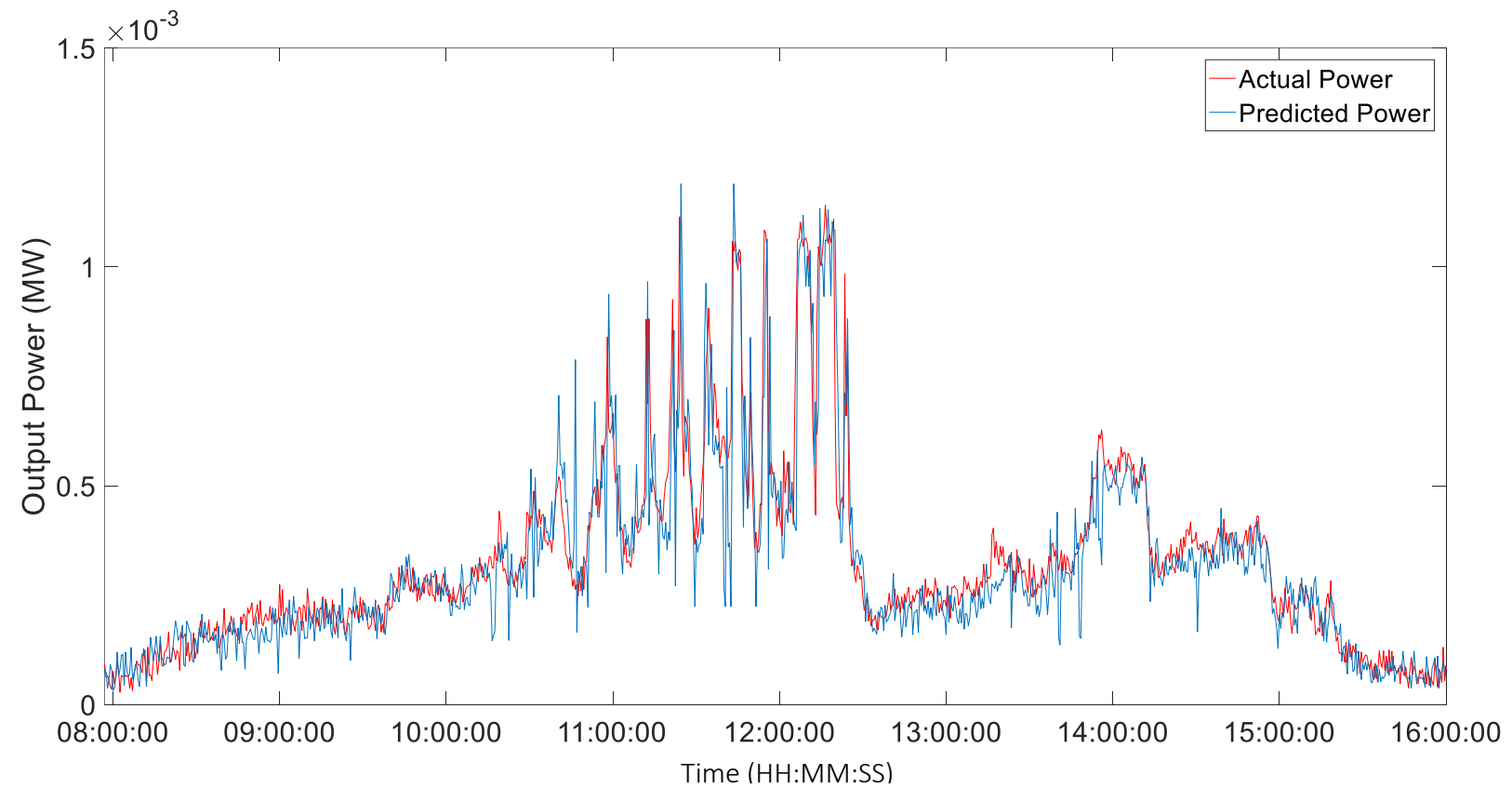


Figure 26: Graph of Actual Power versus Predicted Power on 10th of January 2018

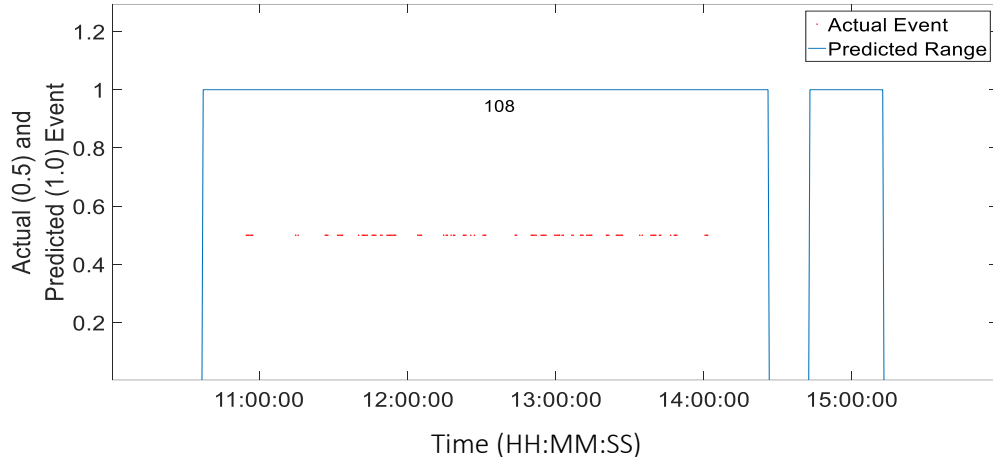


Figure 27: Graph of Predicted and Occurrence of Power Fluctuation Events (Experiment)

Table 9 shows the performances in predicting power fluctuation events during simulation and experiment. From the table, the TS-SOINN predicts 99.72% of the power fluctuation events in a month during the experiment, which is higher than the simulation stage by 2.26%. In addition, the experimental stage has a higher false acceptance rate than the simulation stage by 1.48%, which is 11.99%. Both experimental and simulation stages' results are very close. Therefore, the experimental results validate the simulation results.

Table 9: Performances in Predicting Power Fluctuation Events

	Simulation	Experiment
Predicted Power Fluctuation Events (%)	97.46	99.72
False Acceptance Rate (%)	10.51	11.99

6.2 Intelligent Real-Time PMS

This section analyses the performance of the developed intelligent real-time PMS. Firstly, the optimised parameter values for the PMS are obtained. Then its performance in mitigating the power fluctuation events is evaluated. The developed PMS performance is compared with the conventional hourly rule-based controller [2] and dynamic ramp rate controller [16].

The developed PMS, conventional hourly rule-based controller [2] and dynamic ramp rate controller [16] are used to control the BESS to dispatch ancillary power to the power network to smoothen power fluctuation events. The capacity of the battery is set to be 20% rated power of the PV system (54 kWh) for all tested PMS.

6.2.1 Optimisation of Parameters

The update time T_{update} and limiting threshold Th_m are the parameters for the intelligent PMS to be determined. Seven days of data are used to identify the optimum parameters for the developed PMS. Figure 28 shows the percentage of mitigated power fluctuation events versus different update times. From the figure, it is found that the update time of 2.5 minutes has the highest percentage of mitigated power fluctuation events. Thus, 2.5 minutes is selected as the update time.

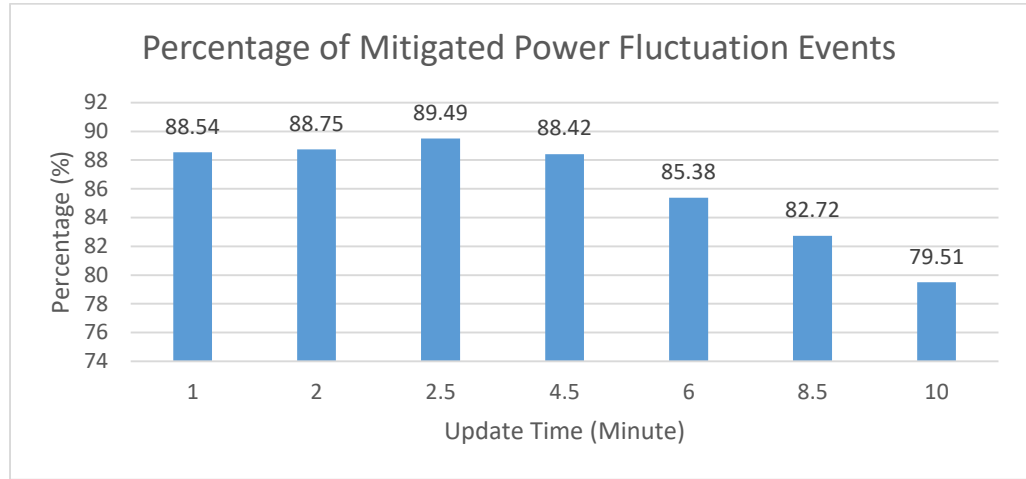


Figure 28: Percentage of Mitigated Power Fluctuation Events versus Different Update Times

Next, the optimal value for the limiting threshold Th_m is determined. Figure 29 shows the percentage of mitigated power fluctuation events against different limiting thresholds. From the figure, 5% of the rated capacity achieves the highest mitigation rate. Therefore, limiting threshold Th_m is set as 5% of the rated capacity of the PV system.

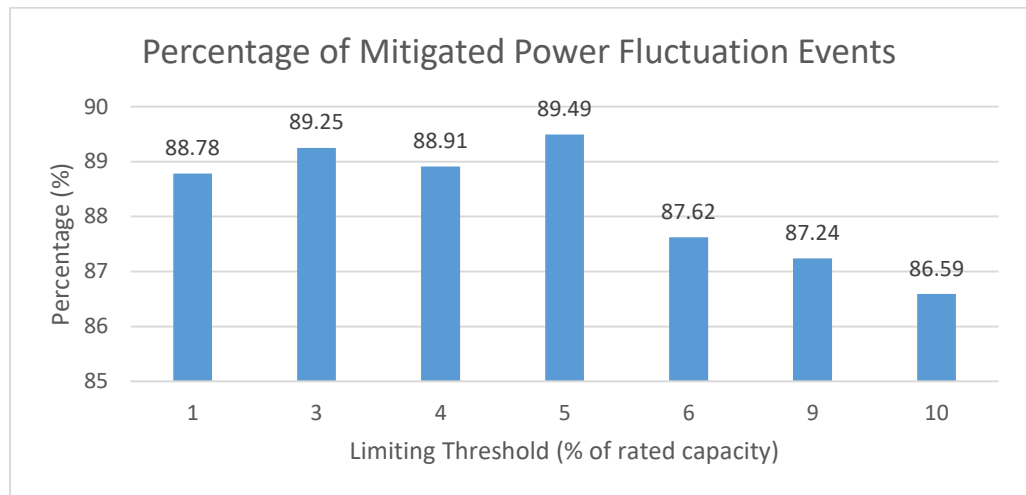


Figure 29: Percentage of Mitigated Power Fluctuation Events against Different Limiting Thresholds

6.2.2 Performance Evaluation

Thirty days of real-life irradiance and temperature from 0900 to 1800 are fed into the modelled PV system to identify the performance of the mitigation engine. The performance of the developed PMS is verified in three stages: 1) the performance of the modelled BESS controller, 2) the PV power and the output power at the PCC, 3) the developed system is compared with the conventional hourly rule-based controller [2] and dynamic ramp rate controller [16] in terms of SOC, number of mitigated events, and generate energy at the PV and PCC.

The BESS controller is a vital element in this work where it converts required energy from DC to alternating current (AC). If the BESS controller is unable to operate according to $P_{BESS,ref}$, the PMS will be unable to smooth power fluctuation events. Figure 30 shows a graph where P_{PV} (red dotted) overlaps with P_{PCC} (blue line) and $P_{PCC,ref}$ (black line). Figure 30 shows that although the red dotted fluctuates largely, the blue line increases and decreases according to the black dashed line. Thus, it proves that the PI controller is able to control the P_{BESS} to output according to the developed PMS.

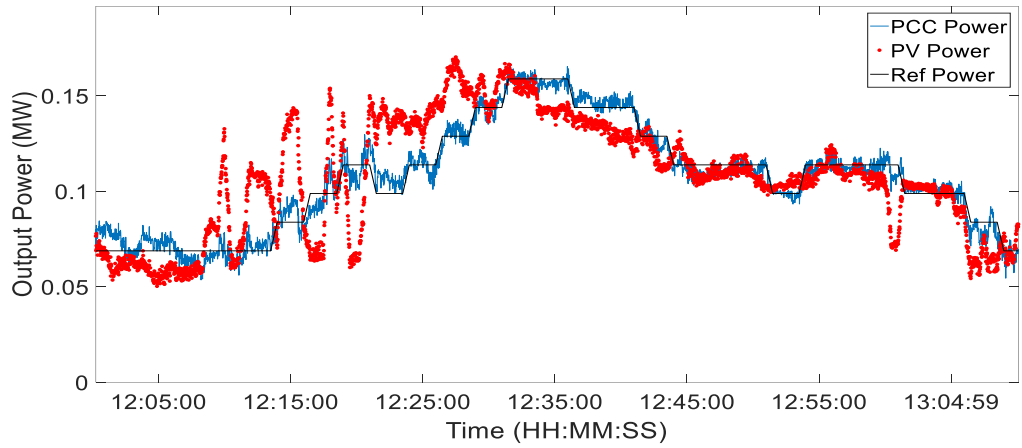


Figure 30: Performance of the BESS Controller

Figure 31 shows the output power of the PV system and the PCC power for a day. From 0900 to 1030, the output power of the PV system and the PCC overlap with each other because the TS-SOINN does not predict any power fluctuation events and the PMS does not switch on. After 1030, although the output power of the PV system increases or decreases greatly within a short time, power at the PCC follows the trend at a slower speed to prevent power fluctuation events. This is because the TS-SOINN predicts a power fluctuation event, and it switches on the PMS. To further verify the above statement, Figure 32 shows the zoomed in version of Figure 31, where the red dots are output power of the PV system and the blue line is power at the PCC. From Figure 32, the red dots fluctuate from 0.14 MW to 0.06 MW from 1323 to 1325. However, power at the PCC maintains the fluctuation level within 10% of rated capacity which is 0.027 MW. This scenario shows that the developed PMS supplies adequate ancillary power to the PCC to reduce fluctuation rate at the PCC.

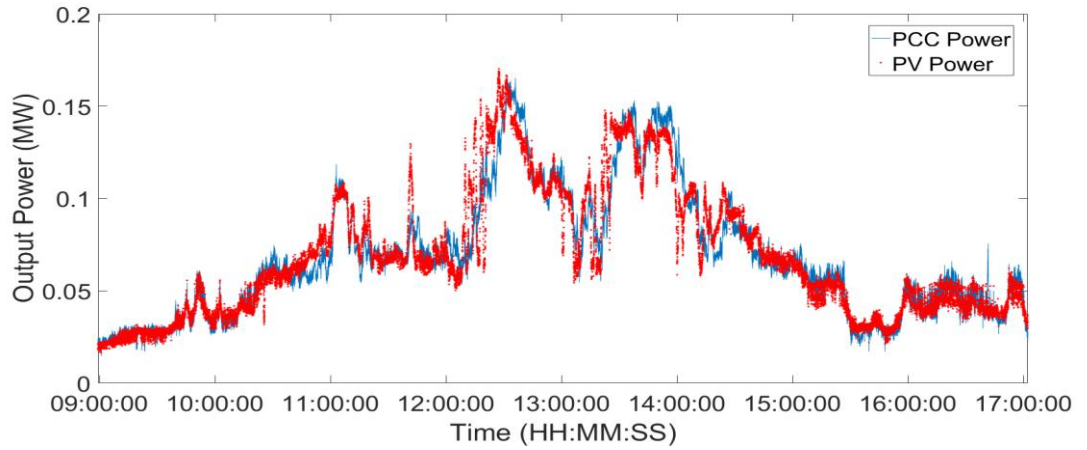


Figure 31: PV Power (Red Dotted) versus PCC Power (Blue Line)

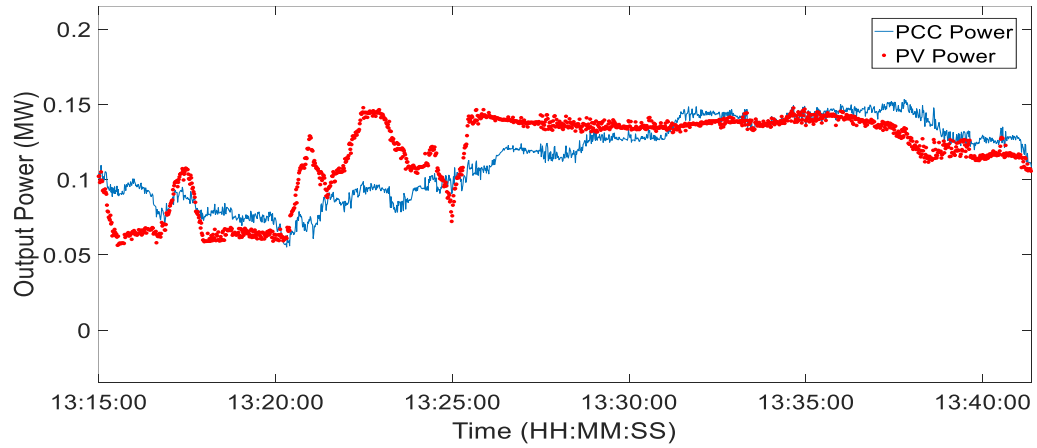


Figure 32: Graph of PCC Power versus PV Power (Zoomed In)

Since the developed intelligent PMS is implemented into the PV grid-tied system, stability of the system needs to be tested. Figure 33 shows the root mean square (RMS) voltage and frequency at the PCC after the developed PMS integrates into the PV grid-tied system. From the RMS voltage and frequency plots, it can be seen that the voltage is within 0.9 P.U and 1.1 P.U, and frequency are within ± 2 Hz. Thus, the PV grid-tied system remains stable after implementation of the developed intelligent PMS.

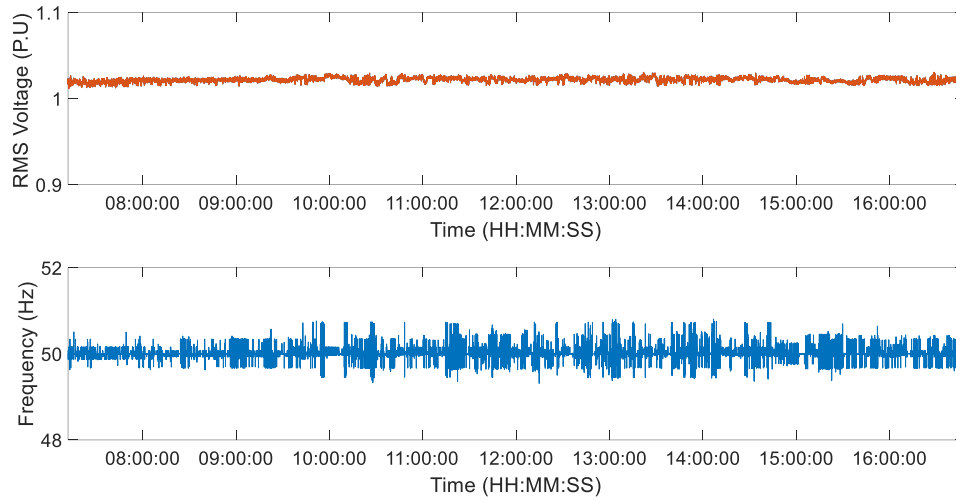


Figure 33: RMS Voltage (Top) and Frequency (Bottom) at the PCC

Table 10 shows the mitigated power fluctuation events by the developed PMS. From Table 10, it has a total of 2365 power fluctuation events. When the developed PMS is integrated into the PV grid-tied system, the total number of events is reduced to 257, which is a reduction of 89.13 %. Unpredicted events by the TS-SOINN algorithm and limitation of the BESS to deal with sudden large increase and decrease of power in an extremely short time are the reasons for the 257 unmitigated events.

Table 10: Number of Mitigated and Unmitigated Event

Power Fluctuation Events	PV System (Unmitigated)	PCC (Mitigated)
Number of events	2365	257
Percentage of events (%)	100	10.87

Chapter 6 – Results & Discussions

The SOC of the battery is then discussed. Figure 34 shows a day output power of the proposed system (top plot) and SOC of the battery (bottom plot). From Figure 34, the SOC of the battery maintains in between 30% to 100%. A sharp increase or decrease in SOC is caused by a sudden increase or decrease of PV power. The short update time (2.5 minutes) reduces the difference between the reference power and the actual PV power. Thus, the SOC of the BESS can maintain within the permissible range.

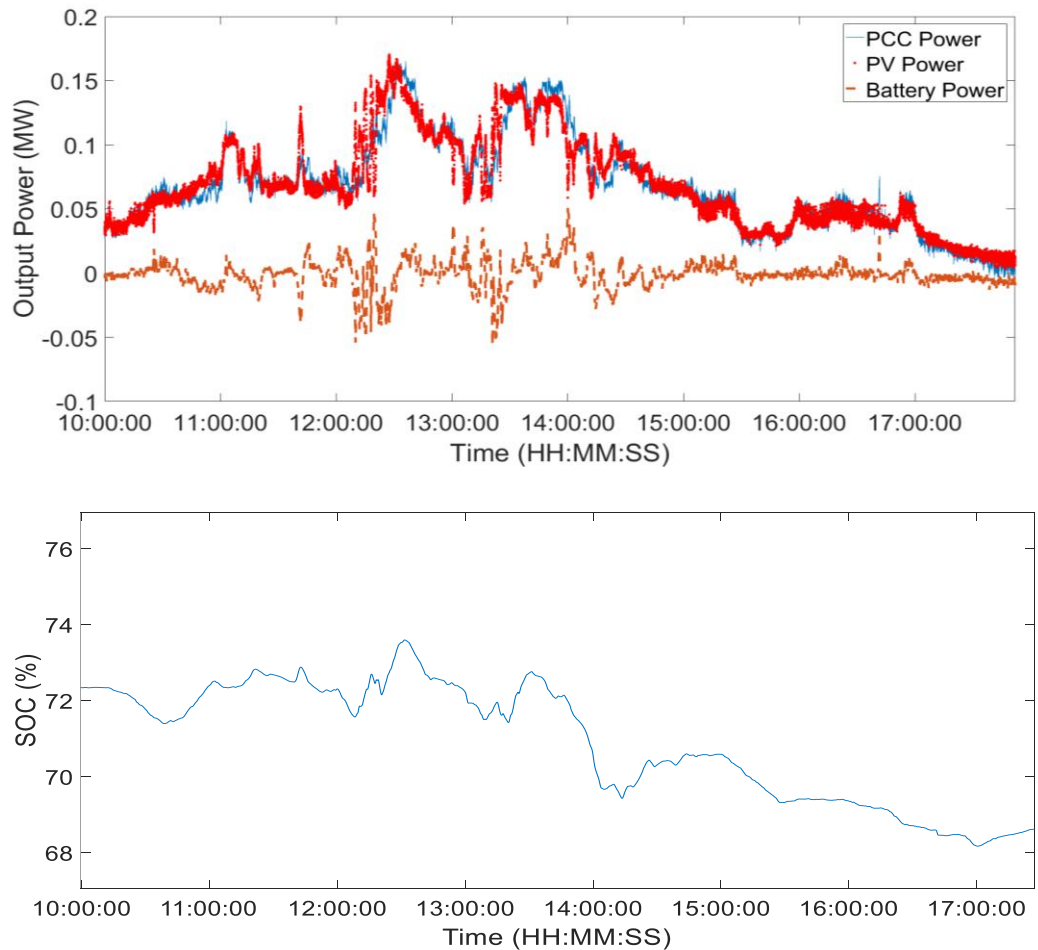


Figure 34: Simulation of PV Grid-Tied System with Developed PMS for a Complete Day. Top Plot: PCC (blue), PV (red), and Battery (brown) Active Power. Bottom plot: Battery SOC

6.2.3 Performance Comparison

Performance of the developed PMS is then compared with the conventional hourly rule-based controller in [2], and dynamic ramp rate control in [16]. Figure 35, Figure 36 and Figure 37 show SOC of BESS in three different days which is controlled by the developed PMS, hourly ruled-based controller, and ramp rate controller. From the figures, the hourly ruled-based controller works within 30% to 100% of SOC. Since the hourly ruled-based controller works at the boundary of 30% and 100%, it indicates the power fluctuation events that happen within that period are unable to be smoothened. From the plots, the developed PMS operates within 50% to 80% of SOC. This shows that the developed PMS is able to operate at all time to mitigate power fluctuation events as the SOC does not work at the boundary region (30% and 100%). For the ramp-rate controller, it works within 60% and 70% of SOC. The smallest SOC operation region is due to the ramp-rate controller is switched on when the ramp rate of output power is more than 450Ws^{-1} .

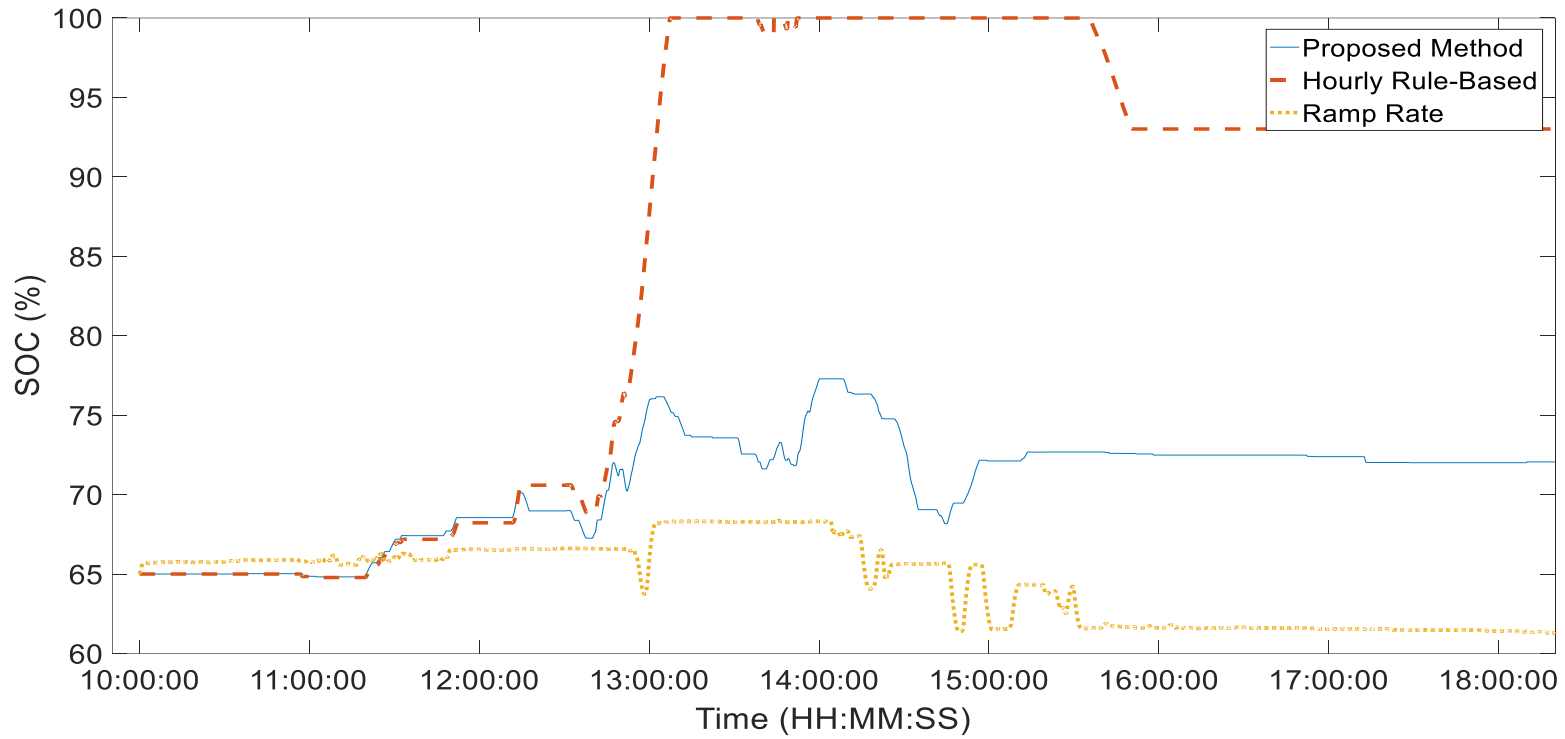


Figure 35: SOC of BESS by the Developed PMS, Hourly Rule-Based and Ramp Rate Controller for day 3

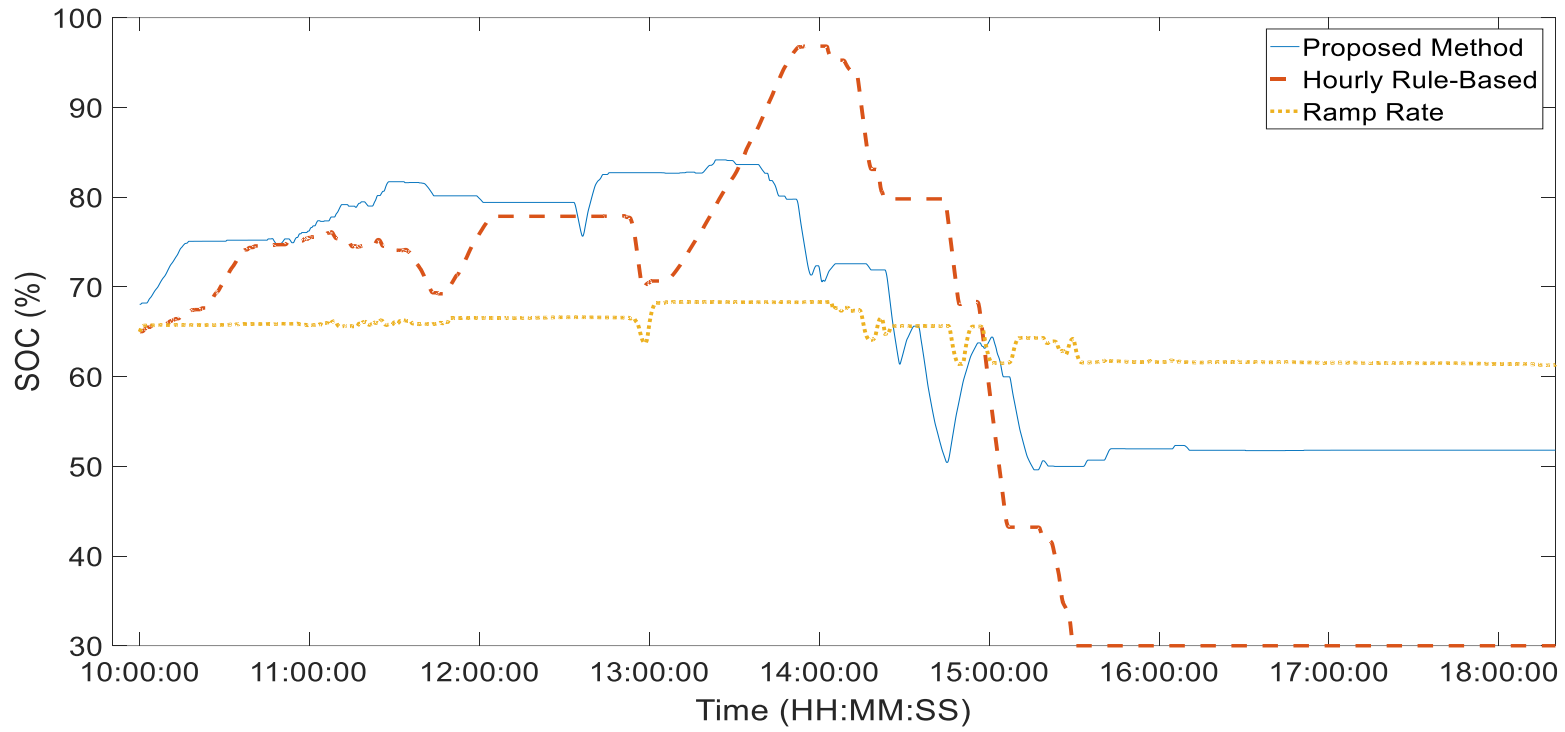


Figure 36: SOC of BESS by the Developed PMS, Hourly Rule-Based and Ramp Rate Controller for day 8

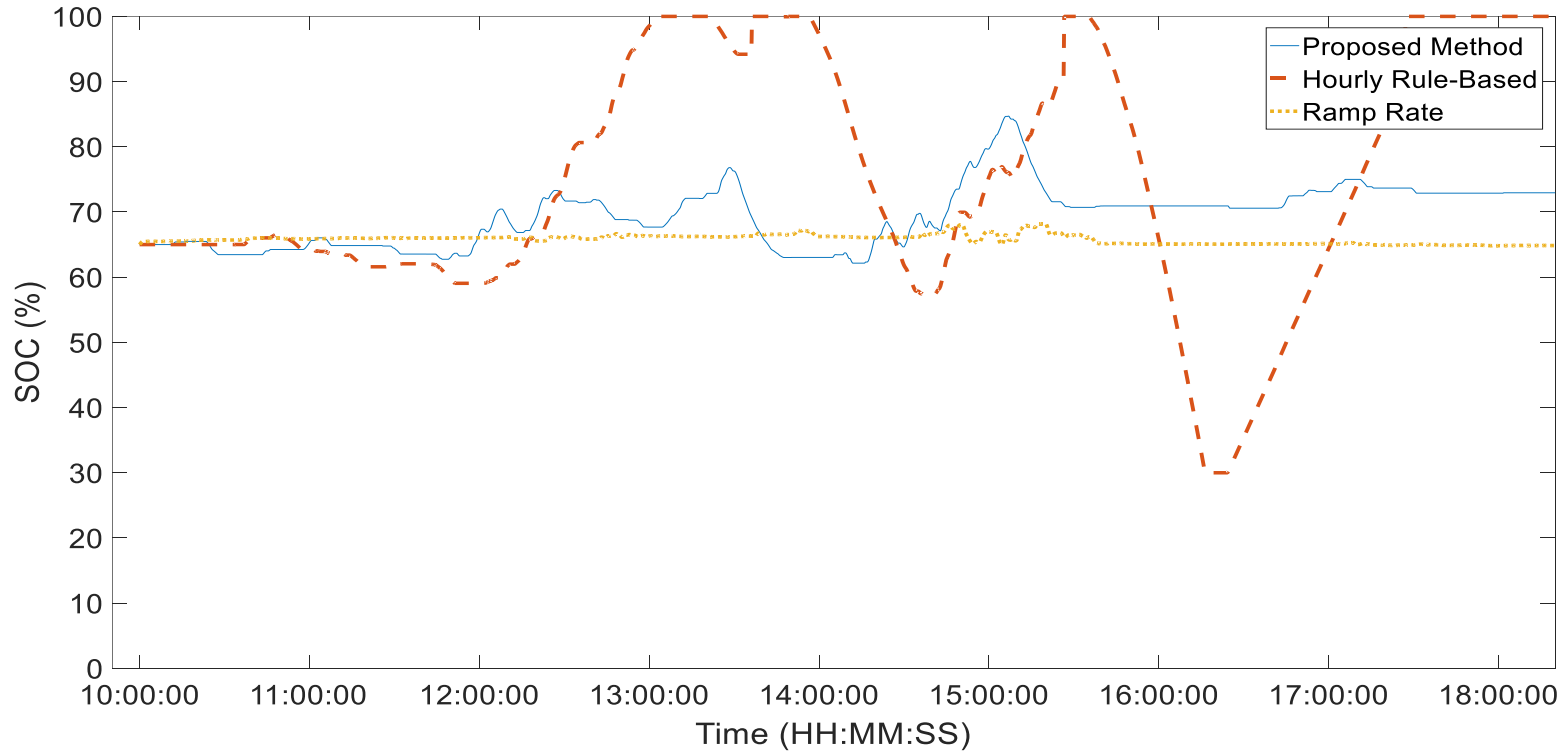


Figure 37: SOC of BESS by the Developed PMS, Hourly Rule-Based and Ramp Rate Controller for day 15

Figure 38 shows the fluctuation rate at the PCC by different methods. From the figure, 7.3% of the data (a month data with 30 seconds resolution) or 2365 events exceed 10% of fluctuation level at the PCC. By implementing the developed PMS, dynamic ramp rate control and hourly rule-based control, the power fluctuation events drop to 0.8%, 3.5% and 4.7%, respectively. The detailed performances are summarised in Table 11.

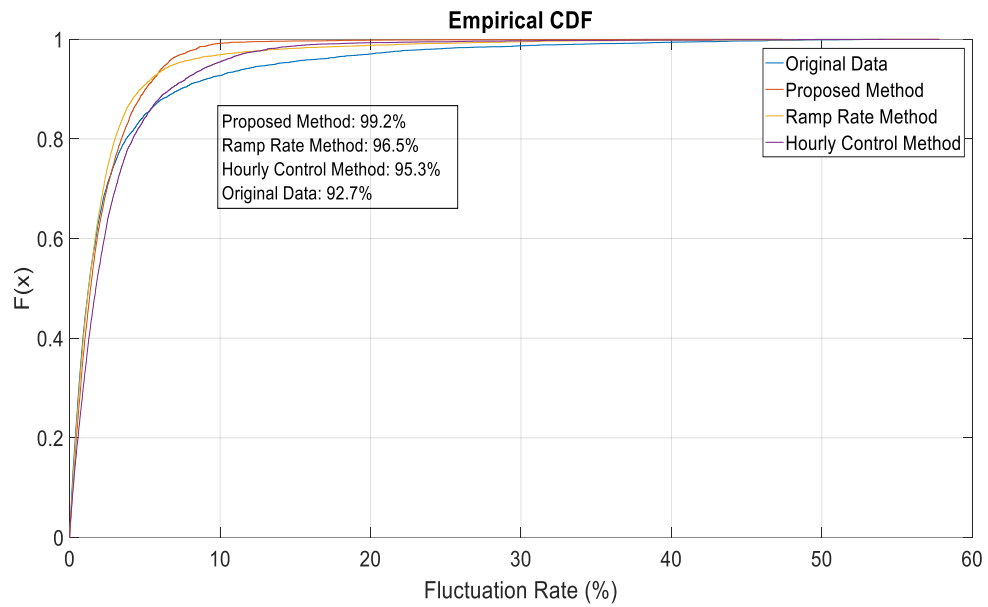


Figure 38: Cumulative Distribution Function Analysis of Ramp Rate at PCC of Original Data (blue), Developed PMS (Red), Ramp Rate Method (Orange), and Hourly Control (Purple)

From Table 11, the developed PMS mitigates 89.13% of power fluctuation events whereas the hourly rule-based controller and the dynamic ramp rate control mitigate 35.60% and 52.05% of power fluctuation events, respectively. This shows that the developed PMS mitigates the most number of

Chapter 6 – Results & Discussions

power fluctuation events with a similar rating of BESS. In another word, the developed PMS mitigates power fluctuation events with a smaller rating of BESS (as hourly rule-based and dynamic ramp rate could mitigate 89.13% power fluctuation events with a higher rating of BESS). This indicates the developed PMS reduces the cost to enhance the reliability of PV grid-tied system.

The hourly rule-based controller has the lowest performance because it dispatches ancillary power in hourly basis. This causes a large difference between reference power and actual PV power, and the BESS has to dispatch a large amount of ancillary power to smoothen the power fluctuation events. As a consequence, the capacity of the BESS reaches its limit and unable to operate. The ramp rate controller has a lower performance than the developed PMS because the characteristic of PI controller is high in overshoot and settling time, but low in steady-state error. Since the ramp rate controller updates the $P_{PCC,ref}$ at every instance, the varying reference signal has a high possibility to experience overshoot from the PI controller. In contrast, the developed PMS updates the $P_{PCC,ref}$ (as it updates for every 2.5 minutes) in a lower frequency, this reduces the chance of overshooting as it has sufficient time to reach steady-state. This can be seen from Figure 39 where the PI error of developed system within ± 0.03 whereas PI error of the ramp rate controller is ± 0.12 . As a result, the ancillary power is unable to behave as the reference signal and causes a lower mitigation rate.

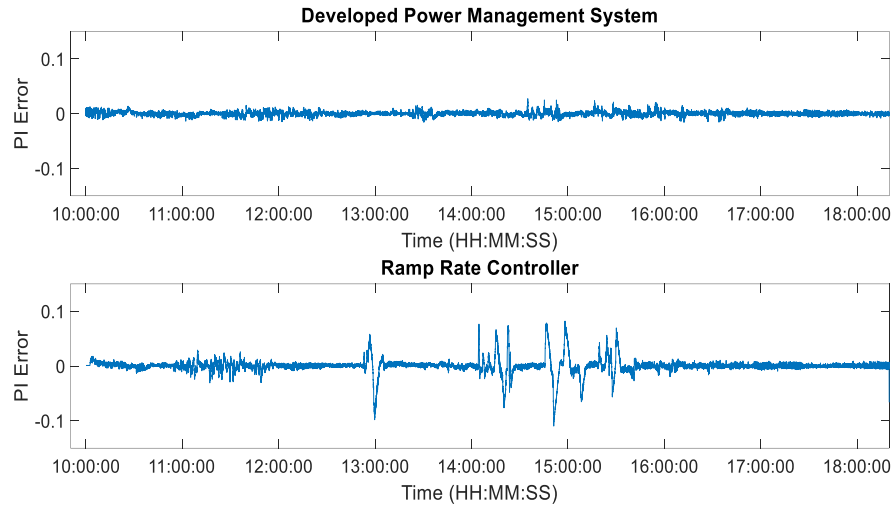


Figure 39: PI Error for Developed System and Ramp Rate Controller

The total energy injected into the grid by different methods is then evaluated. Total energy injected to the grid for a day is 476.35 kWh on average. This number reduces to 467.42 kWh, 449.36 kWh and 469.01 kWh for the developed system, hourly rule-based controller and ramp-rate controller, respectively. The reduction of energy is due to the output power of the PV system increases in high speed and the BESS has to absorb energy to prevent power fluctuation events. From the results, the ramp rate controller outperforms the developed system by 0.33%. It is because the ramp rate controller updates the reference signal rapidly, whereas the developed system updates the reference signal in a lower frequency. However, the developed system reduces the possibility of overshooting by the PI controller and outperforms the ramp rate controller in terms of mitigated events by 37.08%. The developed system

Chapter 6 – Results & Discussions

outperforms the hourly control method in terms of mitigated events and loss of energy by 53.53% and 3.80%, respectively.

To conclude, the developed system mitigates the most power fluctuation events (89.13%), with energy losses of 1.87%. It requires 30% of SOC to achieve these performances. The hourly rule-based controller mitigates the least event which is 35.60%, with energy losses of 5.67%. It also needs to work with a larger operation region compared to the developed system which is 70% to accomplish these results. These results show that the developed system outperforms hourly rule-based controller. Lastly, the ramp rate controller reduces 52.05% power fluctuation events with energy losses of 1.54%. It requires 10% of SOC operation region to obtain these results. These results show that the developed system outperforms the ramp rate controller in terms of mitigated events by 37.08%, whereas the ramp rate controller outperforms the developed system in terms of energy losses and SOC operation region by 0.33% and 20%, respectively.

Chapter 6 – Results & Discussions

Table 11: Summary of PMS Performances

Mitigation Method	Developed System	Hourly Control [2]	Ramp Rate Control [16]
Number of mitigated events	2108	842	1231
Total number of events	2365	2365	2365
Percentage of mitigated events (%)	89.13	35.60	52.05
Energy from the PV (kWh)	476.35	476.35	476.35
Energy from the PCC (kWh)	467.42	449.36	469.01
Energy Loss (%)	1.87	5.67	1.54
SOC Operation Region	50% - 80%	30%-100%	60%-70%

6.3 Summary

In conclusion, the performance of the TS-SOINN is compared with E-SOINN, SOINN-DTW, HBSOINN, SOM, and NARX algorithms in predicting the output power of a PV system and subsequently power fluctuation events. Based on the results in predicting output power, TS-SOINN outperforms tested algorithms in terms of MAE, RMSE, R^2 and s . TS-SOINN also has the highest prediction rate and lowest false acceptance rate in predicting power fluctuation event, which is 97.46% and 10.51%, respectively. These results are validated experimentally.

Next, the performance of the intelligent real-time PMS is evaluated. The performance of the developed PMS is compared with the conventional hourly rule-based controller and the dynamic ramp rate controller. Results show that the developed PMS mitigates 89.13% of the power fluctuation event which outperforms the conventional hourly rule-based controller and the dynamic ramp rate controller.

Chapter 7 Conclusions

The research work reported in the thesis dealt with developing an active learning classification and prediction engine for a PMS to mitigate power fluctuation events in a PV grid-tied system.

The research work sought to investigate and solve the research issues arising from highly fluctuate and random behaviour of PV output power. When the intermittent PV output power has a fluctuation rate of 10% of rated capacity within a minute, it is known as a power fluctuation event. A power fluctuation event could break the supply and demand of electrical power and create other power quality events to the power network such as voltage flicker, frequency fluctuation, and voltage sag. Therefore, when the penetration of the PV system is high, the adverse impact of power fluctuation is more severe. This phenomenon limits the penetration of the PV system to the power networks as the reliability of the PV system is low. The main achievement in this research work is to enhance the reliability of the PV grid-tied system by integrating an intelligent real-time PMS into a PV grid-tied system to mitigate power fluctuation event due to PV system. The intelligent real-time PMS is composed of an active learning classification and prediction engine, and a mitigation engine based on BESS.

The developed TS-SOINN is an active learning classification and prediction engine. It takes in irradiance, temperature and PV output power to forecast output power and subsequently predicts power fluctuation events in a PV grid-tied system. A novel associate memory and a weighted tapped delay line are equipped in the TS-SOINN to advance the current incremental unsupervised learning algorithm to incremental time-series prediction. Both simulation and experimental results showed that the TS-SOINN achieves better performance than SOM, NARX, SOINN-DTW, HBSOINN and E-SOINN in terms of MAE, RMSE, R^2 , s , the prediction rate of power fluctuation events and false acceptance rate.

A mitigation engine based on a BESS with a rule-based controller is then developed to supply ancillary power to the grid to smooth power fluctuation events. The mitigation engine is switched on when the TS-SOINN predicts power fluctuation events. It updates the reference power to the BESS in 2.5 minutes and then supplies the power deficit to the grid accordingly.

A PV grid-tied system is modelled in the PSCAD environment. Performance of the developed intelligent real-time PMS is tested and validated in this modelled PV micro-grid system. Besides, a laboratory scale PV grid-tied system is designed and constructed in the UNM's Solar Cabin to validate the performance of the TS-SOINN algorithm experimentally.

By using real-life environment data, the developed TS-SOINN based real-time prediction engine predicts power fluctuation events with a high prediction rate of 97.46%. The high prediction rate of the TS-SOINN is validated experimentally. In addition, results show that the developed PMS reduces 89.13% of power fluctuation event with an energy loss of 1.87% and the battery's SOC maintains within 30% to 100%. The developed PMS outperforms hourly rule-based controller and the ramp-rate controller by 53.53% and 37.08%, respectively in terms of the mitigated power fluctuation events.

7.1 Future Works

During the development of this research work, it is observed that the response time is slow in a battery. This can be solved by integrating an ESS which has a faster response time such as the supercapacitor. Supercapacitor can mitigate power fluctuation events that occur within few seconds with a large amplitude. It can also serve as a secondary ESS to smooth the power fluctuation when the battery's SOC is less than 30%. Besides, prediction on other power quality events is suggested. Since there are several types of power quality events, it would enhance the reliability of the PV system if these power quality events are predictable.

REFERENCES

- [1] S. Shivashankar, S. Mekhilef, H. Mokhlis, and M. Karimi, "Mitigating methods of power fluctuation of photovoltaic (PV) sources – A review," *Renew. Sustain. Energy Rev.*, vol. 59, pp. 1170–1184, 2016.
- [2] S. Teleke, M. E. Baran, S. Bhattacharya, and A. Q. Huang, "Rule-based control of battery energy storage for dispatching intermittent renewable sources," *IEEE Trans. Sustain. Energy*, vol. 1, no. 3, pp. 117–124, 2010.
- [3] M. Z. Daud, A. Mohamed, and M. A. Hannan, "An improved control method of battery energy storage system for hourly dispatch of photovoltaic power sources," *Energy Convers. Manag.*, vol. 73, pp. 256–270, 2013.
- [4] L. Li, Q. Ding, H. Li, and M. Dan, "Optimal dispatching method for smoothing power fluctuations of the wind-photovoltaic-battery hybrid generation system," *IEEE Innov. Smart Grid Technol. - Asia, ISGT Asia*, no. 20, pp. 1–6, 2012.
- [5] S. Koochi-Kamali, N. A. Rahim, and H. Mokhlis, "Smart power management algorithm in microgrid consisting of photovoltaic, diesel, and battery storage plants considering variations in sunlight, temperature, and load," *Energy Convers. Manag.*, vol. 84, pp. 562–582, 2014.
- [6] Y. Xu *et al.*, "Assessing Short-Term Voltage Stability of Electric Power Systems by a Hierarchical Intelligent System," *IEEE Trans. Neural Networks Learn. Syst.*, vol. 27, no. 8, pp. 1686–1696, 2016.
- [7] J. Rodway, S. Member, P. Musilek, S. Member, S. Misak, and L. Prokop, "Prediction of PV Power Quality: Total Harmonic Distortion of Current," in *IEEE Electrical Power and Energy Conference*, 2013, pp. 1–4.
- [8] S. Furao, T. Ogura, and O. Hasegawa, "An enhanced self-organizing incremental neural network for online unsupervised learning," *Neural Networks*, vol. 20, no. 8, pp. 893–903, 2007.
- [9] R. Hara, H. Kita, T. Tanabe, H. Sugihara, A. Kuwayama, and S. Miwa, "Testing the technologies: Demonstration Grid-connected photovoltaic projects in Japan," *IEEE Power Energy Mag.*, vol. 7, no. 3, pp. 77–85, 2009.
- [10] J. Antonanzas, N. Osorio, R. Escobar, R. Urraca, F. J. Martinez-de-Pison, and F. Antonanzas-Torres, "Review of photovoltaic power forecasting," *Sol. Energy*, vol. 136, pp. 78–111, 2016.
- [11] S. Sobri, S. Koochi-Kamali, and N. A. Rahim, "Solar photovoltaic generation forecasting methods: A review," *Energy Convers. Manag.*, vol. 156, no. May 2017, pp. 459–497, 2018.
- [12] H. T. Siegelmann, B. G. Horne, and C. L. Giles, "Computational capabilities of recurrent NARX neural networks," *IEEE Trans. Syst. Man, Cybern. Part B Cybern.*, vol. 27, no. 2, pp. 208–215, 1997.
- [13] S. Okada, O. Hasegawa, and T. Nishida, "Machine Learning Approaches

- for Time-Series Data Based on Self-Organizing Incremental,” in *International Conference on Artificial Neural Networks*, 2010, pp. 541–550.
- [14] H. Xie, H. Tang, and Y.-H. Liao, “Time Series Prediction Based on NARX Neural Networks: An advanced approach,” in *International Conference on Machine Learning and Cybernetics*, 2009, pp. 1275–1279.
 - [15] T. Kohonen, “The Self-organizing Map,” *Proc. IEEE*, vol. 78, no. 9, pp. 1464–1480, 1990.
 - [16] I. De Parra, L. Marroyo, J. Marcos, and M. Garci, “Control strategies to use the minimum energy storage requirement for PV power ramp-rate control,” *Sol. Energy*, vol. 111, pp. 332–343, 2015.
 - [17] A. Kusko and M. Thompson, *Power Quality in Electrical Systems*, 1 edition. McGraw-Hill Education, 2007.
 - [18] R. B. Digambar, S. K. Ravishankar, and J. Saurabh, “Impact of Distributed Generation on Power System Stability,” in *International Conference on Innovative Mechanisms for Industry Applications*, 2017, pp. 122–125.
 - [19] Y. S. Lim and J. H. Tang, “Experimental study on flicker emissions by photovoltaic systems on highly cloudy region: A case study in Malaysia,” *Renew. Energy*, vol. 64, pp. 61–70, 2014.
 - [20] Y. Noro *et al.*, “Power fluctuation suppression system for large scale PV,” in *2012 IEEE PES Transmission and Distribution Conference and Exposition (T&D)*, 2012, pp. 1–6.
 - [21] M. Farhoodnea, A. Mohamed, H. Shareef, and H. Zayandehroodi, “Power Quality Analysis of Grid-Connected Photovoltaic Systems in Distribution Networks,” *PRZEGLĄD ELEKTROTECHNICZNY*, no. 2a, pp. 208–213, 2013.
 - [22] J. Marcos, L. Narvarte, I. Berazaluze, R. González, and J. Samuel, “Attenuation of Power Fluctuations in Large PV Power Plants: The Use of Prediction to Optimize the Storage System,” in *28th European Photovoltaic Solar Energy Conference and Exhibition*, 2013, pp. 4252–4255.
 - [23] E. . Stewart, T. P. Aukai, S. D. J. MacPherson, B. P. Quach, D. Nakafuji, and R. Davis, “A Realistic Irradiance-based Voltage Flicker Analysis of PV Applied to Hawaii Distribution Feeders,” in *2012 IEEE Power and Energy Society General Meeting*, 2012, pp. 1–7.
 - [24] A. Pan, Y. Tian, H. Zhao, X. Yang, and J. Jin, “Power Quality Analysis of PV System of Summer and Winter,” in *CIRED 2012 Workshop Integration of Renewables into the Distribution Grid*, 2012, pp. 1–4.
 - [25] R. Albarracín and H. Amarís, “Power Quality in distribution power networks with photovoltaic energy sources,” in *8th IEEE International Conference on Environment and Electrical Engineering*, 2009, pp. 360–363.
 - [26] T. Funabashi, T. Senjyul, M. Dattal, A. Yonal, M. Corporation, and E.

- Engineering, "A Coordinated Control Method for Leveling Output Power Fluctuations of Multiple PV Systems," in *The 7th International Conference on Power Electronics*, 2008, pp. 445–450.
- [27] A. O. Al-mathnani, H. Shareef, A. Mohamed, M. A. Mohd Ali, and M. A. Hannan, "Power Quality Improvement using DVR with Two Fast Vector Control," in *The 4th International Power Engineering and Optimization Conference*, 2010, vol. 1, pp. 376–381.
- [28] T. Gao, J. Cao, Y. Xu, H. Zhang, P. Yu, and S. Yao, "From Power Quality to Power Experience," in *4th International Conference on Networking and Distributed Computing*, 2014, pp. 116–120.
- [29] W. Shen and Y. Zhu, "Impacts of Small Photovoltaic Power Station on Voltage Sag in Low-Voltage Distribution Network," in *International Conference on Electrical and Control Engineering (ICECE)*, 2011, pp. 1585–1588.
- [30] K. Yamashita, Y. Kitauchi, and H. Kobayashi, "Influence of voltage sags on the power system with high penetration of photovoltaic power generation," in *2012 IEEE Power and Energy Society General Meeting*, 2012, pp. 1–7.
- [31] F. A. Rahman, "System-Wide Power Quality Monitoring in Malaysia," in *18th International Conference and Exhibition on Electricity Distribution (CIRED)*, 2005, pp. 1–5.
- [32] J. Kilter *et al.*, "Current practice and future challenges for power quality monitoring - CIGRE WG C4.112 perspective," in *2012 IEEE 15th International Conference on Harmonics and Quality of Power (ICHQP)*, 2012, pp. 390–397.
- [33] M. Music, A. Bosovic, N. Hasanspahic, S. Avdakovic, and E. Becirovic, "Integrated Power Quality Monitoring Systems in Smart Distribution Grids," in *2nd IEEE ENERGYCON Conference & Exhibition*, 2012, pp. 501–506.
- [34] H. Zang and Y. Zhao, "Intelligent Identification System of Power Quality Disturbance," in *Global Congress on Intelligent Systems*, 2009, pp. 258–261.
- [35] Z. Ding, Y. Zhu, and C. Chen, "Comprehensive Evaluation of Power Quality Based on Meaningful Classification," in *Critical Infrastructure*, 2010, pp. 1–4.
- [36] P. P. K. Chan, J. Zhu, Z. W. Qiu, W. W. Y. Ng, and D. S. Yeung, "Comparision of Different Classifiers in Fault Detection in Microgrid," in *International Conference on Machine Learning and Cybernetics*, 2011, vol. 3, pp. 1210–1213.
- [37] E. C. Bentley, G. a. Putrus, S. McDonald, and P. Minns, "Power quality disturbance source identification using self-organising maps," *IET Gener. Transm. Distrib.*, vol. 4, no. 10, pp. 1188–1196, 2010.
- [38] G. Mallesham, S. Mishra, and a N. Jha, "Automatic generation control of microgrid using artificial intelligence techniques," in *2012 IEEE*

- Power and Energy Society General Meeting*, 2012, pp. 1–8.
- [39] J. Llanos, D. Sáez, R. Palma-Behnke, A. Núñez, and G. Jiménez-Estévez, “Load profile generator and load forecasting for a renewable based microgrid using Self Organizing Maps and neural networks,” in *The 2012 International Joint Conference on Neural Networks (IJCNN)*, 2012, pp. 1–8.
 - [40] Y. Loewenstern, L. Katzir, and D. Shmilovitz, “The effect of system characteristics on very-short-term load forecasting,” in *12th International School on Nonsinusoidal Currents and Compensation*, 2015, pp. 1–6.
 - [41] I. Rendroyoko and M. Rusli, “Development of Power Quality Control Procedures and Standards to Control the Connection of Non-linear loads in Electric Power Systems,” in *22 nd International Conference on Electricity Distribution*, 2013, pp. 1–6.
 - [42] H. Hao, X. Yonghai, and Y. Lin, “Control Scheme of PV Inverter Under Unbalanced Grid Voltage,” in *2014 IEEE PES General Meeting / Conference & Exposition*, 2014, pp. 1–5.
 - [43] G. C. Pyo, H. W. Kang, and S. I. Moon, “A New Operation Method for Grid-Connected PV Systems Considering Voltage Regulation in Distribution System,” in *IEEE Power and Energy Society 2008 General Meeting: Conversion and Delivery of Electrical Energy in the 21st Century, PES*, 2008, pp. 1–7.
 - [44] H. Hao and Y. Xu, “Control Strategy of PV Inverter under Unbalanced Grid Voltage Sag,” in *2014 IEEE Energy Conversion Congress and Exposition*, 2014, pp. 1029–1034.
 - [45] T. Shou *et al.*, “Harmonic Current Suppression for Three Phase PV Generation System under Unbalanced Grid Voltage,” in *IEEE PES Asia-Pacific Power and Energy Engineering Conference (APPEEC)*, 2013, pp. 1–6.
 - [46] S. Dasgupta, S. K. Sahoo, and S. K. Panda, “Design of a Spatial Iterative Learning Controller for Single Phase Series Connected PV Module Inverter for Grid Voltage Compensation,” in *Power Electronics Conference (IPEC), 2010 International*, 2010, pp. 1980–1987.
 - [47] W. Al-Saedi, S. W. Lachowicz, D. Habibi, and O. Bass, “Power quality enhancement in autonomous microgrid operation using Particle Swarm Optimization,” *Int. J. Electr. Power Energy Syst.*, vol. 42, no. 1, pp. 139–149, 2012.
 - [48] W. T. Jewell, R. Ramakumar, and S. R. Hill, “Study of dispersed photovoltaic generation on the PSO system,” *IEEE Trans. Energy Convers.*, vol. 3, no. 3, pp. 473–478, 1988.
 - [49] J. Marcos, L. Marroyo, E. Lorenzo, and M. Garcia, “Smoothing of PV Power Fluctuations by Geographical Dispersion,” *Prog. Photovoltaics Res. Appl.*, vol. 20, no. 2, pp. 226–237, 2012.
 - [50] A. Murata and K. Otani, “An analysis of time-dependent spatial distribution of output power from very many PV power systems installed

- on a nation-wide scale in Japan,” *Sol. Energy Mater. Sol. Cells*, vol. 47, no. 1–4, pp. 197–202, 1997.
- [51] M. Lave, J. Kleissl, and E. Arias-Castro, “High-frequency irradiance fluctuations and geographic smoothing,” *Sol. Energy*, vol. 86, no. 8, pp. 2190–2199, 2012.
 - [52] T. E. Hoff and R. Perez, “Quantifying PV power Output Variability,” *Sol. Energy*, vol. 84, no. 10, pp. 1782–1793, 2010.
 - [53] T. E. Hoff and R. Perez, “Modeling PV fleet output variability,” *Sol. Energy*, vol. 86, no. 8, pp. 2177–2189, 2012.
 - [54] I. H. Rowlands, B. P. Kemery, and I. Beausoleil-Morrison, “Managing solar-PV variability with geographical dispersion: An Ontario (Canada) case-study,” *Renew. Energy*, vol. 68, pp. 171–180, 2014.
 - [55] J. G. Da Silva Fonseca Junior, T. Oozeki, H. Ohtake, K. ichi Shimose, T. Takashima, and K. Ogimoto, “Regional forecasts and smoothing effect of photovoltaic power generation in Japan: An approach with principal component analysis,” *Renew. Energy*, vol. 68, pp. 403–413, 2014.
 - [56] E. Wiemken, H. G. Beyer, W. Heydenreich, and K. Kiefer, “Power characteristics of PV ensembles: experiences from the combined power production of 100 grid connected PV systems distributed over the area of Germany,” *Sol. Energy*, vol. 70, no. 6, pp. 513–518, 2001.
 - [57] M. Cao, Q. Xu, P. Zeng, X. Xu, and X. Yuan, “An Energy Storage System Configuration Method to Stabilize Power Fluctuation in Different Operation Periods,” in *PES General meeting / Conference & Exposition*, 2014, pp. 1–5.
 - [58] E. Abdelkarim, M. M. Aly, M. Abdelakher, Z. Ziadi, and T. Senjyu, “Supersession of Large Penetration Photovoltaic Power Transients Using Storage Batteries,” in *2013 IEEE 10th International Conference on Power Electronics and Drive Systems (PEDS)*, 2013, pp. 78–83.
 - [59] K. Hossain and H. Ali, “Small Scale Energy Storage for Power Fluctuation Minimization with Spatially Diverged PV plants,” in *Southeastcon*, 2013, pp. 1–6.
 - [60] X. Liu, A. Aichhorn, L. Liu, and H. Li, “Coordinated control of distributed energy storage system with tap changer transformers for voltage rise mitigation under high photovoltaic penetration,” *IEEE Trans. Smart Grid*, vol. 3, no. 2, pp. 897–906, 2012.
 - [61] A. Mills *et al.*, “Dark Shadows,” *IEEE Power Energy Mag.*, vol. 9, no. 3, pp. 33–41, 2011.
 - [62] F. Barbieri, S. Rajakaruna, and A. Ghosh, “Very short-term photovoltaic power forecasting with cloud modeling: A review,” *Renew. Sustain. Energy Rev.*, vol. 75, no. November 2016, pp. 242–263, 2017.
 - [63] V. P. A. Lonij *et al.*, “Forecasts of PV power output using power measurements of 80 residential PV installs,” *Conf. Rec. IEEE Photovolt. Spec. Conf.*, pp. 3300–3305, 2012.
 - [64] V. P. A. Lonij, A. E. Brooks, A. D. Cronin, M. Leuthold, and K. Koch,

- “Intra-hour forecasts of solar power production using measurements from a network of irradiance sensors,” *Sol. Energy*, vol. 97, pp. 58–66, 2013.
- [65] V. P. Lonij, A. E. Brooks, K. Koch, and A. D. Cronin, “Analysis of 80 rooftop PV systems in the Tucson, AZ area,” *Conf. Rec. IEEE Photovolt. Spec. Conf.*, pp. 549–553, 2012.
- [66] S. S. Soman, H. Zareipour, S. Member, O. Malik, and L. Fellow, “A Review of Wind Power and Wind Speed Forecasting Methods With Different Time Horizons,” in *IEEE North American Power Symposium (NAPS) 2010*, 2010.
- [67] S. M. Lawan, W. A. W. Z. Abidin, W. Y. Chai, A. Baharun, and T. Masri, “Different Models of Wind Speed Prediction; A Comprehensive Review,” in *Solar Energy Forecasting and Resource Assessment*, vol. 5, no. 1, J. Kleissl, Ed. Elsevier, 2014.
- [68] Y. Huang, J. Lu, C. Lu, X. Xu, W. Wang, and X. Zhou, “Comparative Study of Power Forecasting,” in *2010 Internatioanl Conference on Power System Technology*, 2010, pp. 1–6.
- [69] C. Joao P. S., *Smart and Sustainable Power System: Operations, Planning, and Economics of Insular Electricity Grids*. Boca Raton: CRC Press, 2015.
- [70] R. Dambreville, P. Blanc, J. Chanussot, and D. Boldo, “Very short term forecasting of the global horizontal irradiance using a spatio-temporal autoregressive model,” *Renew. Energy*, vol. 72, pp. 291–300, 2014.
- [71] P. Addesso, R. Conte, M. Longo, R. Restaino, and G. Vivone, “MAP-MRF cloud detection based on PHD filtering,” *IEEE J. Sel. Top. Appl. Earth Obs. Remote Sens.*, vol. 5, no. 3, pp. 919–929, 2012.
- [72] V. Bjerknes, E. Volken, and S. Brönnimann, “The problem of weather prediction, considered from the viewpoints of mechanics and physics,” *Meteorol. Zeitschrift*, vol. 18, no. 6, pp. 663–667, 2009.
- [73] E. Lorenz, D. Heinemann, H. Wickramaratne, H. G. Beyer, and S. Bofinger, “Forecast of ensemble power production by grid-connected PV systems,” *20th Eur. Photovolt. Sol. Energy Conf.*, pp. 3–9, 2007.
- [74] P. Bacher, H. Madsen, and H. A. Nielsen, “Online short-term solar power forecasting,” *Sol. Energy*, vol. 83, no. 10, pp. 1772–1783, 2009.
- [75] S. Alessandrini, L. Delle Monache, S. Sperati, and G. Cervone, “An analog ensemble for short-term probabilistic solar power forecast,” *Appl. Energy*, vol. 157, pp. 95–110, 2015.
- [76] C. Monteiro, T. Santos, L. A. Fernandez-Jimenez, I. J. Ramirez-Rosado, and M. S. Terreros-Olarte, “Short-term power forecasting model for photovoltaic plants based on historical similarity,” *Energies*, vol. 6, no. 5, pp. 2624–2643, 2013.
- [77] J. G. Da Silva Fonseca, T. Oozeki, T. Takashima, G. Koshimizu, Y. Uchida, and K. Ogimoto, “Photovoltaic power production forecasts with support vector regression: A study on the forecast horizon,” *Conf. Rec. IEEE Photovolt. Spec. Conf.*, pp. 002579–002583, 2011.

- [78] J. G. Da Silva Fonseca, T. Oozeki, T. Takashima, G. Koshimizu, Y. Uchida, and K. Ogimoto, "Use of support vector regression and numerically predicted cloudiness to forecast power output of a photovoltaic power plant in Kitakyushu, Japan," *Prog. Photov.*, vol. 20, pp. 874–882, 2012.
- [79] B. Urquhart, B. Kurtz, E. Dahlin, M. Ghonima, J. E. Shields, and J. Kleissl, "Development of a sky imaging system for short-term solar power forecasting," no. 2013, pp. 875–890, 2015.
- [80] Y. Chu, B. Urquhart, S. M. I. Gohari, H. T. C. Pedro, J. Kleissl, and C. F. M. Coimbra, "Short-term reforecasting of power output from a 48 MWe solar PV plant," *Sol. Energy*, vol. 112, pp. 68–77, 2015.
- [81] Z. Peng, D. Yu, D. Huang, J. Heiser, and S. Yoo, "ScienceDirect 3D cloud detection and tracking system for solar forecast using multiple sky imagers," *Sol. Energy*, vol. 118, pp. 496–519, 2015.
- [82] J. L. Bosch and J. Kleissl, "Cloud motion vectors from a network of ground sensors in a solar power plant," *Sol. Energy*, vol. 95, pp. 13–20, 2013.
- [83] C. W. Chow *et al.*, "Intra-hour forecasting with a total sky imager at the UC San Diego solar energy testbed," *Sol. Energy*, vol. 85, no. 11, pp. 2881–2893, 2011.
- [84] P. M. Ferreira, J. M. Gomes, I. A. C. Martins, and A. E. Ruano, "A neural network based intelligent predictive sensor for cloudiness, solar radiation and air temperature," *Sensors (Switzerland)*, vol. 12, no. 11, pp. 15750–15777, 2012.
- [85] R. Marquez and C. F. M. Coimbra, "Intra-hour DNI forecasting based on cloud tracking image analysis," *Sol. Energy*, vol. 91, pp. 327–336, 2013.
- [86] R. H. Inman, H. T. C. Pedro, and C. F. M. Coimbra, "Solar forecasting methods for renewable energy integration," *Prog. Energy Combust. Sci.*, vol. 39, no. 6, pp. 535–576, 2013.
- [87] A. Azadeh, A. Maghsoudi, and S. Sohrabkhani, "An integrated artificial neural networks approach for predicting global radiation," *Energy Convers. Manag.*, vol. 50, no. 6, pp. 1497–1505, 2009.
- [88] A. Mellit, S. A. Kalogirou, L. Hontoria, and S. Shaari, "Artificial intelligence techniques for sizing photovoltaic systems: A review," *Renew. Sustain. Energy Rev.*, vol. 13, no. 2, pp. 406–419, 2009.
- [89] C. Chen, S. Duan, T. Cai, and B. Liu, "Online 24-h solar power forecasting based on weather type classification using artificial neural network," *Sol. Energy*, vol. 85, no. 11, pp. 2856–2870, 2011.
- [90] S. K. H. Chow, E. W. M. Lee, and D. H. W. Li, "Short-term prediction of photovoltaic energy generation by intelligent approach," *Energy Build.*, vol. 55, pp. 660–667, 2012.
- [91] C. Craggs, E. M. Conway, and N. M. Pearsall, "Statistical investigation of the optimal averaging time for solar irradiance on horizontal and vertical surfaces in the UK," *Sol. Energy*, vol. 68, no. 2, pp. 179–187,

- 2000.
- [92] C. F. M. Coimbra and J. Kleissl, "Overview of Solar-Forecasting Methods and a Metric for Accuracy Evaluation," in *Solar Energy Forecasting and Resource Assessment*, Elsevier, 2013, pp. 171–194.
 - [93] P. Kanirajan and V. Suresh Kumar, "Power quality disturbance detection and classification using wavelet and RBFNN," *Appl. Soft Comput.*, vol. 35, pp. 470–481, 2015.
 - [94] H. Quan, D. Srinivasan, and A. Khosravi, "Short-term load and wind power forecasting using neural network-based prediction intervals," *IEEE Trans. Neural Networks Learn. Syst.*, vol. 25, no. 2, pp. 303–315, 2014.
 - [95] J. Bai, W. Gu, X. Yuan, Q. Li, F. Xue, and X. Wang, "Power Quality Prediction, Early Warning, and Control for Points of Common Coupling with Wind Farms," *Energies*, vol. 8, no. 9, pp. 9365–9382, 2015.
 - [96] A. Hebboul, F. Hachouf, and A. Boulemnadjel, "A New Incremental Neural Network for Simultaneous Clustering and Classification," *Neurocomputing*, vol. 169, pp. 89–99, 2015.
 - [97] A. Hebboul, M. Hacini, and F. Hachouf, "An Incremental Parallel Neural Network for Unsupervised Classification," in *7th International Workshop on Systems, Signal Processing and their Applications*, 2011, pp. 400–403.
 - [98] M. Oral, E. L. Oral, and A. Aydin, "Supervised vs. Unsupervised Learning for Construction Crew Productivity Prediction," *Autom. Constr.*, vol. 22, pp. 271–276, 2012.
 - [99] M. Tscherepanow, M. Kortkamp, and M. Kammer, "A hierarchical ART network for the stable incremental learning of topological structures and associations from noisy data," *Neural Networks*, vol. 24, no. 8, pp. 906–916, 2011.
 - [100] S. Jain, S. Lange, and S. Zilles, "Some natural conditions on incremental learning," *Inf. Comput.*, vol. 205, no. 11, pp. 1671–1684, 2007.
 - [101] G. A. Carpenter and S. Grossberg, "Art of Adaptive Pattern Recognition By a Self-Organizing Neural Network.," *Computer (Long. Beach. Calif.)*, vol. 21, no. 3, pp. 77–88, 1988.
 - [102] Y. Prudent and A. Ennaji, "A new learning algorithm for incremental self-organizing maps," in *13th European Symposium on Artificial Neural Networks*, 2005, pp. 7–12.
 - [103] B. Fritzke, "A Growing Neural Gas Network Learns Topologies," *Adv. Neural Inf. Process. Syst.* 7, vol. 7, no. 1, pp. 625–632, 1995.
 - [104] T. M. Martinetz, "Competitive Hebbian learning rule forms perfectly topology preserving maps," in *International Conference on Artificial Neural Networks*, 1993, pp. 427–434.
 - [105] T. M. Martinetz, S. G. Berkovich, and K. J. Schulten, "'Neural-Gas' network for vector quantization and its application to time-series prediction," *IEEE Trans. Neural Networks*, vol. 4, no. 4, pp. 558–569, 1993.

- [106] S. Furao and O. Hasegawa, “An incremental network for on-line unsupervised classification and topology learning,” *Neural Networks*, vol. 19, no. 1, pp. 90–106, 2006.
- [107] C. M. Bishop, *Pattern Recognition and Machine Learning*. Cambridge: Springer-Verlag New York, 2006.
- [108] O. Tremblay, M. Ieee, L. Dessaint, S. M. Ieee, and A. Dekkiche, “A Generic Battery Model for the Dynamic Simulation of Hybrid Electric Vehicles,” in *Vehicle Power and Propulsion Conference*, 2007, pp. 284–289.
- [109] “Compact DAQ 9178 Technical Specification.” [Online]. Available: <http://www.ni.com/pdf/manuals/374046a.pdf>. [Accessed: 25-Apr-2015].
- [110] “NI 9209 Technical Specification.” [Online]. Available: http://www.ni.com/pdf/manuals/376909c_02.pdf. [Accessed: 25-Apr-2015].
- [111] “NI 9203 Technical Specification.” [Online]. Available: http://www.ni.com/pdf/manuals/374070a_02.pdf. [Accessed: 25-Apr-2015].
- [112] “SP Lite 2 Pyranometer Technical Specification.” [Online]. Available: <http://www.kippzonen.com/Product/9/SP-Lite2-Pyranometer#.WZNLMIWg-Uk>. [Accessed: 10-Oct-2014].